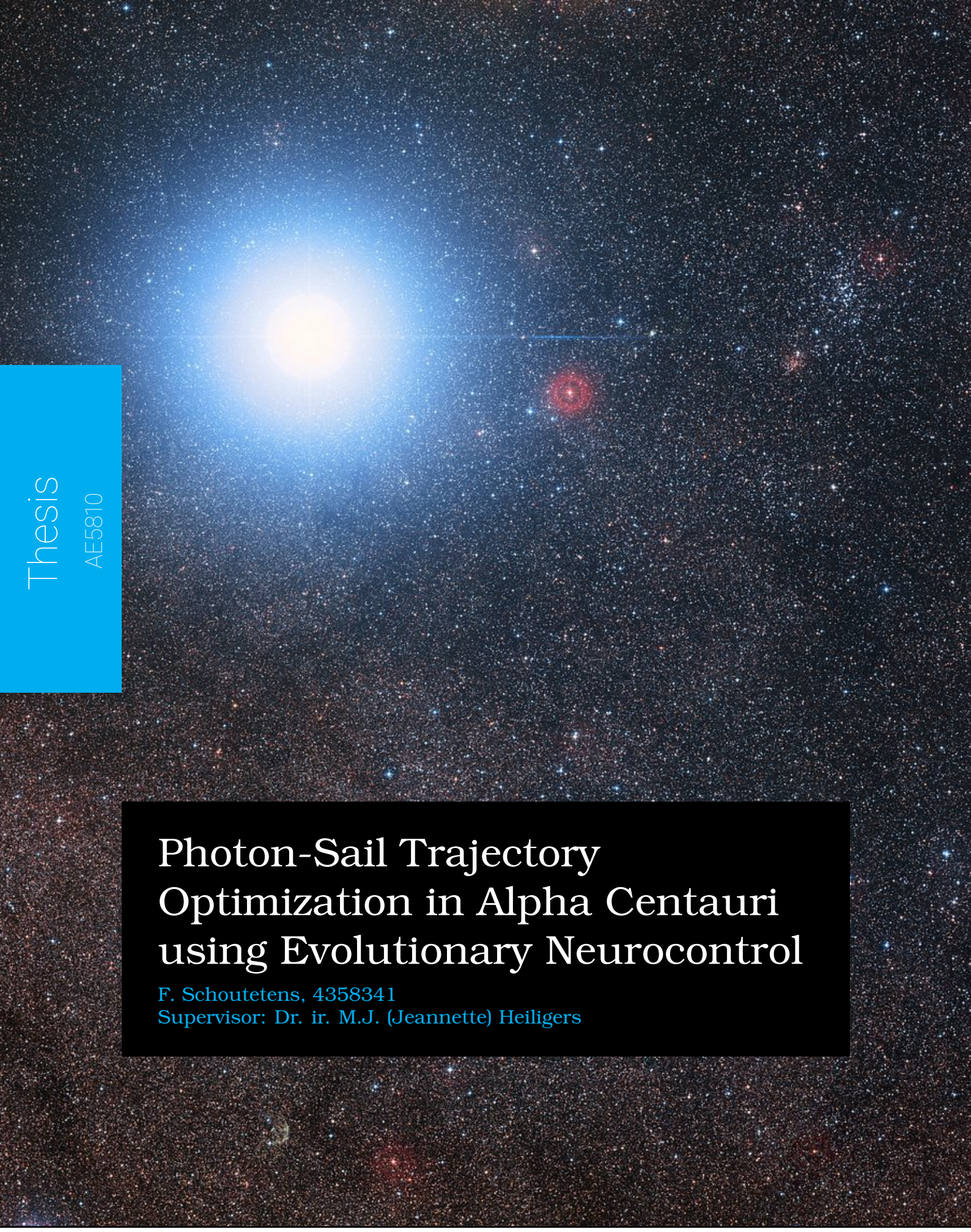

Thesis
AE5810

Photon-Sail Trajectory Optimization in Alpha Centauri using Evolutionary Neurocontrol

F. Schoutetens, 4358341
Supervisor: Dr. ir. M.J. (Jeannette) Heiligers

TU Delft Delft University of Technology

Aerospace Engineering

October 6, 2019

Title page figure taken from https://www.newscientist.com, Retrieved June, 2018

Photon-Sail Trajectory Optimization in Alpha Centauri using Evolutionary Neurocontrol

by

Frederic Schoutetens

Dissertation for the degree of

Master of Science: Aerospace Engineering

at The Astrodynamics and Space Missions Section,
Delft University of Technology,

to be defended publicly on Tuesday October 22, 2019 at 13:00.

Student number:	4358341	
Supervisor:	Dr. ir. M.J. (Jeannette) Heiligers	
Project duration:	January 7, 2019 – October 22, 2019	
Thesis committee:	Prof. dr. ir. P. N. A. M. Visser - TU Delft,	Committee chair
	Dr. ir. M.J. (Jeannette) Heiligers - TU Delft,	Supervisor
	Dr. A. Menicucci - TU Delft,	External examinator
	Prof. dr. ir. B. Dachwald - FH-Aachen,	External supervisor

An electronic version of this thesis is available at `http://repository.tudelft.nl/`.

TU Delft

"...provide ships or sails adapted to the heavenly breezes, and there will be some who will brave that void."

Johannes Kepler to Galileo in 1610.

Preface

This thesis is the result of eight months of performing research on photon sails and interstellar travel to Alpha Centauri, with the following title:

Photon-Sail Trajectory Optimization in Alpha Centauri using Evolutionary Neurocontrol.

The first words of gratitude are for those who provide me with love and support throughout my entire life: my parents, Marc and Ingrid, and my brother, Benoît. I could not become who I am now without your unconditional love. I am forever grateful for giving me everything I need in order to be where I want to be. Their dedication gave me a boost to be where I am right now and will encourage me to perform at my best in the future.

The author of this work would also like to thank Dr. ir. Jeannette Heiligers for her inspiration, cooperation and thorough feedback throughout the process of this thesis research. Your scientific knowledge, professional attitude, enthusiasm and critical mindset have been an essential component towards the realization of this work. I hope this research on interstellar travel can be continued together in the future.

This thesis would also not be possible without the help of Prof. dr. ir. Bernd Dachwald, who cooperated by sharing his solar-sailing knowledge and expertise in InTrance. Furthermore, I would like to thank Dr. ir. Andreas Ohndorf for his input during the exploration of InTrance as software tool for this work.

Last but not least, I want to pay tribute to all my friends with whom I could spend the past five years at TU Delft. These include my friends from the graduation room of the ninth floor. A most special acknowledgement goes to Hendrik Gaens, Wouter Van Gijseghem and the De Leeuw twins, whom I consider as friends for a lifetime.

Frederic Schoutetens
Delft, October 6, 2019

Summary

In 2016, Yuri Milner announced Breakthrough Starshot, an initiative to prove the concept of ultra-fast light-driven nanocraft, thereby laying the foundations for the inaugural launch of an interstellar mission to Alpha Centauri within the next generation. The target time of flight to reach Alpha Centauri is 20 years, corresponding to a velocity of 20% of the speed of light, achieved by accelerating a sail with a laser beam emitted from Earth. The scientific goal of this mission is to help achieve one of mankind's biggest desires: to find signs of extraterrestrial life, with Proxima b - an Earth-like exoplanet in the habitable zone of Alpha Centauri C - as the primary target.

The mission as proposed by the Breakthrough Starshot project is a fly-through mission, with a velocity such that the spacecraft would travel through Alpha Centauri's binary star system in approximately a day. To increase the scientific yield of this interstellar mission, this thesis proposes to decelerate at Alpha Centauri.

From this, the objective of the thesis work was defined as follows:

To contribute to interstellar travel to Alpha Centauri using a photon sail by designing the deceleration trajectory in the binary Centauri AB system to get captured into an orbit about one of its binary stars.

For this purpose, the optimal control problem that needs solving is to find the optimal path of the sail and the optimal orientation of the sail such that the spacecraft is able to decelerate into a capture orbit about one of Alpha Centauri's stars within the shortest travel time.

By surpassing the proposal of the Breakthrough Starshot project by enabling the spacecraft to be captured around one of the binary stars, the range of mission applications at Alpha Centauri is enhanced. This thesis therefore also investigates transfer trajectories between the binary stars and orbit raising from the center of the star's habitable zone to its outer edge.

InTrance, an intelligent spacecraft trajectory optimization tool using neurocontrol evolution, was adapted to be suitable as the optimal control solver to determine the time-optimal trajectories of this three-phased mission proposal. This tool combines artificial intelligence, machine learning and evolutionary algorithms with the aim to find the (near-to) global optimal solution by optimizing the steering strategy of the sail.

Investigating capture, transfer and orbit raising for four different lightness numbers resulted in the following outcome:

1. The baseline sail technology used in this work was a Sunjammer-like sail. Such a spacecraft would need approximately 20,000 years to arrive at Alpha Centauri into an orbit about Alpha Centauri A. Therefore, sending a sail today would presumably mean that it would be overtaken by a more-developed photonic sail launched in the future.

2. Although the Breakthrough Starshot project aims to travel to Alpha Centauri within 20 years, a travel time of approximately 2000 years was found in case the sail would be captured into the binary star system, instead of performing a flyby. However, once arrived, the sail would be capable to explore the binary star system by transferring between the stars and by increasing its orbit from the center of the habitable zone to its outer edge, for example.

3. A futuristic graphene-based sail could travel from our Solar System to Alpha Centauri and could be captured into an orbit about Alpha Centauri B within less than 80 years. However, it is found to be extremely challenging for such a high-technological sail to perform transfer trajectories or orbit raising, because of its large lightness number. Therefore, it is suggested to jettison the sail at arrival.

4. Although it is technically possible to perform this mission with a conventional one-sided reflective sail, the travel time from our Solar System to Alpha Centauri would be eight times longer than for a sail that is reflective on both sides. Therefore, current technology would need to be innovated such that this interstellar mission can be performed with a two-sided reflective sail.

When looking into the future, there is an abundance of potential for interstellar exploration in Alpha Centauri. A first recommendation would be to improve the model of the sail from an ideal model to a real model with non-perfect reflectivity of the sail. Next, a better understanding of the orbital dynamics of a photon sail in a binary star system could be realized by an in-depth study of periodic orbits about artificial equilibrium points, such as the area at the L_1-point to simultaneously observe Alpha Centauri A and B. Finally, the next target for a fascinating research project is suggested to be a rendezvous with Proxima b, Alpha Centauri C's Earth-like planet. Contributing to realizing a mission to this exoplanet using a photon sail could well lead to the next giant leap for mankind.

Contents

List of Figures

List of Tables

1 Introduction

The idea of using a photon sail to travel to Alpha Centauri - the closest neighbouring star system to the Sun - goes against intuition as the sail does not use propellant to travel in between the stars. However, on April 12 2016, Yuri Milner announced the Breakthrough Starshot project[1], based on the dream of both scientists and science fiction enthusiasts to travel among the stars. Within the next generation, this project's goal is to demonstrate that Alpha Centauri, and more specifically Proxima Centauri, can be reached within 20 years of travel time, corresponding to a speed of 20% of the speed of light. This first launch to Alpha Centauri would make use of a laser beamer to accelerate ultra-fast light-driven nanocraft to relativistic speeds to fly through and transmit images of the star system, consisting of the recently-discovered Earth-sized potentially habitable planet Proxima b.

Before interstellar missions can become a reality, hard engineering challenges remain to be solved. Lubin's roadmap to interstellar travel formulated the essential components for Milner's leap to the stars, reviving the possibility of interstellar travel by describing the recent technological advances in material sciences, laser propulsion, and the development of high-performance wafer-scale spacechips attached to sails [1]. The latter concept of using a sail to accelerate a space probe is no innovation. Solar sailing recently lifted off with JAXA's IKAROS mission (2010) - the first interplanetary solar sail mission - followed by NASA's NanoSail-D2 mission (2010), and The Planetary Society's LightSail-1 mission (2015) [2–4]. Even more recently, LightSail-2 proved successful orbit raising about Earth, demonstrating the possibility of generating continuous thrust from photons hitting a highly reflective sail, surpassing the conventional methods of spacecraft propulsion depending on the expulsion of mass [5]. Where propellant-based propulsion systems make effective interstellar travel impossible - with travel times of up to thousands of years - light sails provide an energy efficient alternative, achieving high velocities using a relatively weak, but continuous acceleration. The capabilities of solar sailing are used to the fullest extent in high-energy and long-duration missions, such as highly non-Keplerian orbits, advanced space weather warning and pole-sitter missions [6–10].

For interstellar travel, high temperatures during close encounters with stars - where the acceleration is largest, though the sail is prone to melting - and the loss of effective propulsion away from the star form the key challenges [11]. Alternative to performing a close stellar encounter, the high flux of coherent light from lasers has been proposed to solve the problem of decreasing acceleration with distance to the Sun [12]. Interstellar vehicles propelled by terrestrial laser beams were first studied in the 1960s [13, 14]. However, using this technology, there is no straightforward way to decelerate at arrival [15].

Research teams are currently considering these new means of interstellar travel, focusing on lightweight high-velocity photon sails, using either lasers or stellar radiation. It was suggested to only make use of two astrophysical aspects to end up in an orbit at the destination: the gravity of the stars and their stellar radiation [16]. With a strong, ultralight material as graphene for a sail covered with a highly reflective coating, travel times of 95 years and maximum arrival speeds of 4.6% of the speed of light would result in a successful deceleration into Alpha Centauri with arrival at Proxima Centauri. By making use of photogravitational assists in a more clever way, the transfer from Earth to Alpha Centauri was found to be approximately 75 years, corresponding to a velocity of 5.7% of the speed of light [17]. Furthermore, the MIRA Collaboration performed research on artificial equilibrium points, AEPs, in Alpha Centauri for a solar balloon spacecraft, before inves-

[1] See the Breakthrough Starshot initiative at `https://breakthroughinitiatives.org/initiative/3`, Retrieved August 14 2019

tigating capture and transfer trajectories for a stellar-photon sailcraft in the elliptical restricted three-body problem [18, 19].

After providing the background of this thesis research, the goals of this thesis research are discussed in section 1.1, while the outline of this thesis report is provided in section 1.2.

1.1. Research Objective and Questions

Contrary to the idea of the Breakthrough Starshot project - performing a flyby at Proxima Centauri and thus traversing the system within hours - this work focuses on decelerating in Alpha Centauri, hence improving the scientific yield of the interstellar mission. While previous work on capture into Alpha Centauri focused on arriving at Proxima Centauri, this work puts emphasis on the binary star system of Alpha Centauri, Centauri AB. In addition, this thesis performs research on the feasibility of capturing into the binary system of Alpha Centauri by utilizing an intelligent spacecraft trajectory optimization tool, InTrance, based on artificial intelligence, machine learning and evolutionary algorithms. By proposing a time-optimal mission that enables the exploration of the binary system of Alpha Centauri, this thesis contributes to the investigation of the feasibility of interstellar travel to Alpha Centauri. As a result, the objective of this research reads as follows:

To contribute to interstellar travel to Alpha Centauri using a photon sail by designing the deceleration trajectory in the binary Centauri AB system to get captured into an orbit about one of its binary stars.

The primary goal of this research is thus to find a time-optimal capture phase for a photon sail using only photon pressure and the gravitational attraction of the stars. This leads to the following list of research questions:

1) Is it possible to get captured into an orbit about Centauri A or B?

2) What is the maximum injection speed at which the spacecraft can still be captured into an orbit about Centauri A or B?

3) What is the required performance of the sail for interstellar travel to Alpha Centauri?

After answering these research questions, this work can be considered as a valuable contribution to interstellar travel to Alpha Centauri by adding innovative knowledge to the contemporary research of orbital dynamics of a photon sail in a binary star system like Alpha Centauri. During the process of this thesis, two additional research topics were added after the capture phase of the mission was answered successfully: transfer trajectories between the stars and orbit raising about a star. The goal of these additional mission phases is to find time-optimal solutions.

1.2. Report Outline

This thesis work is written in the format of a draft journal paper that may be submitted to the "Journal of Guidance, Control and Dynamics", which is published by the American Institute of Aeronautics and Astronautics. The paper can be found in chapter 2. According to the guidelines[2] issued by the American Institute of Aeronautics and Astronautics, the paper is initialized with an abstract, followed by the introduction. The core of the paper starts with a discussion of Alpha Centauri, after which the photon sail dynamics is explained with respect to the elliptical restricted three-body problem, elaborating on the novel force model for a sail subjected to two radiative bodies. Thereafter, a range of mission applications is discussed before presenting the proposed mission scenario. Then, after explaining the optimal control problem and discussing InTrance as the trajectory optimization tool, the results with accompanying sensitivity analyses are presented. The paper comes to an end with the conclusion. The third chapter of this report covers another conclusion. However, in this conclusion, the aim is to answer the research questions listed above. In addition, a list of recommendations for future work is provided in chapter 3. Finally, the thesis work is concluded with an appendix on verification and validation, and an appendix providing the input configuration files for InTrance.

[2]See the guidelines at `https://www.aiaa.org/home/events-learning/events/Technical-Presenter-Resources`, Retrieved August 18 2019

2

Journal Article

In this chapter, the stand-alone journal article can be found. This draft paper presents the core work of this thesis research. Aside from minor changes to fulfil the requirements of a journal article, it is ready for submission.

Photon-Sail Trajectory Optimization in Alpha Centauri using Evolutionary Neurocontrol

Frederic Schoutetens *
Delft University of Technology, 2629 HS, Delft, The Netherlands

With the increased interest for interstellar exploration after the discovery of exoplanets and the proposal of the Breakthrough Starshot project to perform a fly-through mission of Alpha Centauri to capture the first images of an Earth-like exoplanet, this paper investigates the optimization of photon-sail trajectories in Alpha Centauri for various mission applications. The prime objective is to find the optimal steering strategy for the photonic sail to get captured in Alpha Centauri after a minimum-time transfer from Earth. By extending the idea of the Breakthrough Starshot project with a deceleration phase at arrival, the mission's scientific yield is increased. In addition to capture into an orbit at the center of the habitable zone of one of the stars, a transfer trajectory to an orbit around the other star and an orbit-raising maneuver to the outer edge of the habitable zone are also investigated and added to the proposed mission scenario. The trajectories are optimized for minimum time of flight with the trajectory optimization tool InTrance, which makes use of evolutionary neurocontrol. The results show that an increase in technological development is required to obtain a feasible time of flight of approximately one century, using a two-sided reflective sail. The optimized time of flight from our Solar System until capture in Alpha Centauri ranges from 20,000 years for current sail technology to less than 80 years for a futuristic graphene-based ultralight sail. The latter allows a maximum injection speed into Alpha Centauri of 5.5% of the speed of light. The results in this work show an average improvement of 30% in terms of time of flight for lightness numbers smaller than a graphene-based sail. A sail as proposed by the Breakthrough Starshot project, however, would need over 2000 years to travel from our Solar System until capture about Alpha Centauri B, such that a fly-through mission that arrives within a lifetime is arguably the best option for a near-term mission to Alpha Centauri.

*Graduate Student, section of Astrodynamics and Space Missions, department of Space Engineering, Faculty of Aerospace Engineering, F.R.J.Schoutetens@student.tudelft.nl

Nomenclature

Roman Symbols

a	=	semi-major axis	[AU]
$\bar{a}$	=	acceleration	[m/s^2]
$\mathbf{a}$	=	acceleration vector	[m/s^2]
A	=	sail area	[m^2]
c	=	speed of light	[m/s]
e	=	eccentricity	[-]
$\mathbf{f}$	=	thrust normal vector	[N]
F	=	force	[N]
$\mathbf{F}$	=	force vector	[N]
g	=	standard acceleration due to gravity	[m/s^2]
i	=	inclination	[deg]
J	=	cost function	[-]
K	=	scaling factor	[-]
l	=	mean longitude	[deg]
L	=	luminosity	[W]
M	=	mass	[kg]
n	=	mean motion	[deg/yr]
$\tilde{n}$	=	minimum number of stellar radii	[-]
$\hat{\mathbf{n}}$	=	sail normal vector	[-]
P	=	stellar radiation pressure	[Pa]
r	=	distance	[AU]
$\mathbf{r}$	=	position vector	[AU]
$\dot{\mathbf{r}}$	=	velocity vector	[AU/d]
$\ddot{\mathbf{r}}$	=	acceleration vector	[AU/d^2]
R	=	radius	[m]
$\hat{\mathbf{s}}$	=	unit vector from Alpha Centauri's barycenter to the Sun	[-]
t	=	time	[s]
T	=	orbital period	[yr]
T_0	=	epoch of periapsis	[yr]
$\tilde{T}$	=	temperature	[K]

$\mathbf{T}$	=	rotation matrix	[-]
u	=	sign of the direction of the star's acceleration with respect to sail's normal vector	[−]
$\mathbf{u}$	=	control vector	[deg, deg]
v	=	velocity	[km/s]
ΔV	=	velocity increment	[km/s]
w	=	weight	[-]
$\mathbf{x}$	=	state vector	[m, m/s]

Greek Symbols

α	=	sail cone angle	[deg]
β	=	lightness number	[-]
δ	=	sail clock angle	[deg]
ϵ	=	relation for stellar radiation pressure between Alpha Centauri's binary stars	[-]
ζ	=	sail's absorptivity	[-]
θ	=	true anomaly	[deg]
μ	=	gravitational parameter	[m^3/s^2]
$\bar{\mu}$	=	dimensionless mass of secondary star	[-]
ρ	=	semi-latus rectum	[AU]
ω	=	argument of periapsis	[deg]
$\bar{\omega}$	=	magnitude of the angular velocity of the rotating frame	[rad/s]
$\bar{\boldsymbol{\omega}}$	=	angular velocity vector of the rotating frame	[rad/s]
Ω	=	longitude of ascending node	[deg]

Superscripts

$\hat{\square}$	=	unit vector
$\dot{\square}$	=	differentiation with respect to true anomaly

Subscripts

$\square_0$	=	at 1 AU distance
$\square_\odot$	=	solar unit
$\star$	=	star's property
A	=	Alpha Centauri A
b	=	begin
B	=	Alpha Centauri B
$bary$	=	barycenter

$bary, A$	=	Alpha Centauri A w.r.t barycenter
$bary, B$	=	Alpha Centauri B w.r.t barycenter
c	=	characteristic
f	=	final
h	=	normal to the orbital plane, pointing along the orbital angular momentum vector
i	=	incident photons
inj	=	injection
nom	=	nominal
r	=	radial
SC	=	spacecraft
SRP	=	stellar radiation pressure
t	=	tangential
T	=	target
$t.c.$	=	termination condition

Other notations

$^\circ$	=	degree
$'$	=	minute
$''$	=	second

I. Introduction

At 146 astronomical units (AU) away from the Sun and at a velocity of less than 0.01 AU/day, it would take Voyager 1 approximately 75,000 years to reach Alpha Centauri, the closest star system from Earth at approximately 275,000 AU. A photon-sail propelled spacecraft could surpass the conventional methods of spacecraft propulsion and substantially reduce the travel time to Alpha Centauri by exclusively making use of the radiation pressure from a star as a means to drive a spacecraft forward. This technology recently lifted off with JAXA's IKAROS mission - the first interplanetary solar-sail mission - followed by NASA's NanoSail-D2 mission and The Planetary Society's LightSail-1 and LightSail-2 missions [1–4]. Each of these missions proved the possibility of generating continuous thrust from photons hitting a highly reflective sail [5].

The Breakthrough Starshot project* is an initiative that aims to demonstrate that an ultra-fast light-driven sail can be used for a first interstellar mission to Alpha Centauri. The goal is to arrive after 20 years of travel time - which corresponds to a velocity of 20% of the speed of light or approximately 35 AU/day - and to fly through the system while transmitting images back to Earth of the recently-discovered Earth-sized and potentially habitable planet Proxima

*See the Breakthrough Starshot initiative at `https://breakthroughinitiatives.org/initiative/3`, Retrieved August 14, 2019

b. According to this mission scenario, the spacecraft would fly through Alpha Centauri's binary star system within approximately a day.

To increase the scientific yield of such an interstellar mission, the feasibility to decelerate at Alpha Centauri is worth investigating, such that the spacecraft remains in the system. This problem of deceleration presents novel and cutting-edge research, with the objective to decelerate using the gravitational attraction and photonic pressure of the stars. Initial results were obtained by Heller and Hippke (2017), who assumed a graphene-based sail covered with a highly reflective coating. To decelerate at Alpha Centauri, they obtained travel times of 95 years and maximum arrival speeds of 4.6% of the speed of light [6]. By making better use of photogravitational assists, the travel times were reduced by Heller et al. (2017) to 75 years, which allows an injection speed in Alpha Centauri of 5.7% of the speed of light [7]. Another research group, the MIRA Collaboration, focused on the computation of artificial equilibrium points in Alpha Centauri for a solar balloon spacecraft, before investigating capture and transfer trajectories for a stellar-photon sailcraft in the elliptical restricted three-body problem [8, 9].

This research contributes to the investigation of the feasibility of interstellar travel to Alpha Centauri by designing time-optimal trajectories for various mission applications. Where previous work focused on arriving at Proxima Centauri, the prime objective of this work is to solve the optimal control problem of a photon sail being captured into a bound orbit around either Alpha Centauri A or Alpha Centauri B, where the orbit is located in the center of the habitable zone of the star. These trajectories are optimized using the intelligent spacecraft trajectory optimization tool InTrance, that utilizes neurocontroller evolution based on artificial intelligence, machine learning and evolutionary algorithms. Instead of traversing the star system within hours, capture into the system opens up new mission capabilities. Therefore, two follow-up mission applications are proposed, namely a transfer orbit from one star to the other and an orbit-raising maneuver about a star. This paper thus presents a time-optimized mission proposal that allows capture into Alpha Centauri with subsequent transfer and orbit-raising trajectories by applying two astrophysical effects - photon pressure and gravitational attraction - to maneuver through Alpha Centauri, without the need for on-board fuel.

The paper is structured as follows. After introducing the star system, the dynamical framework is described for a photon sail in the elliptical restricted three-body problem, discussing the force model for a sail subjected to two radiative forces. Thereafter, the mission applications are discussed, after which a mission scenario is proposed. Next, the optimal control problem with the associated solver for trajectory optimization is explained. This leads to the discussion of the obtained results followed by accompanying sensitivity analyses, before concluding this paper.

II. Alpha Centauri

Alpha Centauri has scientific importance and is highly ranked to be the first target in future interstellar exploration, because it allows a better understanding of our Sun, and knowledge on the evolution of our Solar System formation [9]. More intriguingly, by visiting Alpha Centauri, Earth-like exoplanets could be discovered, due to the similarity of two

Table 1 Radius, mass and luminosity of the stars in Alpha Centauri expressed in solar units.

Star	Radius $R_\odot$	Mass $M_\odot$	Luminosity $L_\odot$
Alpha Centauri A	1.2234[a]	1.1055[a]	1.519[b]
Alpha Centauri B	0.8632[a]	0.9373[a]	0.5002[b]
Alpha Centauri C	0.1542[a]	0.1221[a]	0.0015[c]

Notes: [a] = [10], [b] = [11], [c] = [12].

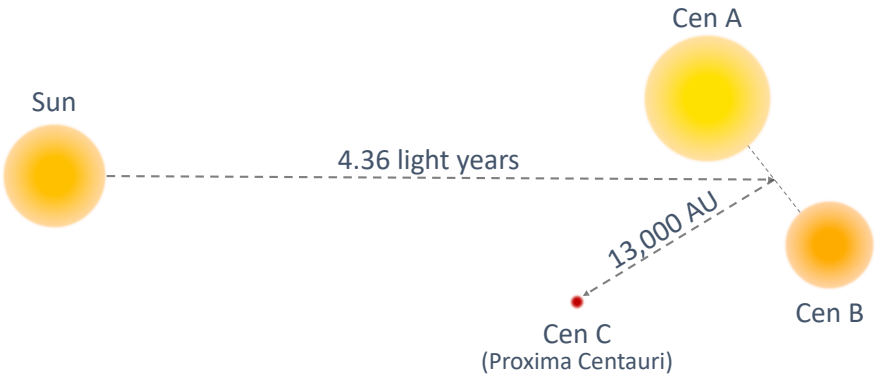

Fig. 1 Graphical view of Alpha Centauri (dimensions not to scale, size of stars to scale).

of the stars of Alpha Centauri with the Sun. This section continues with a discussion on the composition of the star system in Section II.A, accompanied by a comparison with our Solar System. Thereafter, the orbital elements of Alpha Centauri are investigated in Section II.B, in order to define the entry conditions for a sail traveling from Earth.

A. Composition of Alpha Centauri

At a distance of 4.36 light years or approximately 275,000 AU away from the Sun, Alpha Centauri is the closest star system to the Sun, making it an obvious target for future interstellar exploration missions [13]. Alpha Centauri is a triple star system, consisting of Alpha Centauri A, Alpha Centauri B - forming the binary star system Alpha Centauri AB - and Alpha Centauri C, the latter being positioned slightly closer at 4.22 light years away from the Sun [10]. A schematic view of Alpha Centauri is shown in Figure 1. The binary stars Alpha Centauri A and B - from now on referred to as Cen A and Cen B - are solar-like, with their high metallic content implying the existence of planets originating from a stellar disc [14]. While Cen A is larger and more luminous than the Sun, Cen B is smaller and cooler than our Sun. Alpha Centauri C - officially termed Proxima Centauri and from now on referred to as Cen C - is the smallest and faintest of the triple star system [10]. Proxima Centauri b - the prime target of the Breakthrough Starshot project - is an Earth-sized exoplanet discovered in 2016, orbiting in the habitable zone of Cen C [12]. This habitable zone ranges from 0.04 AU to 0.08 AU [15]. Table 1 shows the relation between the Alpha Centauri stars and the Sun in terms of radius, mass and luminosity.

Table 2 Equatorial coordinates of Alpha Centauri, J2000 [16].

Star	Right Ascension [h m s]	Declination [° ′ ″]
Alpha Centauri A	14 39 36.5	-60 50 02
Alpha Centauri B	14 39 35.1	-60 50 14
Alpha Centauri C	14 29 43.0	-62 40 46

Table 3 Orbital elements of Centauri B about Centauri A [18].

Parameter	Unit	Value
Semi-major axis a	[AU]	23.517
Eccentricity e	[-]	0.5208
Inclination i	[deg]	79.320
Longitude of ascending node Ω	[deg]	205.064
Argument of periapsis ω	[deg]	232.006
Orbital period T	[yr]	79.929
Epoch of periapsis T_0	[yr]	1955.604

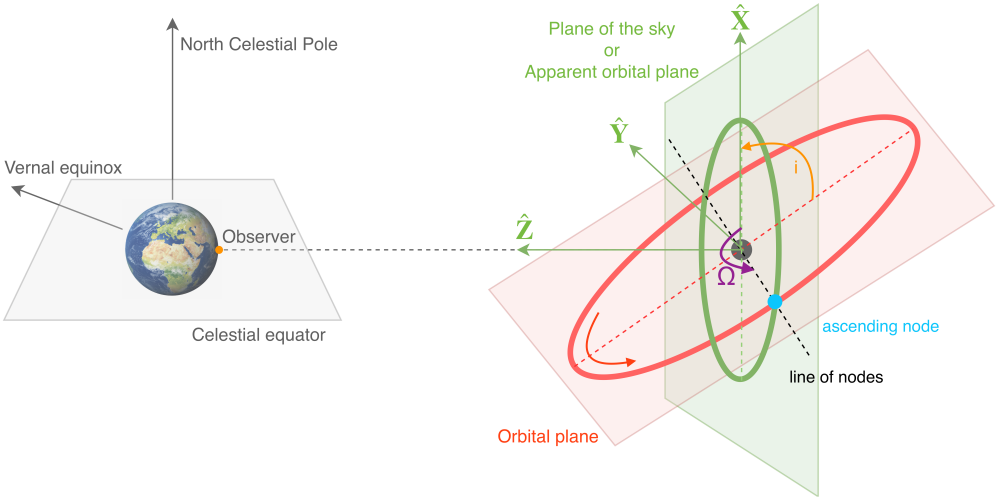

Fig. 2 Schematic view of a binary stars' orbital plane and apparent orbital plane (plane tangent to celestial sphere). Note: this figure serves as an arbitrary illustration and is not to scale.

B. Orbital Elements

Ptolemaios was the first to position Alpha Centauri on the celestial sphere in the 2nd century [17]. 19 centuries later, technology makes it possible to measure the relative position between Cen A and Cen B with a precision of 10 mas (milli arcsecond), which translates into an accuracy of 0.01 AU [18]. To specify the coordinates of the stars of Alpha Centauri, the equatorial coordinate system is used, a right-handed system with its origin at the center of the Earth, the celestial equator as the reference plane and the vernal equinox as the reference direction [19]. The equatorial coordinates of Alpha Centauri are presented in Table 2 and are obtained from the RECONS database [16].

1. Alpha Centauri A and B

Combining the orbital motion, the parallactic motion (the difference in a star's position against the background due to different orbital positions of Earth [20]), and the proper motion (the change in position of a star due to its motion relative to the Earth [20]) of Alpha Centauri's barycenter, the trajectory and corresponding orbital elements of Cen A and Cen B can be defined [18]. By astronomical convention, the orbital elements for a binary system are generally specified as the motion of the secondary star - Cen B - relative to the primary star - Cen A - as shown in Table 3. Both stars orbit their barycenter in elliptical orbits with an orbital period, T, of approximately 80 years and a periapsis of 11.3 AU, equivalent to the distance between Saturn and the Sun, and an apoapsis of 35.8 AU, equivalent to the distance between Neptune and the Sun. Note that these orbital elements define the apparent motion of Alpha Centauri as seen from Earth: the orbital trajectory is thus projected on the plane of the sky which is the plane tangent to the celestial sphere at the star's position, as shown in Figure 2. In this figure, the orbital plane of an arbitrary orbit is depicted in red, and the plane of the sky in green. Furthermore, the figure shows the observer frame $\mathcal{B}(\hat{\mathbf{X}}, \hat{\mathbf{Y}}, \hat{\mathbf{Z}})$ with the coordinates (X, Y, Z), where the $\hat{\mathbf{X}}$-axis points due north and is the perpendicular projection of the direction from the observer to the North Celestial Pole onto the plane of the sky [21]. The $\hat{\mathbf{Z}}$-direction is defined towards the observer and the $\hat{\mathbf{Y}}$-direction completes the right-handed reference frame. The longitude of the ascending node, Ω, is measured eastward starting from northern direction, as illustrated with the purple arrow in Figure 2. The ascending node in a binary star system is defined as "the node where the secondary star moves away from the observer with respect to the plane of the sky", as depicted with the blue dot in Figure 2 [22]. Furthermore, the inclination, i, is defined as "the angle from the orbital plane to the plane of the sky", depicted with the orange arrow in Figure 2 [21]. The projection of the true relative orbit of Cen B on the plane of the sky results in its apparent relative orbit as shown in Figure 3a, where the star's position at the indicated years are depicted with blue dots.

Instead of describing the motion of the companion star about the primary star, a barycentric view of the orbital motion of the binary system is more intuitive. Acknowledging Newton's first law in a binary star system, the stars are always on opposite sides of the barycenter, implying that the barycenter is found on the line connecting both stars - which is mathematically described in Eq. 1 - such that the distance between the stars is the sum of the distances of the stars with respect to the barycenter, see Eq. 2.

$$M_A \, \mathbf{r}_{bary,A} + M_B \, \mathbf{r}_{bary,B} = 0 \tag{1}$$

$$\left\| \mathbf{r}_{bary,A} - \mathbf{r}_{bary,B} \right\| = \|\mathbf{r}\| = r \tag{2}$$

In Eqs. 1 and 2, M is the stellar mass, $\mathbf{r}$ is the position vector, r is the distance between the stars, $\mathbf{r}_{bary}$ is the star's position vector with respect to the barycenter, $r_{bary} = \left\| \mathbf{r}_{bary} \right\|$, and the subscripts "$A$" and "$B$" refer to Cen A and

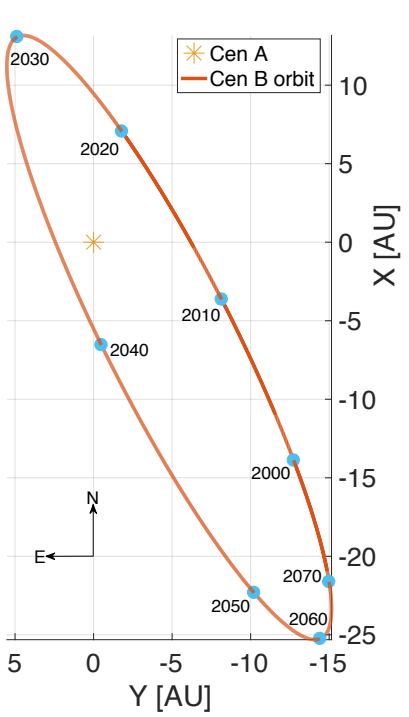

(a) Orbit of Cen B about Cen A as seen from Earth.

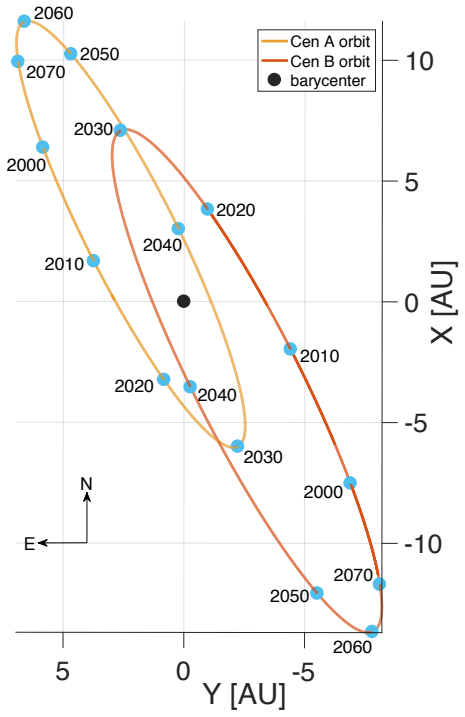

(b) Orbits of Cen A and Cen B about the barycenter as seen from Earth.

Fig. 3 Apparent orbital trajectories in the plane of the sky.

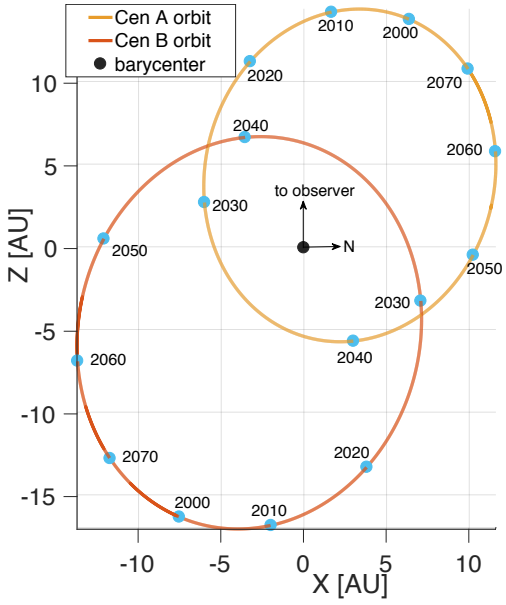

Fig. 4 Orbital trajectories of Cen A and Cen B about the barycenter in the XZ-plane.

Cen B, respectively, such that the distance of the star with respect to the barycenter is denoted by $r_{bary,A}$, as an example for Cen A. From Eq. 1, it follows that $M_A\,\mathbf{r}_{bary,A} = -M_B\,\mathbf{r}_{bary,B}$, which results in the following expression for the distances of the stars with respect to their barycenter [21]:

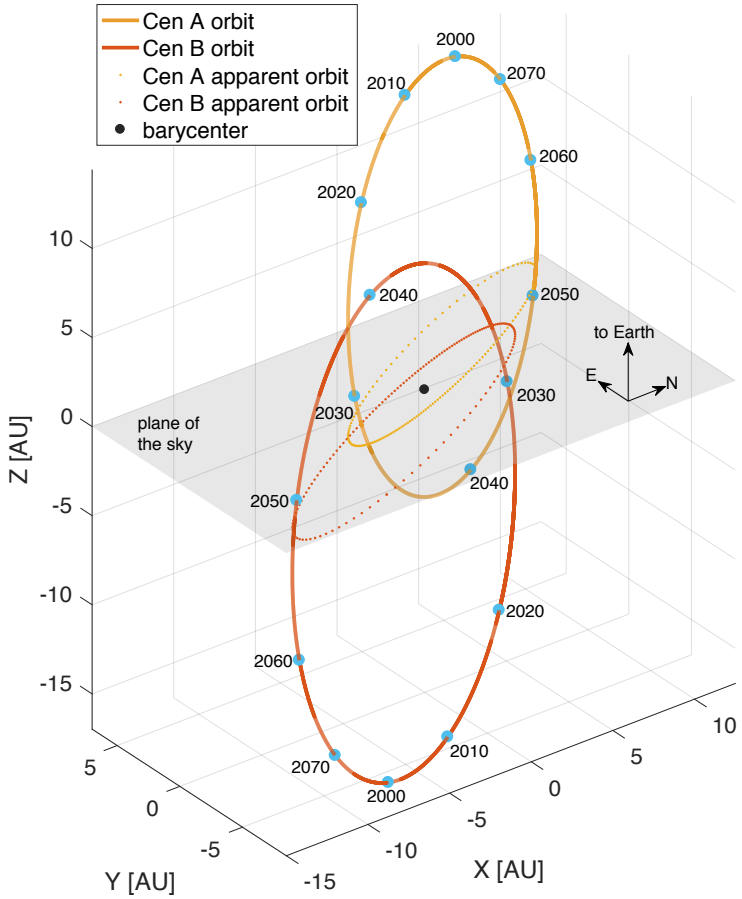

Fig. 5 Orbital trajectories of Cen A and Cen B about the barycenter, 3D-view with the projection of the orbits on the plane of the sky representing the apparent orbits as dots.

$$\mathbf{r}_{bary,A} = -\frac{M_B}{M_A + M_B}\mathbf{r} \quad \text{and} \quad \mathbf{r}_{bary,B} = \frac{M_A}{M_A + M_B}\mathbf{r} \tag{3}$$

In terms of Keplerian elements, the semi-major axes of the star's orbits about the barycenter, a_A and a_B, are scaled as described in Eq. 4, while the orbits have the same eccentricity due to conservation of momentum.

$$a_A = \frac{M_B}{M_A + M_B}a \quad \text{and} \quad a_B = \frac{M_A}{M_A + M_B}a \tag{4}$$

With a semi-major axis of 23.517 AU between Cen A and Cen B (see Table 3), Eq. 4 results in semi-major axes of 10.790 AU and 12.726 AU for Cen A and Cen B, respectively. Although the semi-major axes are not the same, both stars orbit the barycenter with the same orbital period. Because the binary stars orbit their barycenter in the same plane, both orbits have the same inclination, but the argument of periapsis differs by 180°. The absolute motion of the stars about the barycenter as seen from Earth is shown in Figure 3b. From the absolute motion of the stars as seen from the XZ-plane as shown in Figure 4, it is clear that a spacecraft coming from our Solar System passes Cen A's orbit first

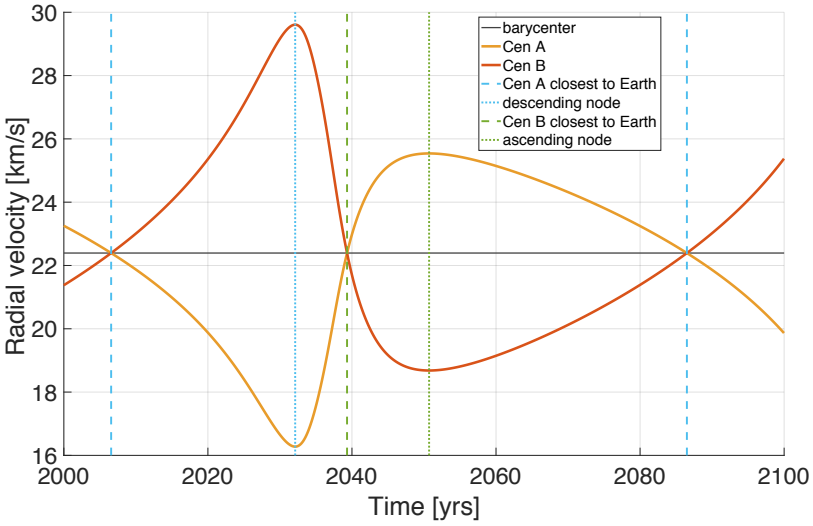

Fig. 6 Radial velocity of Cen A and Cen B, pointing out the epochs of ascending and descending node, and the epochs when Cen A and Cen B are closest to Earth.

before encountering Cen B's orbit. Finally, Figure 5 gives the configuration of Alpha Centauri in three dimensions, including the projection of Cen A's and Cen B's orbits on the plane of the sky.

As stated above, the orbital elements as listed in Table 3 consider the stars' movement with respect to the Earth against the background sky. This means that the positions of the stars change, although slowly. Examining the kinematics of the Alpha Centauri system, it will be closest to the Sun in approximately 28,000 years, after which it will slowly move away from our Solar System [23]. The proper motion of the barycenter of Cen A and Cen B is approximately 3619.9 mas per year towards the west and 693.8 mas per year towards the north, which translates into a proper motion of approximately 6.143 arcmin (minutes of arc) each century, or 1.0238° each millennium [18]. For the scope of this research, the proper motion of the stars is not taken into account, since it only changes very slowly over hundreds of years. Combining this proper motion with the parallax motion, the barycentric velocity can be determined, resulting in a velocity of 22.97 km/s in western direction and 4.40 km/s in northern direction. Finally, the average radial velocity - the projection of the velocity vector on the line of sight - can be found using spectroscopy to be 22.39 km/s in the direction of our Solar System [18]. The radial velocities, v_r, of Cen A and Cen B are calculated as:

$$v_r = v_{r,bary} + K(\cos(\omega + \theta) + e\cos\omega) \tag{5}$$

combined with either the scaling factor, K, for Cen A:

$$K_A = -\frac{M_B}{M_A + M_B}\frac{n\,a\sin i}{\sqrt{1-e^2}} \tag{6}$$

or the scaling factor for Cen B:

Table 4 Orbital elements of Alpha Centauri A and B about their barycenter, J2000.

Parameter	Unit	Centauri A	Centauri B
Semi-major axis a	[AU]	10.790	12.726
Eccentricity e	[-]	0.5208	0.5208
Inclination i	[deg]	0.0	0.0
Longitude of ascending node Ω	[deg]	0.0	0.0
Argument of periapsis ω	[deg]	180.0	0.0
Mean longitude l	[deg]	19.959	199.959

$$K_B = \frac{M_A}{M_A + M_B} \frac{n\, a \sin i}{\sqrt{1 - e^2}} \tag{7}$$

In Eqs 5 - 7, $v_{r,bary}$ is the barycenter's radial velocity, ω is the argument of periapsis, θ is the true anomaly, e is the eccentricity, $n = \frac{2\pi}{T}$ is the star's mean motion and a is Cen B's semi-major axis with respect to Cen A, see Table 3. Figure 6 shows the result of the expression in Eq. 5, together with the barycentric radial velocity (horizontal black line), the epoch when Cen A is closest to Earth in 2007 and 2086 (blue dashed line), the descending node - the node in the plane of the sky where Cen B moves towards the observer - in 2032 (blue dotted line), the epoch when Cen B is closest to Earth in 2039 (green dashed line), and the ascending node in 2051 (green dotted line). This means that Cen B is closer to Earth than Cen A in the time period from 2032 to 2051, 19 years within a period of almost 80 years. The epochs in Figure 6 correspond with the Alpha Centauri configuration as shown in Figure 4, while the radial velocities comply with what is found by Pourbaix et al. (2002) [24], and by Pourbaix and Boffin (2016) [25] as well as the radial velocities from the Ninth Catalog of Spectroscopic Binary Orbits[†] [26]. Note that these references defined the positive radial velocity away from Earth, while the positive radial velocity in this work is defined towards Earth.

In addition to describing the orbits of Cen A and Cen B with respect to the observer frame $\mathcal{B}(\hat{\mathbf{X}}, \hat{\mathbf{Y}}, \hat{\mathbf{Z}})$, it is also convenient to describe them with respect to the Barycentric Stellar Reference System (BSRS) $\mathcal{J}_1(\hat{\mathbf{x}}, \hat{\mathbf{y}}, \hat{\mathbf{z}})$ centered in the barycenter of Cen A and Cen B with the coordinates (x, y, z). In this frame, the $\hat{\mathbf{x}}$-axis coincides with the orbits' major axis, positive towards periapsis of Cen B, the $\hat{\mathbf{z}}$-axis points along the angular momentum vector and the $\hat{\mathbf{y}}$-axis completes the right-handed frame. The frame transformations used to go from frame $\mathcal{B}(\hat{\mathbf{X}}, \hat{\mathbf{Y}}, \hat{\mathbf{Z}})$ to $\mathcal{J}_1(\hat{\mathbf{x}}, \hat{\mathbf{y}}, \hat{\mathbf{z}})$ is discussed in the Appendix. The result of the transformation from the apparent plane to the orbital plane is shown in Figure 7, with the corresponding orbital elements listed in Table 4, from which it is clear that Cen A's orbit is smaller due to its larger mass. The frame as shown in Figure 7 is used in this work to optimize the trajectories in Alpha Centauri. In addition, the optimized trajectories can also be presented in a body-fixed reference frame: the Cen A-fixed reference frame or the Cen B-fixed reference frame, with the corresponding star as its center with the coordinates (x_A, y_A, z_A) and (x_B, y_B, z_B), respectively. The transformation from the inertial BSRS-frame to the body-fixed reference frame is simply

[†]See the ninth catalogue of spectroscopic binary orbits at `http://sb9.astro.ulb.ac.be`

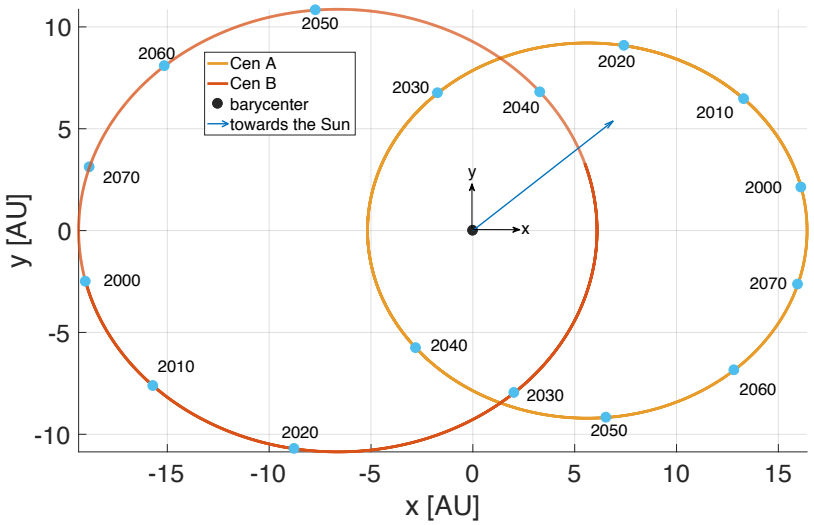

Fig. 7 Orbital trajectories of Cen A and Cen B about the barycenter in the xy-plane (orbital plane), with the blue arrow indicating the Sun's direction (inclined with 10.68° with respect to the orbital plane).

Table 5 Relevant orbital elements of Centauri C about the barycenter of the binary star system [10].

Parameter	Unit	Value
Semi-major axis a	[AU]	8,700
Eccentricity e	[-]	0.50
Orbital period T	[yr]	547,000
Epoch of periapsis T_0	[yr]	285,017

a translation from the barycenter of Cen A and Cen B to the star. Finally, to design capture trajectories, it is crucial to know from what direction the spacecraft enters the system. With the expression as presented in Eq. 31 in Appendix A, the unit vector from Alpha Centauri's barycenter to the Sun, $\hat{\mathbf{s}}$, can be calculated as $\hat{\mathbf{s}} = [0.774; 0.605; 0.185]$. The Sun's direction is also shown in Figure 7, which is inclined with 10.68° with respect to the orbital plane, i.e. the complementary angle of the inclination as listed in Table 3.

2. Alpha Centauri C

To conclude the orbital elements of Alpha Centauri, the relevant elements of the smallest star - Cen C - relative to the barycenter of Cen A and Cen B are listed in Table 5. Since the discovery of Cen C one century ago, there has been a debate on whether this distant star is actually part of a triple star system. Indeed, Cen C is far away from Cen A and Cen B, with a periapsis of 4,300 AU and an eccentricity of 0.5. Currently, Cen C is close to its apoapsis of 13,000 AU, equivalent to approximately 433 times Neptune's orbit about the Sun. However, current research is confident that Cen C is gravitationally bounded to the binary [10]. Nonetheless, from the perspective of mission analysis and the scope of this research, Cen C - with an orbital period of over half a million years - and its gravitational effect on the spacecraft will be neglected.

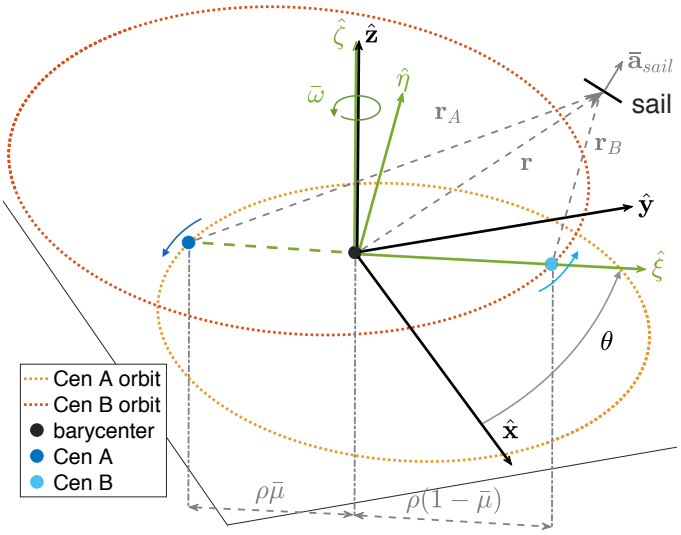

Fig. 8 Barycentric Stellar Reference System $\mathcal{J}_1(\hat{\mathbf{x}}, \hat{\mathbf{y}}, \hat{\mathbf{z}})$ and Barycentric Rotational Reference System $\mathcal{J}_2(\hat{\xi}, \hat{\eta}, \hat{\zeta})$ in Alpha Centauri's binary system.

III. Photon-Sail Dynamics

After discussing the target star system, the fundamental astrodynamical concepts for photon sailing in Alpha Centauri are discussed in this section. In this work, the motion of three objects are considered: the Alpha Centauri binary stars and a photon sailcraft. These three bodies are considered as point masses in the BSRS $\mathcal{J}_1(\hat{\mathbf{x}}, \hat{\mathbf{y}}, \hat{\mathbf{z}})$, see Figure 8. Contrary to the classical three-body problem, the motion of the sailcraft is not only dependent on the gravitational forces acting between the bodies, but also on the radiative force from both stars on the sailcraft. The motion of the sailcraft in Alpha Centauri is investigated in the framework of the elliptical restricted three-body problem and is discussed in Section III.A. Thereafter, the influence of the sail on the spacecraft's motion is examined in Section III.B.

A. Elliptical Restricted Three-Body Problem

The dynamics of a sailcraft in a three-body problem are often simplified to the restricted three-body problem (R3BP), because the mass of the sailcraft is much smaller than the two stars. Therefore, the assumption can be made that the gravitational attraction of the sailcraft on the two stars can be neglected. Due to the highly elliptical orbits of Cen A and Cen B, the R3BP cannot be simplified into the well-known circular restricted three-body problem (CR3BP) [27–29]. Instead, in this work, the elliptical restricted three-body problem (ER3BP) is used to describe the sailcraft's motion in the binary star system [8, 9, 30, 31]. In addition to the BSRS, Figure 8 also presents the rotational reference system employed in the ER3BP, the Barycentric Rotational Reference System (BRRS) $\mathcal{J}_2(\hat{\xi}, \hat{\eta}, \hat{\zeta})$. Its origin is the barycenter of Cen A and Cen B, the $\hat{\xi}$-axis connects the stars and is directed towards Cen B, while the $\hat{\zeta}$-axis is directed perpendicular to the orbital plane of the stars, hence coincident with the z-axis of the BSRS. The $\hat{\eta}$-axis completes the right-handed reference frame. Note that the BRRS rotates with a non-uniform angular velocity about the $\hat{\zeta}$-axis,

$\bar{\omega}$, due to the elliptical nature of the binary star system. As a result, it is more convenient to model the dynamics of the ER3BP in a rotating-pulsating reference frame - the Barycentric Pulsating Reference System (BPRS) $\mathcal{J}_3(\tilde{\xi}, \tilde{\eta}, \tilde{\zeta})$. The rotating-pulsating coordinates $(\tilde{\xi}, \tilde{\eta}, \tilde{\zeta})$ are related to the rotating coordinates (ξ, η, ζ) through the equations $\xi = \rho\tilde{\xi}$, $\eta = \rho\tilde{\eta}$ and $\zeta = \rho\tilde{\zeta}$, with the semi-latus rectum $\rho = \frac{1-e^2}{1+e\cos\theta}$ [31]. In addition, a new set of normalized units are introduced: the sum of the stars' masses as the unit of mass. Introducing the mass ratio $\bar{\mu} = \frac{M_B}{M_A+M_B} = 0.4588$, the dimensionless masses of Cen A and Cen B can then be denoted by $1-\bar{\mu}$ and $\bar{\mu}$, respectively. The distance between the stars is selected as the unit of length and $1/\bar{\omega}$ as the unit of time, resulting in $\bar{\omega} = 1$, such that one orbital period of the binary system is represented by 2π radians [31]. Furthermore, the position of the sail with respect to Cen A and Cen B in rotating-pulsating coordinates $\tilde{\xi}, \tilde{\eta}, \tilde{\zeta}$ can be expressed as:

$$\tilde{\mathbf{r}}_A = \left[(\tilde{\xi} + \rho\bar{\mu}),\ \tilde{\eta},\ \tilde{\zeta}\right]^T \quad \text{and} \quad \tilde{\mathbf{r}}_B = \left[(\tilde{\xi} + \rho\bar{\mu} - \rho),\ \tilde{\eta},\ \tilde{\zeta}\right]^T \tag{8}$$

In the BPRS, the motion of the sailcraft in Alpha Centauri can be expressed as described in Eq. 9, with U as expressed in Eq. 10 and where the differentiation is with respect to the true anomaly θ [31]. The eccentricity e is 0.5208 (see Table 3). Note that when $e = 0$, Eq. 9 reduces to the description of the dynamics in the CR3BP.

$$\ddot{\mathbf{r}} + 2\bar{\boldsymbol{\omega}} \times \dot{\mathbf{r}} + \tilde{\zeta}\bar{\boldsymbol{\omega}} = \frac{1}{1 + e\cos\theta}(\nabla U + \mathbf{a}_{sail}) \tag{9}$$

$$U = \frac{1}{2}(\tilde{\xi}^2 + \tilde{\eta}^2 + \tilde{\zeta}^2) + \frac{1-\bar{\mu}}{\|\mathbf{r}_A\|} + \frac{\bar{\mu}}{\|\mathbf{r}_B\|} \tag{10}$$

In Eq. 9, the first two terms on the left hand side are the kinematic and coriolis accelerations, respectively, while the right hand side consists of the effective potential - a combination of the centripetal acceleration and the gravitational potential - and the sail's acceleration vector, $\mathbf{a}_{sail}$ [5]. The latter is the only term that is still to be defined and is discussed in Section III.B.

B. Sail Model

Multiple models exist to represent the force of the stellar radiation pressure (SRP) that acts on the sail, based on different assumptions for the sail's optical characteristics. The most simplified model assumes a perfectly reflecting flat sail with a uniformly radiating star. That model is called the ideal sail model and is applied in this work, where it must be realized that such a model is only suitable for a preliminary mission feasibility analysis.

1. Ideal Sail

The calculation for the SRP-force acting on the sail is based on a two-momentum-transfer between stellar photons and the sail and is illustrated in Figure 9a. The figure shows that the total SRP-force, $\mathbf{F}_{SRP}$, is a combination of the force

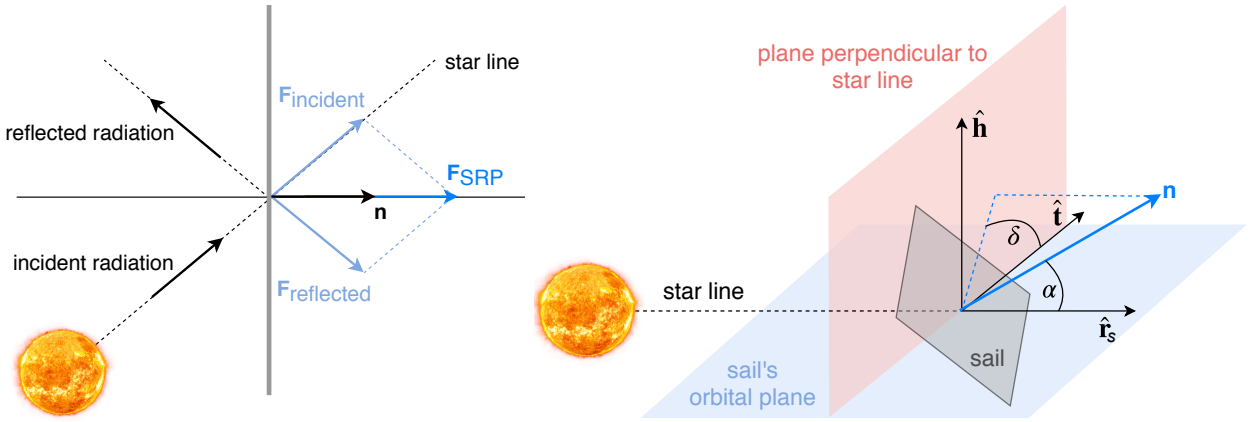

(a) Ideal sail model: incident and reflected radiation combined into SRP-force $\mathbf{F}_{SRP}$.

(b) Sail normal vector n with the clock angle δ and cone angle α.

Fig. 9 Definition of the ideal sail model and the sail normal vector.

from the incident SRP, $\mathbf{F}_{incident}$, and the force from the reflected radiation, $\mathbf{F}_{reflected}$. From geometry, the following expression can be found for the SRP-force:

$$\mathbf{F}_{SRP} = 2PA\cos^2\alpha\,\mathbf{n} \tag{11}$$

This expression in Eq. 11 is dependent on the stellar radiation pressure, P, and the sail's area, A.

2. Sail Orientation

The SRP-force acting on the sail can be expressed by introducing the sail normal vector $\mathbf{n}$. This vector is perpendicular to the sail's surface. As a result of the two-momentum-transfer and the assumption of the ideal sail, the SRP-force is aligned with the sail's normal vector $\mathbf{n}$. The clock angle, δ, and the cone angle, α, define the sail's attitude as shown in Figure 9b in the orthonormal reference frame $\mathcal{O}(\hat{\mathbf{r}}_s, \hat{\mathbf{t}}, \hat{\mathbf{h}})$. This frame has its origin at the sail, with $\hat{\mathbf{r}}_s$ directed along the star-sail-line, with $\hat{\mathbf{h}}$ normal to the sail's orbital plane directed to the orbital angular momentum vector, and with $\hat{\mathbf{t}}$ completing the right-handed reference frame [32]. The clock angle is defined as the angle between the projection of the sail normal vector $\mathbf{n}$ on the plane perpendicular to the star line and the tangential unit vector $\hat{\mathbf{t}}$ [32]. The cone angle is defined as the angle between the sail normal and the star line: $\alpha = \arccos(\mathbf{n}\cdot\hat{\mathbf{r}}_s)$. Using the definitions for the cone and clock angle, the sail normal vector can be resolved along the $\mathcal{O}(\hat{\mathbf{r}}_s, \hat{\mathbf{t}}, \hat{\mathbf{h}})$-frame:

$$\mathbf{n} = \cos\alpha\,\hat{\mathbf{r}}_s + \cos\delta\sin\alpha\,\hat{\mathbf{t}} + \sin\delta\sin\alpha\,\hat{\mathbf{h}} \tag{12}$$

In the BPRS, the explicit components of the sail normal vector, $\mathbf{n} = (n_{\tilde{\xi}}, n_{\tilde{\eta}}, n_{\tilde{\zeta}})$, are given by:

Table 6 Lightness number relation for Cen A and Cen B for a sail with $\beta = 1$ in our Solar System.

Lightness number	Sun	Cen A	Cen B
β	1.0	1.374	0.534

$$
\begin{aligned}
n_{\tilde{\xi}} &= \frac{\tilde{\xi} - \rho\bar{\mu}}{\tilde{r}_A}\cos\alpha - \frac{(\tilde{\xi} - \rho\bar{\mu})\tilde{\zeta}}{\tilde{r}_2\tilde{r}_A}\sin\alpha\sin\delta + \frac{\tilde{\eta}}{\tilde{r}_2}\sin\alpha\cos\delta \\
n_{\tilde{\eta}} &= \frac{\tilde{\eta}}{\tilde{r}_A}\cos\alpha - \frac{\tilde{\eta}\tilde{\zeta}}{\tilde{r}_2\tilde{r}_A}\sin\alpha\sin\delta - \frac{\tilde{\xi} - \rho\bar{\mu}}{\tilde{r}_2}\sin\alpha\cos\delta \\
n_{\tilde{\zeta}} &= \frac{\tilde{\zeta}}{\tilde{r}_A}\cos\alpha + \frac{\tilde{r}_2}{\tilde{r}_A}\sin\alpha\sin\delta
\end{aligned}
\tag{13}
$$

where $\tilde{r}_A = \sqrt{(\tilde{\xi} + \rho\bar{\mu})^2 + \tilde{\eta}^2 + \tilde{\zeta}^2}$ is the Cen A-sail distance and $\tilde{r}_2 = \sqrt{(\tilde{\xi} - \rho\bar{\mu})^2 + \tilde{\eta}^2}$ [27]. Note that the sail normal vector is always directed away from the star: $\mathbf{n}\cdot\hat{\mathbf{r}}_s \geq 0$, while for an ideal sail model, the sail normal vector is coincident with the thrust unit vector, which simplifies the analysis of the sail's steering problem [32].

3. Sail Lightness Number

A variation to the expression for the SRP-force as shown in Eq. 11 can be found by introducing the lightness number β, a sail performance parameter defined as the ratio of the SRP-acceleration to the gravitational acceleration, as shown in Eq. 14 [5].

$$\beta = \frac{a_c}{a_0} \tag{14}$$

In Eq. 14, a_c is the characteristic acceleration, the SRP-acceleration when the sail is at a distance of one AU facing the star, while $a_0 = \frac{\mu}{r_0^2}$, with μ representing the star's gravitational parameter and r_0 representing a distance of one AU [5]. Using Eqs. 11 and 14, the SRP-acceleration vector, $\mathbf{a}_{SRP}$, can be expressed as:

$$\mathbf{a}_{SRP} = \beta\frac{\mu}{r^2}\cos^2\alpha\,\mathbf{n} \tag{15}$$

4. Dynamical System for Sailcraft Configurations in a Binary Star System

When considering a sail in Alpha Centauri's binary system, the SRP-acceleration is a combination of Cen A's SRP-acceleration and Cen B's SRP-acceleration, resulting in an adapted force model with respect to the acceleration model as shown in Eq. 15, as the latter expression represents the SRP-acceleration on the sail produced by the light from a single star. Also, new conventions are introduced. First of all, in this work, the attitude of the sail - defined through the cone and clock angle - is described with respect to Cen A. Furthermore, Cen A and Cen B have different characteristics than the Sun, such that the lightness number changes accordingly. To maintain the lightness number as a convenient

performance parameter as presented in Eq. 15, the lightness number is also defined with respect to Cen A and a new dimensionless parameter, ϵ, is introduced such that $\epsilon\beta$ represents the sail lightness number with respect to Cen B [8]. This parameter ϵ is a physical property based on the masses and luminosities of the binary stars and can be computed as:

$$\epsilon = \frac{L_B M_A}{L_A M_B} \approx 0.3884 \tag{16}$$

where L is the star's luminosity, see Table 1. Table 6 shows the relation for the lightness number with respect to the Sun, Cen A and Cen B. In Table 6, a lightness number of one with respect to the Sun is used. It is clear that a sail about Cen A has a substantially better performance, since Cen A is considerably more luminous, see Table 1. While the sail in our Solar System would match the Sun's gravitational acceleration, the SRP-acceleration of the sail with respect to Cen A is considerably larger than the gravitational acceleration. Relative to Cen B, the same sail is not capable to counter the gravitational acceleration, on account of the substantially smaller luminosity.

When evaluating a sail under influence of SRP of two stars, the SRP-accelerations from both stars have to be considered, as illustrated in Figure 10a. Thus, the sail's total SRP-acceleration becomes:

$$\mathbf{a}_{sail} = \mathbf{a}_A + \mathbf{a}_B \tag{17}$$

with $\mathbf{a}_A$ and $\mathbf{a}_B$ Cen A's and Cen B's SRP-accelerations acting on the sail, respectively. Note that in this work, the effects of special relativity are neglected, which was found to be a realistic assumption for velocities <10% of the speed of light, c, [6]. Likewise, other physical aspects such as the Doppler blueshift or redshift are not considered.

Furthermore, there is the ability to consider various sail configurations, as discussed hereafter.

One-sided Reflective Sail

The one-sided reflective sail, illustrated in Figure 10b, is the most conventional sail configuration and complies with current sail technology. This sail configuration consists of a reflective coating on one side of the sail, while the other side is covered with a high-emissivity coating that is used for passive thermal control by re-radiation [5]. While such a sail performs well in our Solar System, this configuration imposes a constraint on the sail's trajectory in a binary star system. The emissive side cannot be exposed to incident photons, which is highlighted with the red cross in Figure 10b. Thus, the sail should be oriented such that the sail's reflecting side is facing both Cen A and Cen B at any time, see Figure 10a.

Considering the ER3BP as discussed in Section III.A, the acceleration for a one-sided reflective sail can be expressed as shown in Eq. 18, with the constraint on the sail's attitude shown in Eq. 19.

$$\mathbf{a}_{sail} = \beta \frac{1-\bar{\mu}}{r_A^2} (\hat{\mathbf{r}}_A \cdot \hat{\mathbf{n}})^2 \, \hat{\mathbf{n}} + \epsilon\beta \frac{\bar{\mu}}{r_B^2} (\hat{\mathbf{r}}_B \cdot \hat{\mathbf{n}})^2 \, \hat{\mathbf{n}} \tag{18}$$

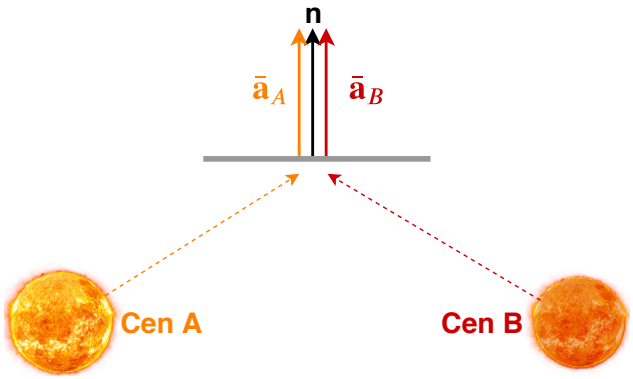

(a) the scenario of additive SRP-acceleration components.

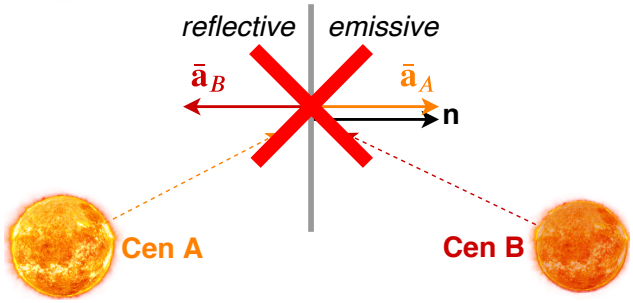

(b) One-sided reflective sail.

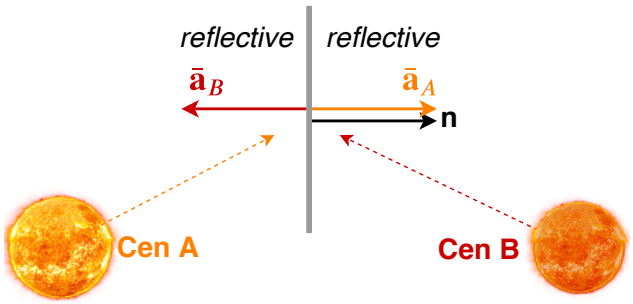

(c) Two-sided reflective sail.

Fig. 10 Overview of the sail configurations.

$$\hat{\mathbf{r}}_A \cdot \hat{\mathbf{n}} \geq 0 \quad \text{and} \quad \hat{\mathbf{r}}_B \cdot \hat{\mathbf{n}} \geq 0 \tag{19}$$

In Eq. 18, the notation $\hat{\square}$ refers to the unit vector and $\hat{\mathbf{r}}_A \cdot \mathbf{n} = \cos^2 \alpha$, as was adopted in Eqs. 11 and 15.

Two-sided Reflective Sail

Where the one-sided reflective sail has one side functioning as a thermal controller, the two-sided reflective sail has a reflective coating on both sides of the sail. Although this technology is not available yet, this work assumes that this technology will become available in the near-future. This sail configuration asks for an adapted expression for the sail's acceleration, since photons are allowed to collide with both sides of the sail. Thus, the separate acceleration components

of Cen A's SRP-acceleration and Cen B's SRP-acceleration can be pointing in the same or the opposite direction, see Figures 10a and 10c.

The sail's acceleration for the two-sided reflective sail in the ER3BP is expressed in Eq. 20, where the new variable u is introduced and expressed in Eq. 21.

$$\mathbf{a}_{sail} = \beta \frac{1-\bar{\mu}}{r_A^2} (\hat{\mathbf{r}}_A \cdot \hat{\mathbf{n}})^2 \, \hat{\mathbf{n}} + u \, \epsilon \, \beta \frac{\bar{\mu}}{r_B^2} (\hat{\mathbf{r}}_B \cdot \hat{\mathbf{n}})^2 \, \hat{\mathbf{n}} \tag{20}$$

$$u = \begin{cases} 1 & \text{if } \hat{\mathbf{r}}_B \cdot \hat{\mathbf{n}} \geq 0 \\ -1 & \text{otherwise} \end{cases} \tag{21}$$

Since the sail's normal vector is defined with respect to Cen A, the normal vector may never point towards Cen A, recalling the constraint: $\hat{\mathbf{r}}_A \cdot \mathbf{n} \geq 0$. u indicates whether Cen B's SRP-acceleration component acting on the sail is aligned with this normal vector (u = 1) or not (u = -1), see respectively Figures 10a and 10c. Thus, the one-sided reflective sail is obtained when $u = 1$. Note that the separate acceleration component $\mathbf{a}_B$ cannot point towards Cen B: $\hat{\mathbf{a}}_B \cdot \hat{\mathbf{r}}_B \geq 0$.

IV. Mission Analysis

With the dynamical system defined in Section III, this section explores possible targets in Alpha Centauri in Section IV.A. From this knowledge, the mission baseline and scenario are defined in Section IV.B.

A. Target Destinations in Alpha Centauri

While the inaugural mission to Alpha Centauri is presumably a flyby mission, there are various other targets that can be considered that add to the complexity of the mission by including a capture phase. Such missions are explored hereafter.

1. Orbits about the Stars

A first possible target is an orbit about one of the binary stars. From a science and mission analysis point of view, interesting targets about the stars might exist in their habitable zones. The habitable zone of Cen A is found to be between 1.171 AU and 2.063 AU, whereas for Cen B the habitable zone is between 0.693 AU and 1.241 AU [15].

2. Artificial Equilibrium Points

The ER3BP - discussed in Section III.A - facilitates interesting targets for promising missions to observe the binary star system, especially when complimented with photon sail acceleration. Artificial equilibrium points (AEPs) are such destinations that make observational missions appealing, since the continuous propulsive acceleration of the sail

enables the displacement of the positions of the classical Lagrange points [8]. While AEPs enabled by sails have been investigated extensively for in the dynamics of our own Solar System ([27, 33, 34]), AEPs in a system with two radiative stars have been investigated to a much lesser extent [8, 30].

In the rotating-pulsating ER3BP, it is possible to show the existence of AEPs in the orbital plane of the two stars. Considering the plane of the system, $\tilde{\zeta} = 0$, equilibrium points exist for the condition that both the velocity and acceleration are zero, resulting in the sail remaining stationary within the three-body system: $\dot{\mathbf{r}} = 0$ and $\ddot{\mathbf{r}} = 0$ [5]. Substituting this equilibrium condition in Eq. 9 results in the expression as shown in Eq. 22 that needs to be satisfied in order to find equilibrium solutions.

$$\nabla U + \mathbf{a}_{sail} = 0 \tag{22}$$

Taking the vector product of the sail's normal vector $\mathbf{n}$ with Eq. 22 results in Eq. 23, realizing that the sail's acceleration vector $\mathbf{a}_{sail}$ is oriented in the direction of the sail's normal vector [5].

$$\nabla U \times \mathbf{n} = 0 \Rightarrow \mathbf{n} = \frac{\nabla U}{|\nabla U|} \tag{23}$$

Equation 23 states that an equilibrium solution is found when the sail's normal vector is always directed opposite to the effective potential, which is the sum of the gravitational accelerations from the stars and the centripetal acceleration acting on the sail [31]. In Eq. 24, the required lightness number to ensure equilibrium for a two-sided reflective sail is given by making use of the expression for the two-sided reflective sail's acceleration as described in Eq. 20. Note that, for a one-sided reflective sail, u in Eq. 20 should be one at all times.

$$\beta = \frac{\nabla U}{\frac{1-\bar{\mu}}{r_A^2}(\hat{\mathbf{r}}_A \cdot \mathbf{n})^2 \mathbf{n} + u\epsilon\frac{\bar{\mu}}{r_B^2}(\hat{\mathbf{r}}_B \cdot \mathbf{n})^2 \mathbf{n}} \tag{24}$$

Although the expressions in Eqs. 22 and 23 are the same for both the circular and elliptical R3BP, there are two substantial differences between the elliptical and circular case, due to the ellipiticity in the former case. Firstly, in the CR3BP, the equilibrium solutions are invariant, while in the ER3BP, the location of the equilibrium points change, depending on the position of the stars and thus their true anomaly [33]. Secondly, contrary to the CR3BP, the ER3BP does not exhibit out-of-plane equilibrium points [33]. Imposing the equilibrium conditions $\dot{\mathbf{r}} = 0$ and $\ddot{\mathbf{r}} = 0$ in Eq. 9 for the three-dimensional case, $\tilde{\zeta} \neq 0$, the remaining term $\tilde{\zeta}\bar{\omega}$ prevents finding three-dimensional equilibrium solutions. However, Baoyin and McInnes (2006) have proposed to use active control to perform a mission at an out-of-plane AEP, which then offers various mission capabilities. Also, a periodic Halo orbit near a planar AEP would contribute to a mission by enabling non-planar observations, giving a better overview of the system's configuration of planets and other celestial objects.

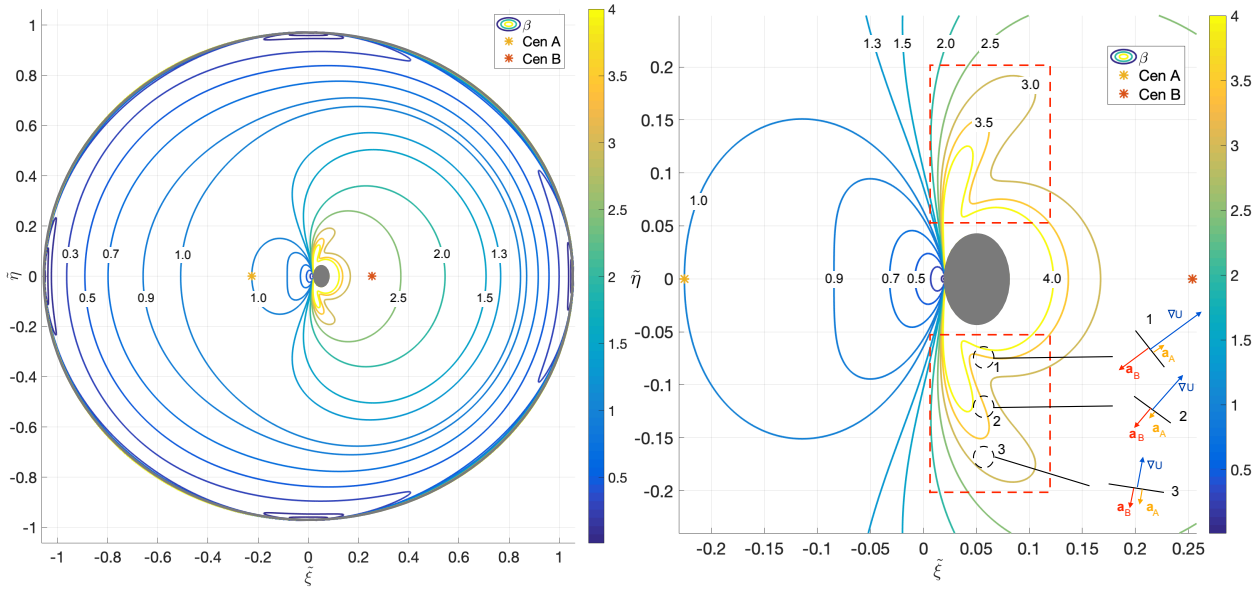

(a) Full configuration space. **(b) Detailed view.**

Fig. 11 Lightness number contour plot for two-sided reflective sail, $\theta = 0°$.

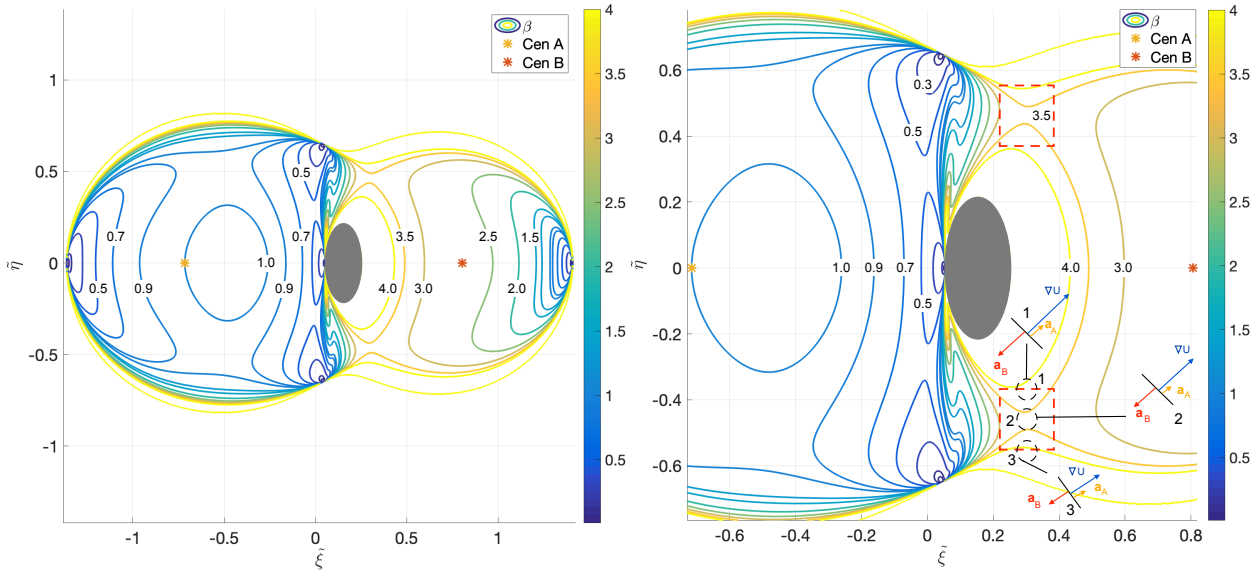

(a) Full configuration space. **(b) Detailed view.**

Fig. 12 Lightness number contour plot for two-sided reflective sail, $\theta = 180°$.

Figures 11 and 12 show contour plots of the lightness number required to achieve equilibrium for the two-sided reflective sail: Figure 11 illustrates the case when the binary star system is at its periapsis, $\theta = 0°$, while Figure 12 shows the case when Cen A and Cen B are at apoapsis, $\theta = 180°$. In each of these figures, the grey areas indicate forbidden areas, where the sail's SRP-acceleration is pointing in the same direction as the effective potential such that the required lightness number would have to be negative to be able to counteract the acceleration component of the effective potential,

which is unattainable. When the true anomaly increases, the distance between the stars increases, which substantially stretches the equilibrium curves due to the large eccentricity. Furthermore, there are two areas of interest where these equilibrium curves differ notably from the equilibrium curves for a single radiating body [5]. The first one - referred to as lobes - is highlighted with the red dotted lines in Figure 11b. Within the red dotted area of Figure 11b, three sails are depicted (1 to 3), showing a representation of the sail's orientation with the accelerations of the SRP of the stars and the effective potential. When examining the lobes in the $\tilde{\eta}$-direction (for a constant $\tilde{\xi}$-coordinate), an increase in lightness number can be noticed, which can be explained by a decrease in total sail acceleration before the separate sail accelerations from Cen A and Cen B align in the same direction (from 1 to 2 in Figure 11b). When opting for an AEP that is close to the $\tilde{\xi}$-axis, the separate sail accelerations oppose each other (sail 1 in Figure 11b). Moving away from the $\tilde{\xi}$-axis, at some point the separate accelerations align in the same direction (sail 2 and 3 in Figure 11b). However, before these accelerations point in the same direction, the total acceleration is small, resulting in the need for a larger lightness number, which causes the lobe-pattern (from sail 1 to 2 in Figure 11b). The second area of interest is highlighted with red dotted lines in Figure 12b with three sails depicted to represent the sail's orientation with the accelerations of the SRP of the stars and the effective potential. In these areas where the lightness number is locally minimal for a constant $\tilde{\xi}$-coordinate, saddle points are noticeable. This can be explained by the fact that the difference between the effective potential component and the sail acceleration is minimal at the saddle point due to a decrease in the SRP-acceleration from Cen A. Based on the direction of the effective potential and thus the orientation of the sail, the required lightness number to create an equilibrium point changes. At the saddle points, the orientation of the sail is such that the separate sail acceleration components from Cen A and Cen B are optimally combined such that the required lightness number reaches a minimum. This means that the SRP-acceleration from Cen A is minimal at the saddle point. This results in a decrease in the required lightness number away from the stars due to an increasingly better sail orientation (sail 1 to 2 in Figure 12b), until the saddle point (sail 2 in Figure 12b), after which the sail acceleration decreases more than the component of the effective potential as the SRP-acceleration from Cen A increases (sail 3 in Figure 12b). Hence, after the saddle point (sail 3 Figure 12b), the sail reaches a less optimal orientation, resulting in an increase in lightness number.

Finally, Figure 13 displays the system at periapsis, but now for the one-sided reflective sail. The results for the one-sided reflective sail only differ from those for the two-sided reflective sail (see Figure 11) in the area in between Cen A and Cen B. Since the sail cannot be subjected to photon impacts on both sides, the forbidden area for the one-sided reflective sail increases.

B. Mission Scenario

To allow a full, thorough and long-duration exploration of the Alpha Centauri system, the following mission scenario is proposed, see Figure 14. What makes this mission most different from the Breakthrough Starshot mission, is that this

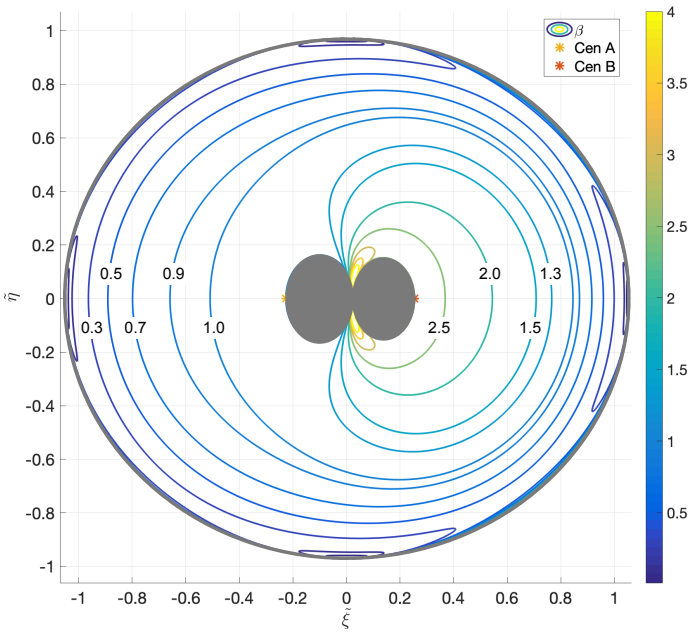

Fig. 13 Full configuration space of lightness number contour plot for one-sided reflective sail, $\theta = 0°$.

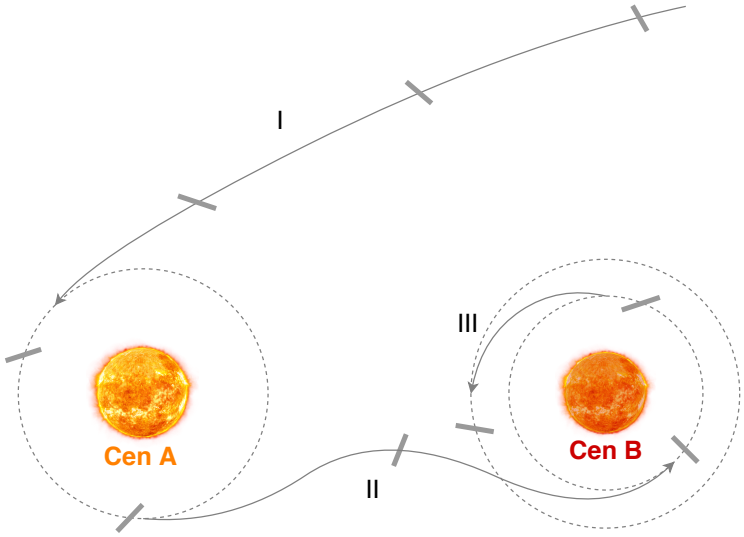

Fig. 14 Graphical view of the mission scenario. Phase I: capture, phase II: transfer trajectory, III: orbit raising.

proposal uses the photonic sail to get captured into an orbit about one of the stars, which is designated as phase I in Figure 14. The desired capture orbit is decided to be in the center of the habitable zone of either of the stars. This means that the target orbit is a circular orbit at 1.617 AU from Cen A, while the capture orbit about Cen B is 0.967 AU. When orbiting one of the stars, close observations of the star and its habitable zone can be made. The second phase of the mission is to transfer to the other star, allowing observations of both stars and their habitable zones within a single mission, see phase II in Figure 14. The target of this transfer trajectory is again a circular orbit in the center of the

Table 7 Orbital elements of the initial condition for an orbit about Cen A or Cen B.

Parameter	Unit	Cen A	Cen B
Semi-major axis a	[AU]	1.617	0.967
Eccentricity e	[-]	0.0	0.0
Inclination i	[deg]	0.0	0.0
Longitude of ascending node Ω	[deg]	0.0	0.0
Argument of periapsis ω	[deg]	0.0	0.0
Mean longitude l	[deg]	free	free

habitable zone. After arriving at the second star, a third and final phase of the mission can be performed, which is to raise the orbit to the outer edge of the habitable zone, see phase III in Figure 14.

V. Trajectory Optimization

With the mission scenario decided upon, the optimal control problem to be solved and the tool used to solve the problem are described in this section. Since photon-sail trajectory optimization in Alpha Centauri is a challenging and novel mission scenario, it requires an innovative trajectory design tool. Therefore, the optimization problem is solved using InTrance, a low-thrust optimization software that is modified in this work for trajectory optimization in Alpha Centauri. First, the optimal control problem is defined in Section V.A, after which the optimal control solver is discussed in Section V.B.

A. Optimal Control Problem

At a specific point in time, t, the state of a spacecraft, $\mathbf{x}_{SC}(t)$, is described by its position, $\mathbf{r}_{SC}(t)$, and velocity, $\dot{\mathbf{r}}_{SC}(t)$, in the BSRS. For low-thrust trajectory optimization using a photon sail, the optimal control problem is to find the optimal sail control vector history that changes the state of the spacecraft, $\mathbf{x}_{SC}(t) = (\mathbf{r}_{SC}(t), \dot{\mathbf{r}}_{SC}(t))$, from its initial state at the start of the trajectory t_b, $\mathbf{x}_{SC}(t_b)$, to its desired target state at the final time of the trajectory t_f, $\mathbf{x}_{SC}(t_f)$, using the control vector $\mathbf{u} = [\alpha\, \delta]^T$ in an optimal way along a trajectory that satisfies the dynamic constraint $\dot{\mathbf{x}}_{SC}(t) = (\dot{\mathbf{r}}_{SC}(t), \ddot{\mathbf{r}}_{SC}(t))$ - which is a function of $\mathbf{x}_{SC}(t)$ and $\mathbf{u}(t)$ with the spacecraft's acceleration $\ddot{\mathbf{r}}_{SC}(t)$ - and terminal constraint at the target, T, $\mathbf{r}_{SC}(t_f) = \mathbf{r}_T(t)$, while minimizing the cost function, J [32, 35]. The objective of this optimization problem is to minimize the transfer time, which is formulated as:

$$J = t_f - t_b \tag{25}$$

Note that $\mathbf{u}$ is bounded to: $0° \leq \alpha \leq 90°$ and $-180° \leq \delta \leq 180°$, while this work assumes that the sail attitude can be changed instantaneously. Apart from these path constraints, a constraint on the minimum distance to both stars is enforced which is elaborated on in Section VI.A. Furthermore, the initial condition for the last two phases of the mission

is a planar circular orbit at the center of the habitable zone of one of the stars, as shown in orbital elements in Table 7, which shows that the mean longitude, l, is the only orbital elements that can be changed by the user. Note that the initial conditions as shown in Table 7 are applied regardless of the outcome of the previous phase of the mission. Additionally, for the star transfer, boundary constraints on the final distance and relative velocity with respect to the target are defined as:

$$r_{SC}(t_f) \leq \begin{cases} 1.617\,\text{AU} & \text{from Cen A} \\ 0.967\,\text{AU} & \text{from Cen B} \end{cases} \quad \text{and} \quad \dot{r}_{SC}(t_f) \leq 100\,\text{m/s from } \dot{r}_A \text{ or } \dot{r}_B \tag{26}$$

with $\dot{r}_A$ and $\dot{r}_B$ the velocity of Cen A and Cen B, respectively. Similarly, the boundary constraints for the phase of orbit raising are defined as:

$$r_{SC}(t_f) \leq 0.01\,\text{AU away from } r_T \quad \text{and} \quad \dot{r}_{SC}(t_f) \leq 100\,\text{m/s from } \dot{r}_T \tag{27}$$

where r_T is the distance of the target orbit from the star: 2.063 AU or 1.241 AU for a target orbit about Cen A or Cen B, respectively, and $\dot{r}_T$ is the velocity at the target orbit. Finally, in case of the one-sided reflective sail, the constraints in Eq. 19 are enforced.

While the objective function in Eq. 25 is suitable for the last two phases of the mission, star transfer and orbit raising, a modified objective function is used for the capture phase of the trajectory into a circular orbit about a star. First of all, it must be noted that the capture problem was approached as a reversed-time escape problem to more easily satisfy the boundary constraint of capture into a circular orbit at the center of the habitable zone of one of the stars. By considering it as a reversed-time escape problem, starting from the targeted orbit, this constraint is automatically satisfied. To reverse the problem in time, the angular momentum of the bodies is inverted. By propagating the escape problem backwards in time, the same control vector history and trajectory is found as the forwards-in-time-propagation of the capture problem.

The minimization of the transfer time then still applies. However, to reduce the computation time, the optimal control problem for escape is not to find the optimal trajectory from an orbit around one of the stars to the sphere of influence of the Alpha Centauri system. Instead, the trajectory is truncated at the point along the trajectory where both the gravitational attraction and the SRP-acceleration of Cen A and Cen B are negligible. An example of the decrease in gravitational acceleration and SRP-acceleration for a sail as proposed by the Breakthrough Starshot project is shown in Figure 15. The propagation ends when both the gravitational acceleration and the SRP-acceleration are smaller than 10^{-4} mm/s^2, which is at 600 AU for the case presented in Figure 15. However, the sail would still need to travel over 275,000 AU before reaching our Solar System. With this in mind, the objective function is split in two parts as shown in Eq. 28, making use of the weights w_1 and w_2.

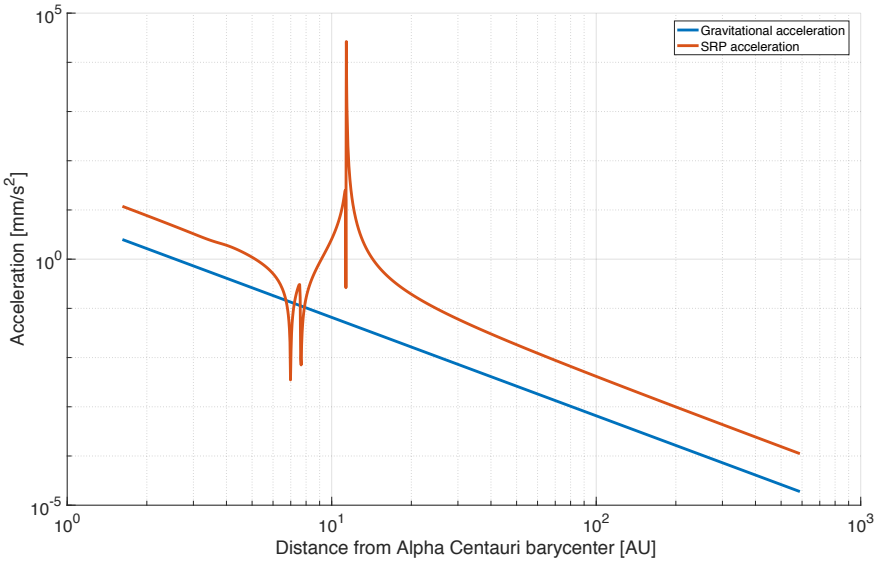

Fig. 15 Example of the decrease in gravitational acceleration and SRP-acceleration away from Alpha Centauri's barycenter for a graphene-like sail with characteristics as proposed by Breakthrough Starshot. Note that the scale is logarithmic.

$$J = w_1(t_{t.c.} - t_b) + w_2(t_f - t_{t.c.}) \tag{28}$$

The first part of the objective function covers the time of flight of the trajectory up to the termination condition, $t_{t.c.}$, of the optimal control problem (e.g., 600 AU away from the barycenter). To find the optimal launch date, the start of the simulation was given a time frame window of 80 years, which is equal to the orbital period of the binary star system. The second part of the objective function is added to account for the travel time from the termination condition until our Solar System. The latter is calculated analytically, which involves the sail's velocity at the termination condition $v_{t.c.}$: $t_f = \frac{r_{Sun} - r_{t.c.}}{v_{t.c.}}$, where r_{Sun} is the distance of the Sun from Alpha Centauri's barycenter, while $r_{t.c.}$ is the distance of the termination condition to the barycenter. This analytical expression assumes that the velocity of the sail remains constant throughout the interstellar phase of the mission. Finally, based on initial test runs, the weights are set to $w_1 = 0.2$ and $w_2 = 0.8$, such that more emphasis is put on minimizing the time of flight of the interstellar part of the trajectory, which directly relates to maximizing the velocity at the termination condition. Regarding this termination condition, the direction of the spacecraft is in the Sun's direction within the boundary condition as:

$$\mathbf{r}_{SC}(t_f) \leq 0.1\% \text{ away from } \mathbf{r}_{t.c.} \tag{29}$$

where $\mathbf{r}_{t.c.}$ is the user-defined position vector of the termination condition (e.g., 600 AU away from the barycenter) in the direction of the Sun.

Note that, although the optimal control problem is approached as an escape problem instead of a capture problem,

the results are presented as a capture problem in the remaining part of this paper.

B. Optimal Control Solver

The optimal control problem defined in the previous section is solved using the existing low-thrust trajectory optimization software InTrance: Intelligent Trajectory optimization using neurocontroller evolution [32, 36].

1. Trajectory Optimization and Evolutionary Neurocontrol

By combining biologically inspired artificial neural networks (ANN) with evolutionary algorithms (EA), InTrance finds the steering strategy that is (close to) the global optimum, without an initial guess [35]. The approach of the applied trajectory optimization algorithm is to calculate the local optimal thrust vector direction at each time step [35]. Using artificial intelligence and machine learning, InTrance finds the optimal trajectory based on the optimal steering strategy [32, 36]. This steering strategy maps the relevant variables, such as the state of the sail and the target, onto the control vector, which is in its turn used in the equations of motion to integrate the trajectory. Therefore, the optimal trajectory is found by learning the algorithm to find the optimal steering strategy. These steering strategies are implemented by the ANN as a neurocontroller, which is a parameterized network function that is defined by an internal parameter set, such as the state variables of the spacecraft or the distance to the target. The goal is to find the optimal parameter set, which is the work of the EA by mapping the parameter set onto a chromosome or individual [35]. Thus, the EA optimizes the initial conditions, such as the launch date and initial state (either Keplerian elements, Cartesian elements or vector state) and the internal parameters of the ANN. As a result, the ENC is a neurocontroller that utilizes an EA to learn and find the optimal parameter set. To conclude, the benefits of the software are that (1) trajectories can be optimized starting from a broad description of the mission while being applicable to a wide variety of mission scenarios, (2) no initial guess is required and (3) no astrodynamics or trajectory optimization expertise is required to perform an optimization run [36].

2. InTrance in Alpha Centauri

In essence, the InTrance software is built up from four libraries: (1) the space library containing the Alpha Centauri binary star system, (2) the ENC-library enclosing the ANN and EA, (3) the spacecraft library for the definition of the sail acceleration model, and (4) the main library combining all these libraries into the toolbox for trajectory optimization. While the ENC remained unmodified in this work, the other libraries required changes. To begin with, a new environment needed to be implemented. Our Solar System was replaced by the Alpha Centauri binary star system, according to the orbital elements as shown in Table 4. Furthermore, there was a need to adapt the force model for the calculation of the sail acceleration, implementing the contribution of the second stellar component on the acceleration. At the same time, a new routine was added to InTrance to carry out simulations for the different sail configurations discussed (one-sided

and two-sided reflective). Moreover, additional alterations were performed to solve the problem of capture. To approach the capture problem as an escape problem, the time rate of change of the Keplerian elements of the bodies involved were inversed. Finally, a dynamic step size control was added to the existing step size control, to ensure smaller step sizes when the sail is close to either of the stars. Since photogravitational assists appeared of crucial importance to loose sufficient kinetic energy and decelerate into a capture orbit, the step size of the integrator is changed based on the sail's entry velocity.

In InTrance, the equations of heliocentric translational motion were already implemented and are used throughout this work to calculate the sail's motion in Alpha Centauri, determined by the gravitational forces of Cen A and Cen B and the sail's SRP-acceleration expressed in the BSRS-frame [32]. Cen A is considered as the central body with Cen B as a disturbing body. For each time step during the trajectory optimization, the control vector - depending on the sail angles α and δ - is calculated by the steering neurocontroller, where the Runge-Kutta-Fehlberg-method of order 4(5) is applied as the numerical integrator of the equations of motion. Furthermore, Lagrange's variational equations are used as the foundation for low-thrust local steering laws to find the optimal transfer trajectory by connecting the change in Keplerian elements with the applied forces [36]. Using these steering laws, the orbital elements can be adjusted with an optimal rate during a low-thrust transfer, resulting in a time-optimal trajectory [35, 37].

VI. Results and Discussion

Using InTrance, the three phases of the proposed mission scenario are optimized: capture into an orbit about one of the stars, transfer to the other star and orbit raising about that star. This scenario is simulated for four different sail materials - corresponding to four different lightness numbers - and two different sail configurations: the two-sided reflective and one-sided reflective sail. These different simulation configurations are discussed in Section VI.A, before presenting the results in Section VI.B. Note that the latter section is the result of performing the same optimization problem for at least five different seed values. Finally, Section VI.C discusses additional results that analyze the sensitivity of the results in Section VI.B.

A. Simulation Configuration

Following the mission proposal presented in Section IV.B, the capture phase is examined first for capture about each of the stars. The subsequent transfer to the other star is based on the outcome of the capture phase. This means that the transfer trajectory is carried out from Cen A to Cen B in case that Cen A is found to be the best star for capture in terms of time of flight. Note that the circular capture orbit is used as the initial condition for the transfer, while the target orbit is again the center of the habitable zone of the target star. Finally, when arriving at the other star, the orbit is raised towards the outer edge of the habitable zone: 2.063 AU for an orbit about Cen A or 1.241 AU for one about Cen B. Before presenting the results for the mission scenario, the key simulation parameters are discussed below.

Table 8 Lightness numbers used for simulations.

Reference in this work	β			Sail Material	Sail Loading [g/m^2]	Reference
	Sun	Cen A	Cen B			
Sail A	0.04	0.057	0.023	Kapton	37	[39]
Sail B	0.765	1.055	0.422	Gold foil	2.0	[6]
Sail C	4.37	6.028	2.411	Composite Graphene-based	0.35	see $*$
Sail D	1779	2453	981	Graphene	0.00086	[6]

$*$: Breakthrough Starshot project: `https://breakthroughinitiatives.org/solicitations/3`, Retrieved August 14, 2019.

1. Minimum distance to the stars

The first parameter of importance is the minimum distance to the stars, as it affects the temperature of the sail. Although the largest accelerations are achieved when as close as possible to the star, the sail could melt when performing such a close photogravitational assist [38]. In addition, there is an increased risk of impact of high-energy particles. Despite the fact that these impacts could help to decelerate the sail during the capture phase by effectively absorbing the high-energy particles, the sail and its payload would be damaged by those impacts. Even though this work assumes an ideal sail with perfect specular reflection, the minimum stellar distance is set to be five stellar radii. This minimum distance is based on the work by Heller et al. (2017), in which a maximum temperature of the sail, $\tilde{T}_{sail}$, is set to be $\tilde{T}_{sail}$ = 100°C (373 K), a limit such that modern silicon semiconductors still function [7]. This temperature can then be used in a relation for the minimum number of stellar radii, $\tilde{n}$, as:

$$\tilde{n} = \sqrt{\zeta} \cdot \left(\frac{\tilde{T}_{\star}}{\tilde{T}_{sail}} \right)^2 \tag{30}$$

where $\tilde{n} = \frac{r_{min}}{R_{\star}}$, ζ is the absorptivity of the sail and $\tilde{T}_{\star}$ is the temperature of the star [7]. The temperatures of Cen A and Cen B are 5790 K and 5260 K, respectively [9]. With a reflectivity of up to 99.95%, the minimum distance is found to be five stellar radii, which equals to 0.02842 AU with respect to Cen A and 0.02005 AU with respect to Cen B.

2. Lightness numbers

Next to the two sail configurations as simulation parameters, the mission scenario was run for four different lightness numbers in an attempt to cover a wide range of technology capability. The lightness numbers shown in Table 8 are expressed with respect to the Sun and Alpha Centauri's binary stars. The four sails are referred to as sails A to D, ordered by the increase in lightness number. The lightness number of the first sail, sail A, is based on current technology and is a Sunjammer-like sail [39]. Sail B is one with a choice of material such that the lightness number is less than one, while the two remaining sails are capable of surpassing the Sun's gravitational acceleration [6]. The sail characteristics as proposed by the Breakthrough Starshot project result in sail C, while sail D is a graphene-class sail that is seen as the

ceiling of the technology of the future. The latter is the sail used in the research by Heller and Hippke (2017). This reference is used as a means to compare the outcome of this work with.

B. Results

The mission scenario from capture until orbit raising is presented hereafter for each of the sails according to the order presented in Table 8. Note that this section only considers prograde orbits about the stars. The results are shown for the two-sided reflective sail, while the results for the one-sided reflective sail are only presented for sail C, which is the sail proposed by the Breakthrough Starshot project. At the end, all different sail configurations will be compared in a combined analysis.

1. Sail A

Figure 16 shows the capture trajectory into Cen A's center of the habitable zone for sail A, with the optimized trajectory in the BSRS as shown in Figure 16a and in a Cen A-fixed reference frame in Figure 16b, where the direction to Cen B is depicted with red arrows. In addition to the orbits, the direction of the SRP-acceleration is represented with green arrows throughout this work. Note that Figure 16a depicts a detail of the closest encounter with Cen A. Although not illustrated here, the sail enters Alpha Centauri with an inclination of approximately 11° due to the relative orientation of the Sun and Alpha Centauri as discussed in Section II.B. However, the photogravitational assist annihilates this inclination, such that the sail remains in the orbital plane of Alpha Centauri after this assist. With this lightness number, the sail is mainly bound to the gravitational attraction of the system, such that the trajectory is an inwards-spiralling motion as seen in Figure 16b. Taking into account the earliest launch date from today, the arrival date would be in the year 20,865 after a transfer time of 18,790 years with a maximum injection speed, v_{inj}, into Alpha Centauri of 0.023% c. It is found that such a lightness number does not fully exploit the binary star system to capture into an orbit about one of the stars. The binary stars are too far away from each other to both have a substantial influence on this sail. To perform capture, it was clear that Cen B could be discarded as the target star. While the transfer time from the Sun until a capture orbit about Cen A would take 18,790 years, capture about Cen B is found to take over 70,000 years.

More information about the capture trajectory of sail A is displayed in Figure 17. Figure 17a shows three different cone angles: the cone angles of the SRP-acceleration induced by Cen A and Cen B, and the cone angle of the total SRP-acceleration with respect to Cen B. Furthermore, a detail during the close encounter is presented with the black arrow indicating the closest encounter. During the close encounter, the sail is oriented to maximize the deceleration at Cen A while the cone angle with respect to Cen B fluctuates during this close maneuver. Since Cen A is the dominant star for this trajectory, the normal vector of the total SRP-acceleration is always directed away from Cen A and the sail is oriented at an angle of approximately 35° with respect to Cen A, which is the optimal cone angle to maximize the transverse component of the SRP-acceleration. The dotted line of the total SRP-acceleration with respect to Cen B

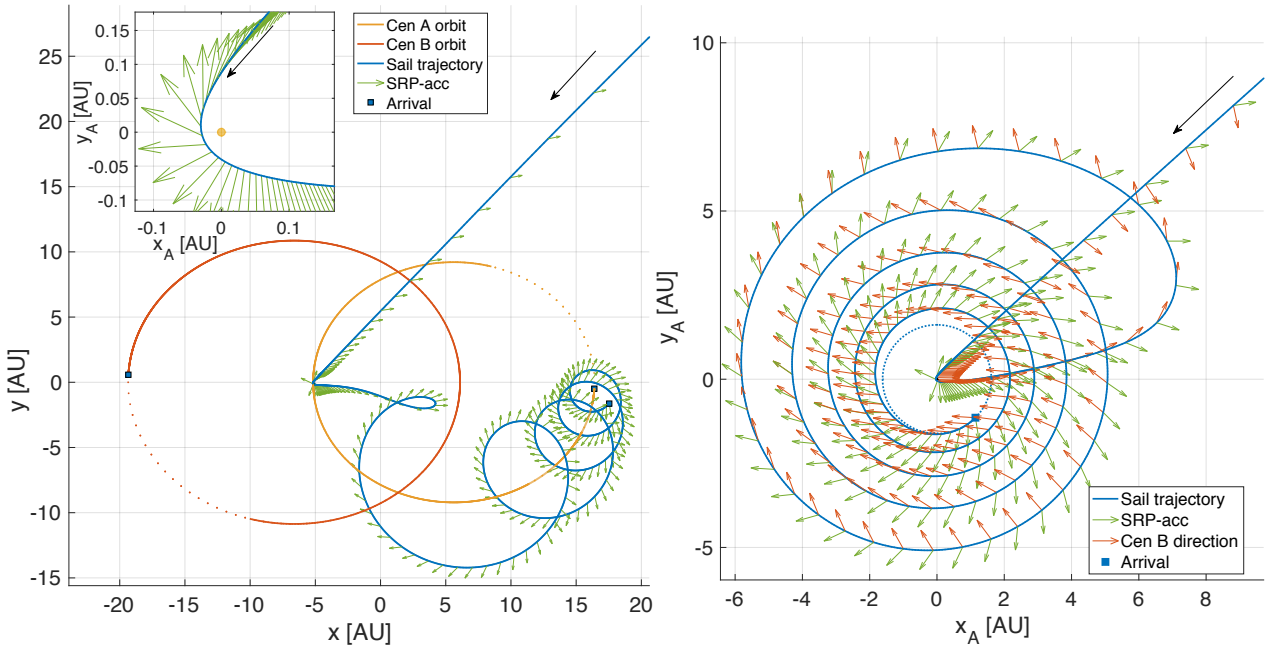

(a) Sail A in the BSRS with detail of closest encounter about Cen A.

(b) Sail A in the Cen A-fixed reference frame.

Fig. 16 Sail A: capture trajectory into an orbit about Cen A.

becomes visible when the SRP-acceleration component of Cen B is opposite to the component of Cen A, such that that cone angle becomes larger than 90°, resulting in a reduced total acceleration. In addition, Figure 17b presents the magnitude of all the accelerations acting on the sail. With a lightness number of that of sail A, the SRP-acceleration is considerably smaller than the gravitational acceleration of Cen A or Cen B. After the photogravitational assist at Cen A, the SRP-acceleration slowly increases as the sail spirals towards Cen A.

The transfer and orbit-raising trajectory of sail A are shown in Figure 18. Since the allowed arrival date is spread over one orbital period of Alpha Centauri to allow for time-optimal results, these trajectories do not immediately follow on the capture trajectory, resulting in a dwell time in between the mission phases to perform scientific observations. The time-optimal transfer from Cen A to Cen B is shown in Figure 18a. The time of flight is approximately 24 years. The sail spirals out of the center of the habitable zone of Cen A and arrives in the habitable zone of Cen B when the binary star system is close to its periapsis. Note that a circular orbit at arrival does not belong to the capabilities of InTrance. Thus, the termination conditions for the target orbit were only limited by the relative distance and velocity to the target, see Eq. 26. Therefore, the resulting orbit is highly eccentric. The orbit-raising phase of sail A from Cen B's center of the habitable zone to its outer edge is shown in Figure 18b, which lasts approximately three years. The direction to Cen A is also depicted. This result is as expected from our knowledge of orbit raising in the Solar System, since the influence of Cen A on the SRP-acceleration is negligible [5].

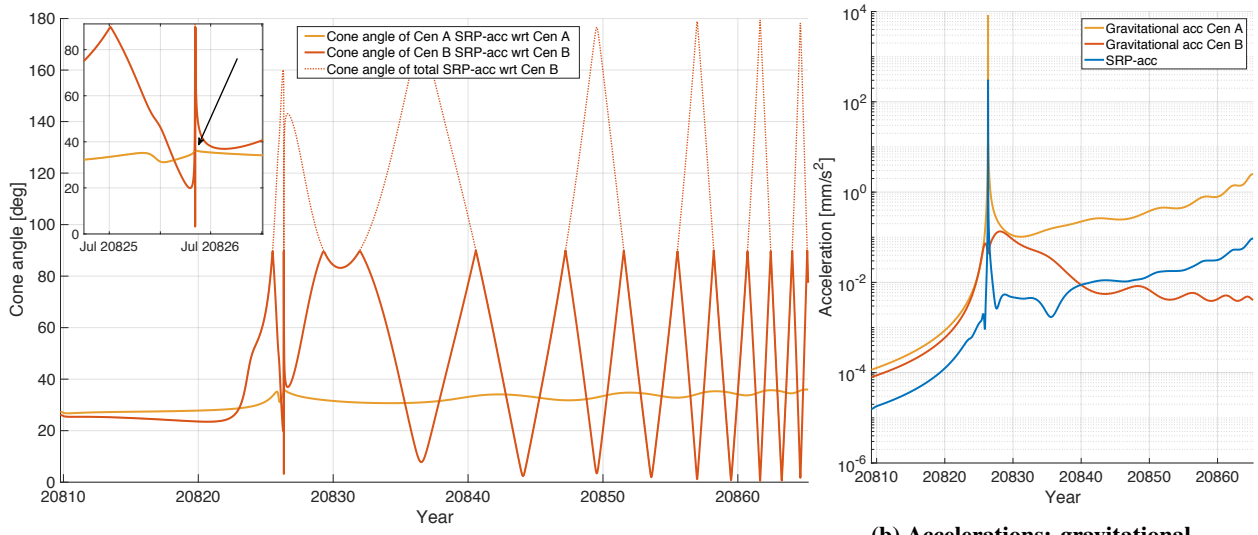

(a) Cone angles of the separate SRP-accelerations with respect to the stars. The dotted line represents the cone angle of the total SRP-acceleration.

(b) Accelerations: gravitational acceleration of Cen A and Cen B, and total SRP-acceleration.

Fig. 17 Sail A: cone angles and accelerations during capture trajectory into an orbit about Cen A.

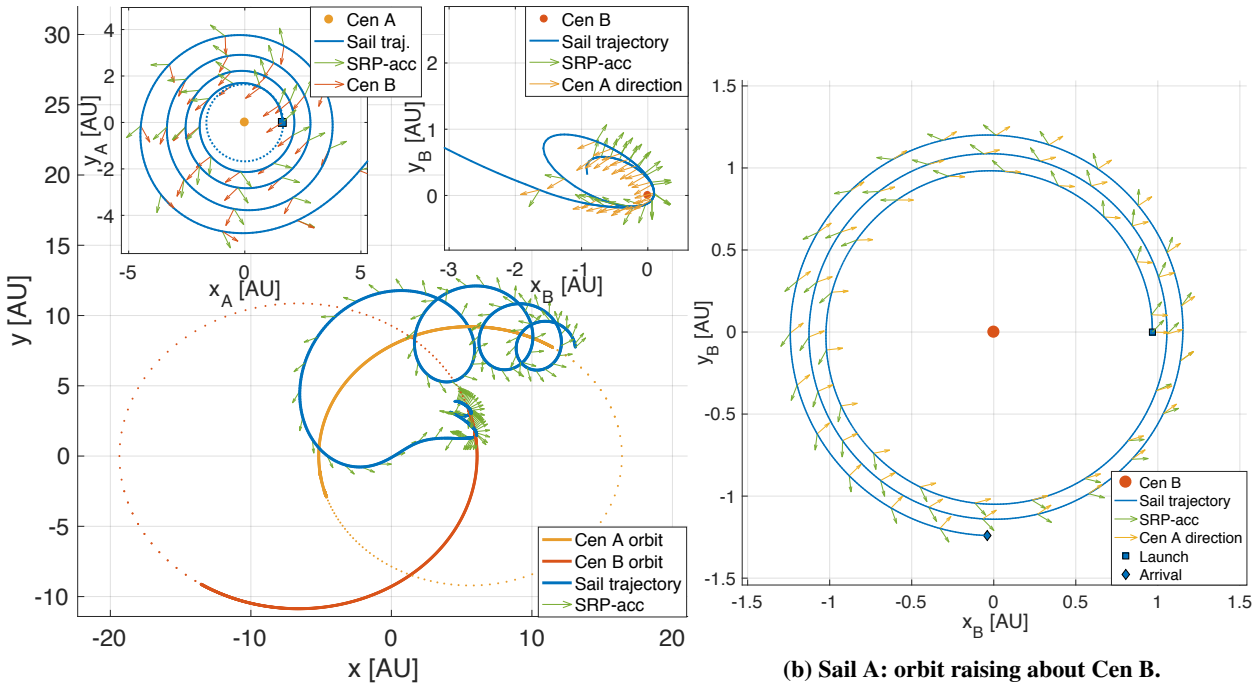

(a) Sail A: transfer trajectory in the BSRS with details of departure at Cen A and arrival at Cen B.

(b) Sail A: orbit raising about Cen B.

Fig. 18 Sail A: transfer and orbit-raising trajectories.

2. Sail B

Figure 19 shows the capture trajectory for sail B. While sail A is not capable of benefiting from the binary star system, the result for sail B shows that for capture around Cen A, Cen B is used to decelerate before arriving in the

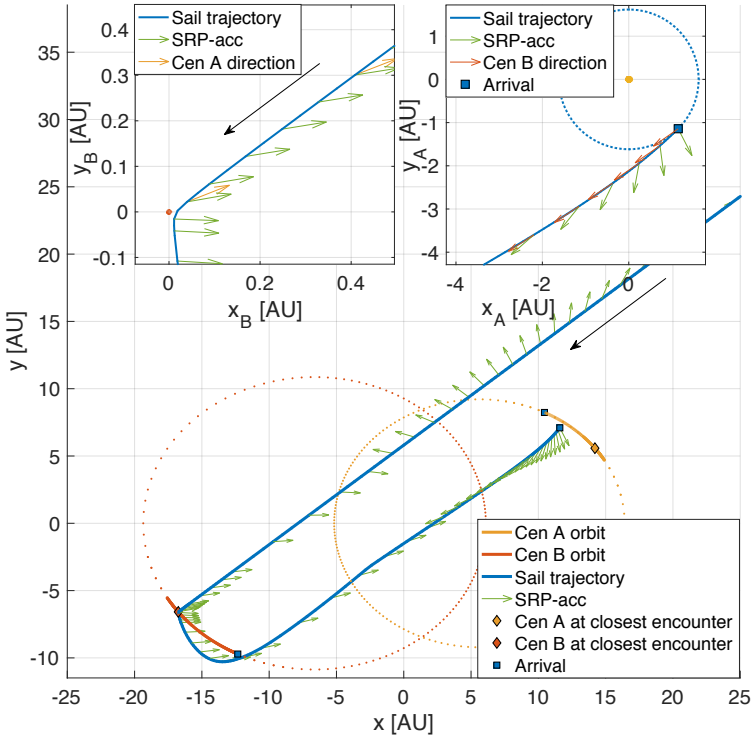

Fig. 19 Sail B: capture trajectory into an orbit about Cen A in the BSRS with details of the closest encounter at Cen B and arrival at Cen A.

center of the habitable zone of Cen A. From Figure 19, it is clear that the photogravitational assist at Cen B is not a conventional gravitational fly-by. Instead, the star is used at its full potential by traveling straight towards it to maximize deceleration, resulting in a so-called bumper-effect, rather than a so-called catapult-effect. This observation is analogous to the work of Heller et al. (2017) [7]. Note that the distance to Cen B reached its minimum during this trajectory. This sail would arrive in the year 4387 after 2293 years of traveling, with 2094 the soonest departure date for this orbital configuration of Alpha Centauri. The injection speed of the sail is found to be 0.19% c.

A three-dimensional view of the capture trajectory is presented in Figure 20a, showing that the entrance of the sail is inclined to Alpha Centauri before the closest encounter with Cen B, after which the sail travels in the orbital plane of Alpha Centauri. In the initial phase before the encounter with Cen B, the SRP-acceleration components are aligned in the same direction, as can be seen in Figure 20b, since the solid lines overlap with the dotted lines. Before the encounter with Cen B, however, there is a phase where Cen A is the dominant star. Nevertheless, the largest deceleration - which is highlighted in the detail of Figure 20b with the arrow pointing to the closest encounter - is experienced close to Cen B, after which the cone angle of the SRP-acceleration of Cen B increases in order to aim for Cen A. In Figure 20b, the transition from Cen B to Cen A as the dominant star is also noticeable in the shift of the cone angle of the total SRP-acceleration at approximately the year 4385. Initially, the total acceleration with respect to Cen A is larger than 90°, after which the total acceleration with respect to Cen B is larger than 90°.

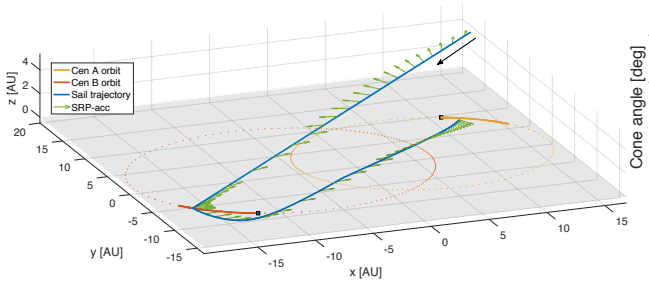

(a) Three-dimensional view of capture trajectory into an orbit about Cen A in the BSRS.

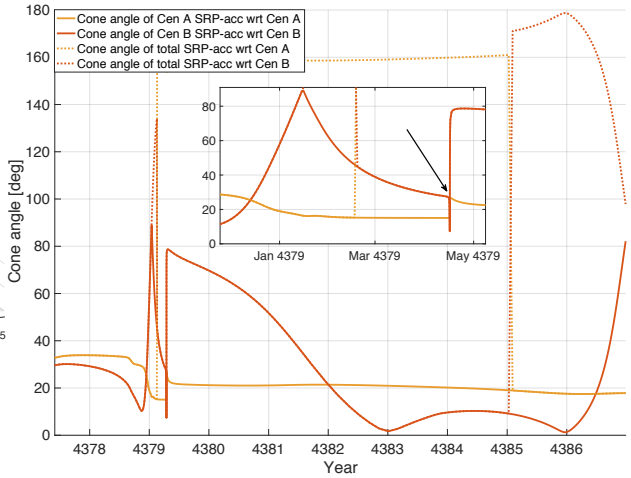

(b) Cone angles of the separate SRP-accelerations with respect to the stars. The dotted lines represent the cone angles of the total SRP-acceleration.

Fig. 20 Sail B: capture trajectory into an orbit about Cen A.

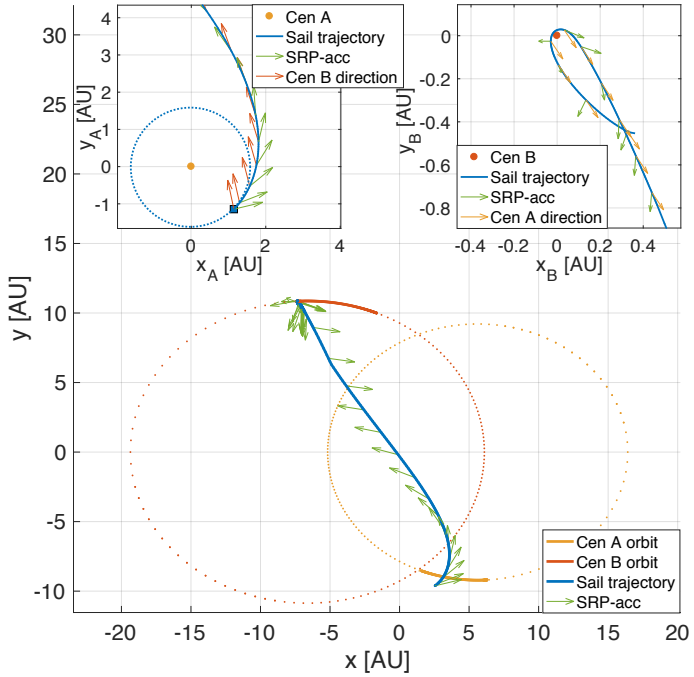

(a) Sail B: transfer trajectory in the BSRS with details of departure from Cen A and arrival at Cen B.

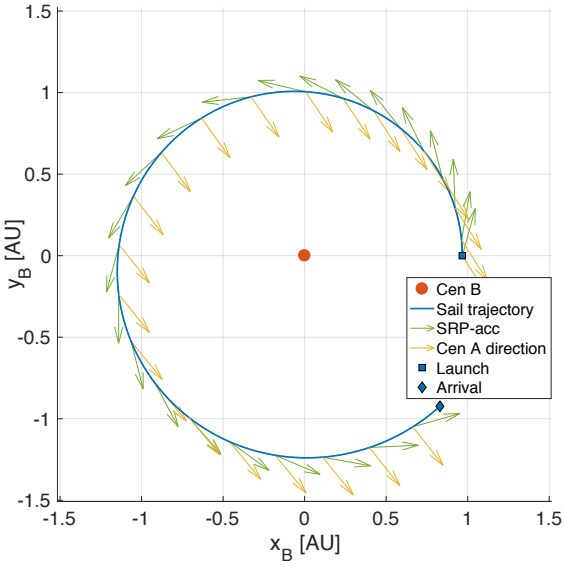

(b) Sail B: orbit raising about Cen B.

Fig. 21 Sail B: transfer and orbit-raising trajectories.

The two remaining phases of sail B are displayed in Figure 21. The transfer trajectory as shown in Figure 21a is from Cen A to Cen B and takes 5.4 years. The fact that the transfer trajectory is the combined mission of escape from Cen A and capture at Cen B is clear from this result. Furthermore, Figure 21a shows that a photogravitational assist at arrival is performed to transfer between the stars as fast as possible, arriving in a non-circular orbit with $a = 0.3$ and

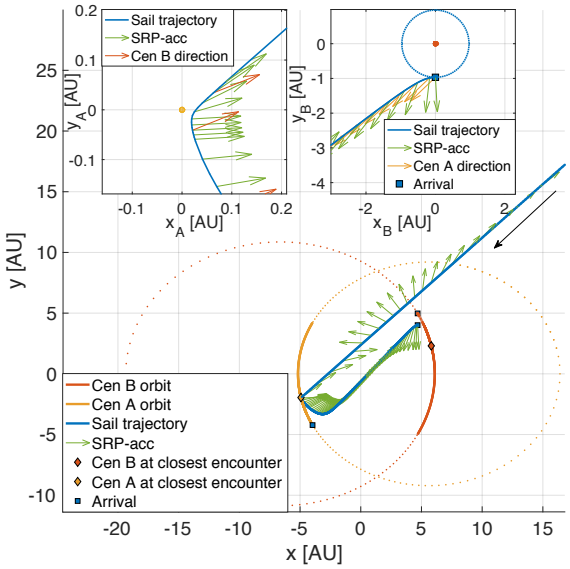

(a) Sail C: capture trajectory in the BSRS with details of encounter with Cen A and arrival orbit about Cen B.

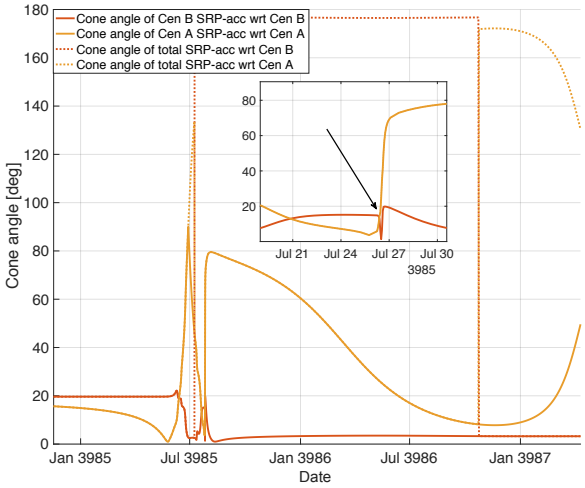

(b) Cone angles of the separate SRP-accelerations with respect to the stars. The dotted lines represent the cone angles of the total SRP-acceleration.

Fig. 22 Sail C: capture trajectory into an orbit about Cen B and the cone angles.

$e = 0.95$. Finally, Figure 21b shows the orbit raising about Cen B from the center of the habitable zone to its outer edge, which takes approximately one year.

3. Sail C

The result for sail C - the sail configuration as proposed by the Breakthrough Starshot project - is shown in Figure 22a, which illustrates that capture with this sail is possible, preferably into an orbit about Cen B. The capture trajectory of sail C is similar to that of sail B, aside from the fact that Cen A is now the star to perform the photogravitational assist at. The increase in lightness number resulted in this change to the more luminous star. This mission would take approximately 2,000 years to perform a photogravitational assist about Cen A with the bumper-effect to end up in a capture orbit about Cen B. With an injection speed of 0.23% c, the earliest arrival date would be the year 3987. Also, note the similarity in the cone angles as shown in Figure 22b compared with Figure 20b for sail B.

The analogy of sail C with sail B is also noticeable for the transfer and orbit-raising trajectories, as shown in Figure 23. The optimized transfer trajectory, see Figure 23a, is performed when Cen A and Cen B are close to each other and takes 2.27 years, which is a shorter time as for the transfer for sail B. However, the transfer time to perform orbit raising at Cen A, see Figure 23b, is found to take longer than the orbit-raising maneuver of sail B about Cen B, 1.8 years. With the lightness number of sail C, the SRP-accelerations are significantly larger than the gravitational acceleration, such that an out-of-plane orientation of the sail is used to perform the relatively small orbit increase to the outer edge of the habitable zone. Therefore, this sail is not efficient to perform orbit raising in Alpha Centauri, since the sail's performance is better than would be required for this orbit-raising maneuver.

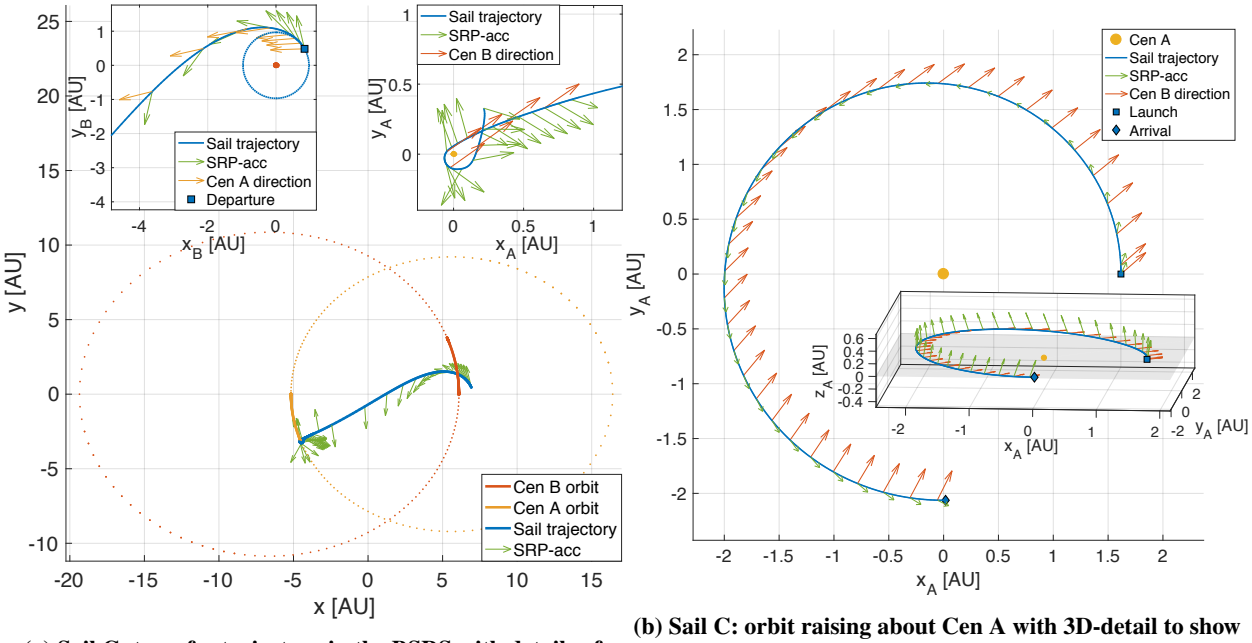

(a) Sail C: transfer trajectory in the BSRS with details of departure from Cen B and arrival at Cen A.

(b) Sail C: orbit raising about Cen A with 3D-detail to show out-of-plane motion.

Fig. 23 Sail C: transfer and orbit-raising trajectories.

Next to presenting the mission scenario for the two-sided reflective sail, this section also presents the result for a one-sided reflective sail. The capture trajectory of sail C for this one-sided reflective sail is presented in Figure 24a, which shows that the time-optimal capture trajectory occurs for capture into an orbit around Cen A with a time of flight of 16,372 years and an injection speed of 0.026% c. Although it is in essence possible, it is found to be unfeasible to travel from our Solar System to Alpha Centauri with a one-sided reflective sail due to the large increase in travel time. Since the photons of Cen A and Cen B can only impact on one side of the sail, the trajectory is highly restricted. This is clear from Figure 24a, which shows that a photogravitational maneuver about one of the stars is not possible. The time of flight from the Sun to Alpha Centauri for this one-sided reflective sail is more than eight times the result for the same lightness number, but with a two-sided reflective sail. The same holds for the transfer time from one star to another. In Figure 24b, it is shown that the trajectory avoids the forbidden areas for the one-sided reflective sail. The sail does not fly in areas where both sides of the sail would be subjected to starlight, such that the transfer time increases to more than 18 years. Due to this forbidden area, the arrival orbit at Cen B is inclined with the orbital plane of Alpha Centauri.

Finally, Figure 25 displays the orbit-raising maneuver for a one-sided reflective sail. Although the one-sided reflective sail is still ill-favored in terms of time of flight, the trajectory is similar to the two-sided reflective sail as shown in Figure 23b. A similar trajectory is the result of a lightness number that is too ambitious for such a maneuver. As seen in the detail of Figure 25, the cone angles remain smaller than 90°, as a result of the constraints for the one-sided reflective sail. The convergence of InTrance shows that such a maneuver is possible, although the trajectory is more

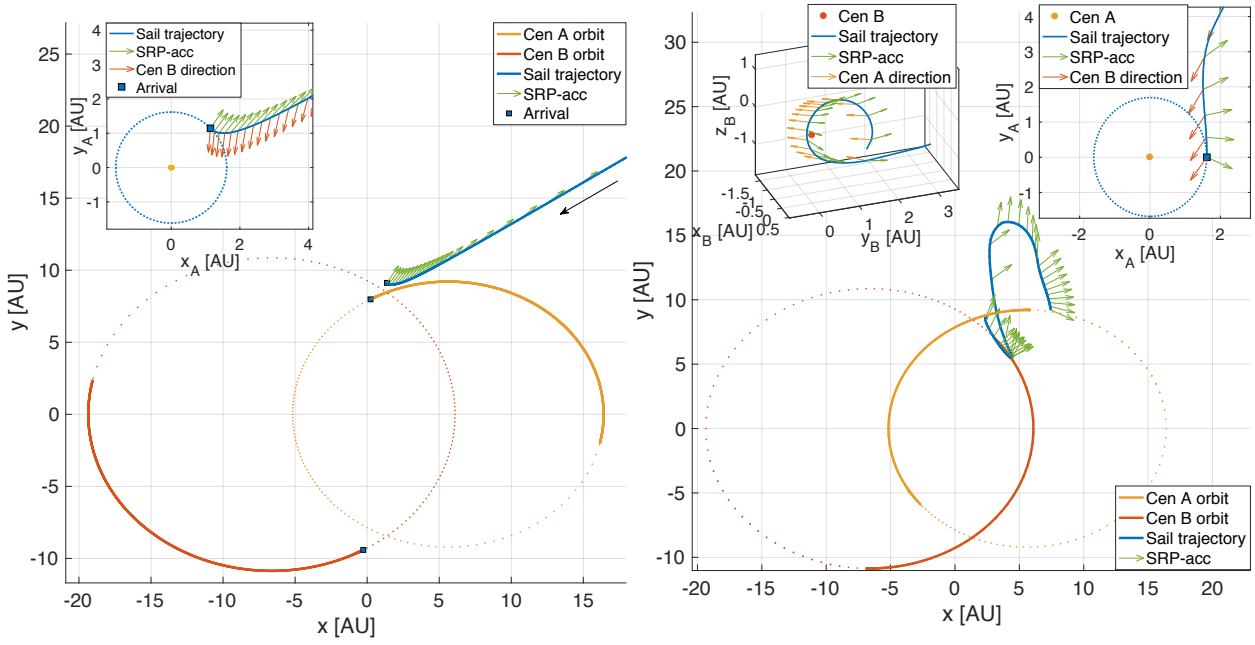

(a) Sail C: capture orbit for a one-sided reflective sail in the BSRS with a detail of the arrival at Cen A.

(b) Sail C: transfer trajectory for a one-sided reflective sail in the BSRS with details of the departure from Cen A and arrival at Cen B.

Fig. 24 Sail C: capture trajectory into an orbit about Cen A and transfer trajectory for a one-sided reflective sail.

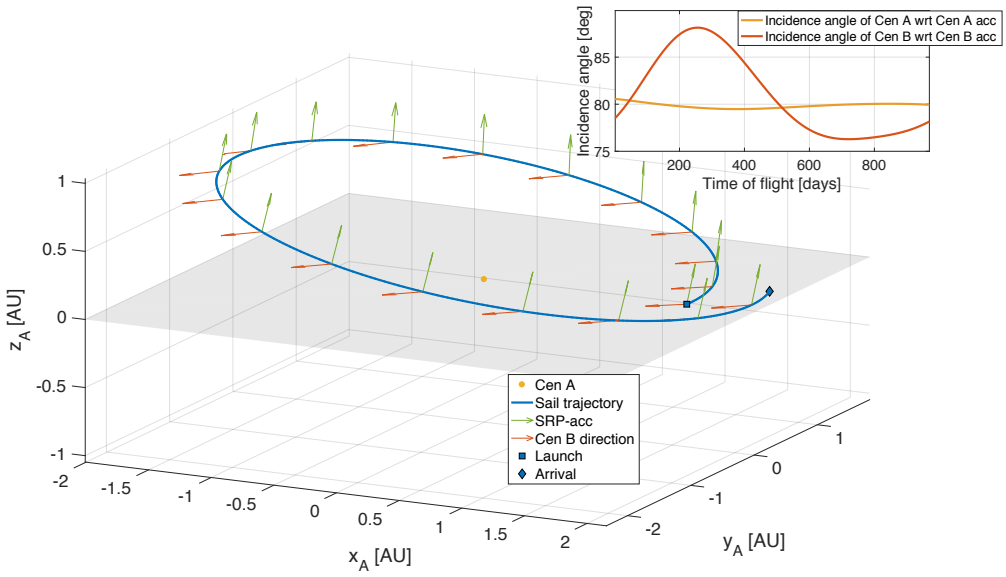

Fig. 25 Sail C: orbit raising about Cen A for a one-sided reflective sail with an overview of the cone angles.

inclined than the one for the two-sided reflective sail, to avoid that both sides of the sail are hit by starlight.

Note that similar results for the one-sided reflective sail are found for the other sail configurations with different lightness numbers. To avoid repetition, however, it was decided not to present these results.

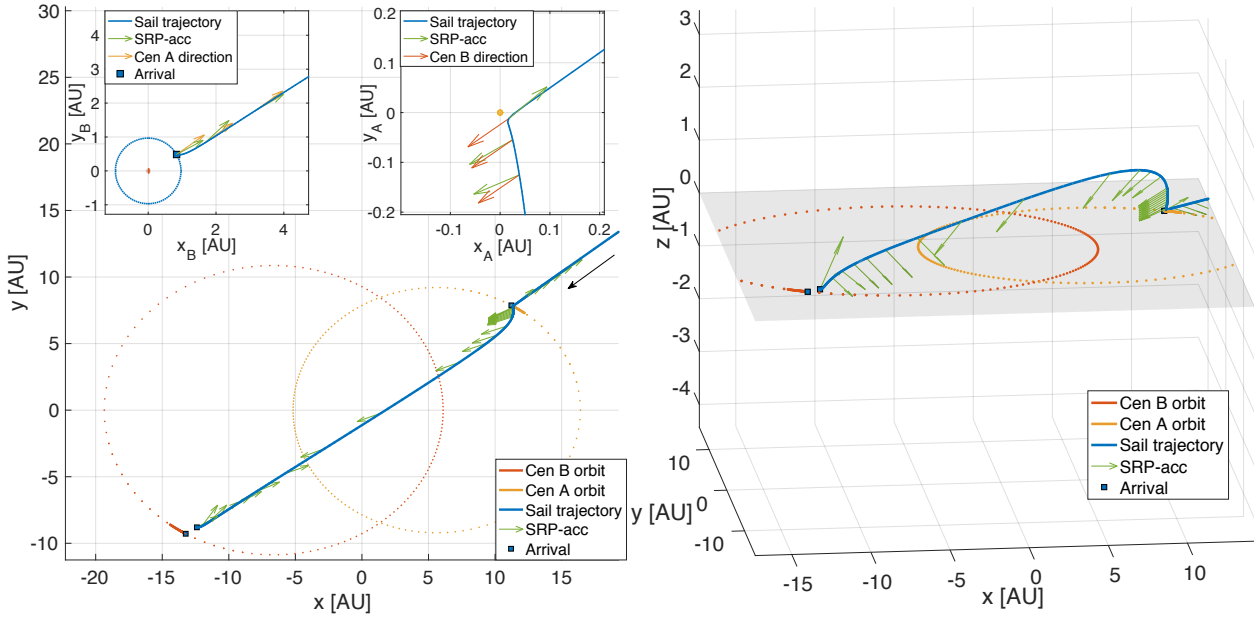

(a) Capture trajectory into an orbit about Cen B in the BSRS.

(b) Sail D: capture trajectory in 3D.

Fig. 26 Sail D: capture trajectory into an orbit about Cen B in the BSRS with details of the closest encounter at Cen A and arrival at Cen B.

4. Sail D

The capture trajectory of the sail with the most optimistic lightness number, sail D, is shown in Figure 26a. Again, a photogravitational assist with the bumper-effect is performed at Cen A, which corresponds to the results of referenced work [6, 7]. Compared to sail C (see Figure 22a), the sail is not deflected as much during the photogravitational assist at Cen A. However, the sail travels out-of-plane after the encounter with Cen A, as shown in Figure 26b, while still being captured into an orbit in the orbital plane of Alpha Centauri. Note that, in Figure 26b, the scale in z-direction is different from those in x- and y-direction to amplify the out-of-plane motion. With this high-technological sail, the arrival date would be in 2172 after traveling over 111 years, which is a significant improvement from sail C in terms of travel time. Note that the departure in the Solar System would be 2060 to ensure the arrival conditions in Alpha Centauri as depicted in Figure 26. The sail would enter Alpha Centauri at 3.9% c, corresponding to 6.75 AU a day.

The cone angles and magnitudes of the accelerations involved are presented in Figure 27, with the arrow indicating the closest encounter at Cen A. From Figure 27a, it is clear that the cone angles go towards 90° after the encounter with Cen A, not to deflect too much away from Cen B. Furthermore, it is important to note that the maximum acceleration, as shown in Figure 27b, is approximately 620 g.

While the results for capture with this sail show promising trajectories, it is found to be challenging to obtain results for the two remaining phases of the mission. As was already discussed, the orbit-raising maneuver for sail C is performed with large cone angles as the produced acceleration would otherwise be too large to conduct the transfer.

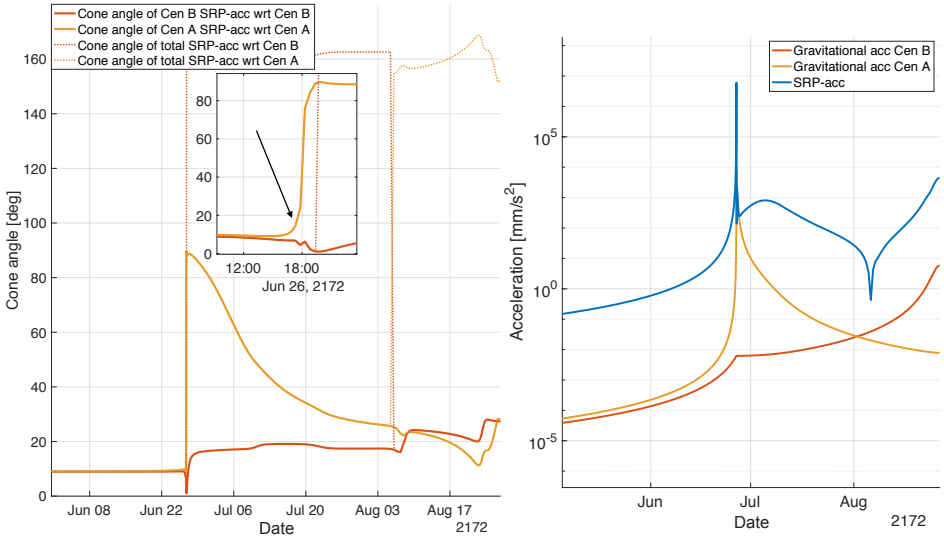

(a) Cone angles of the separate SRP-accelerations with respect to Cen A and Cen B. The dotted lines represent the cone angles of the total SRP-acceleration.

(b) Accelerations: gravitational acceleration of Cen A and Cen B, and total SRP-acceleration.

Fig. 27 Sail D: cone angles and accelerations during capture trajectory into an orbit about Cen B.

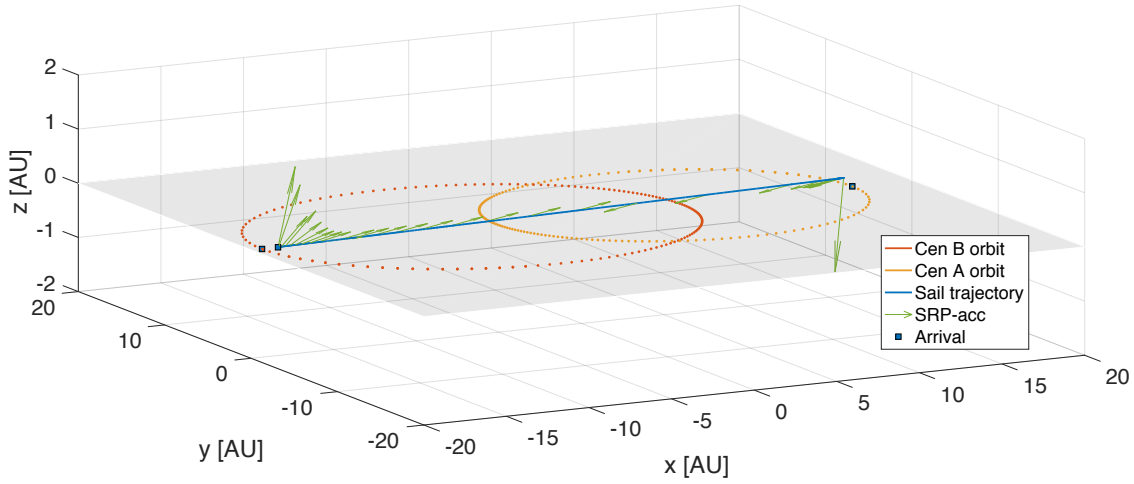

Fig. 28 Sail D: transfer trajectory into an orbit about Cen A in the BSRS.

With an even larger lightness number for sail D, it is found impossible to find an orbit-raising trajectory about Cen A. A transfer trajectory between Cen B and Cen A was obtained as shown in Figure 28. The result is a transfer performed at apoapsis of the system and the distance of 35.8 AU is traveled within four months time. Note that the orientation of the sail while being close to the stars is significantly out-of-plane for the SRP-acceleration not to be too large, in order to make the transfer attainable. For the same transfer at periapsis of the system, it is found to be impossible for the sail to decelerate at arrival. Therefore, it is suggested to jettison the sail after the capture phase, such that the mission ends in an orbit about Cen B.

Table 9 Overview of all results.

		Injection speed	Time of flight (yrs)		
Sail	Configuration	[% c]	Capture	Transfer	Orbit raising
Sail A		0.023	18,790	23.8	3.05
Sail B		0.19	2293	5.4	1.05
Sail C	two-sided reflective	0.23	1950	2.27	1.84
	one-sided reflective	0.026	16,372	18.25	2.72
Sail D		3.9	111.5	0.31	n.a.

Table 10 Comparison of results with time of flight relation of Heller et al. (2017) [7].

Lightness number	Time of Flight [yrs]	Relation $\sqrt{\frac{\beta_{nom}}{\beta}}$ [yrs]	Improvement in %
0.04	18,790	23,514	20.1
0.765	2293	5377	57.4
4.37	1950	2250	13.3

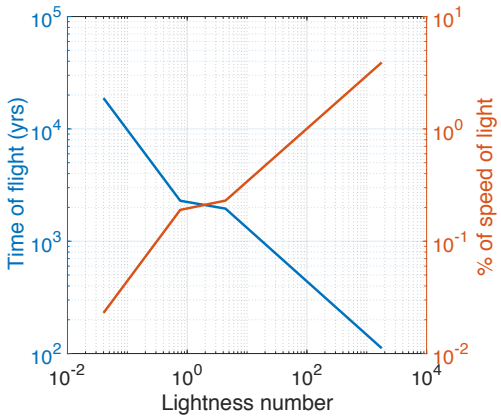

Fig. 29 Overview of the results. The left y-axis shows the time of flight in years, while the right y-axis shows the percentage of speed of light for the investigated lightness numbers.

5. Overview of the results

All the results above are summarized in Table 9. It shows that similar results are obtained for sail B and sail C, since the corresponding lightness numbers are relatively similar. It is also important to note that the one-sided reflective case for sail C shows similar results as those for the two-sided reflective case for sail A. Comparing the one-sided reflective case for sail C with the two-sided reflective case for sail A means it is worth performing research and development on a two-sided reflective sail.

With these results, Figure 29 can be constructed where the time of flight from our Solar System to a capture orbit in Alpha Centauri is displayed on the left axis, while the maximum injection velocity in percentage of speed of light is depicted on the right axis. Comparing these results with Figure 5 of Heller and Hippke (2017), similar results are found for the largest lightness number, i.e., sail D, both with respect to time of flight and optimal configuration of Alpha

Table 11 Time of flight comparison of capture trajectories about Cen A and Cen B. The time of flight indicated in bold is the result presented in Section VI.B.

	Capture into orbit about		
Sail	Cen A [yrs]	Cen B [yrs]	Improvement in %
Sail A	**18,790**	>70,000	73.2
Sail B	**2293**	3618	36.6
Sail C	2409	**1950**	19.1
Sail D	132.3	**111.5**	15.7

Centauri at arrival. The time of flight obtained by Heller and Hippke (2017) is slightly smaller, which is due to the fact that the referenced work performs photogravitational assists at Cen A and Cen B to travel to Proxima Centauri, while this work considers capture into orbits about either Cen A or Cen B. In addition, it is stated in the referenced work that the time of flight of other lightness numbers relate according to $\sqrt{\frac{\beta nom}{\beta}}$, with β_{nom} the lightness number of sail D [7]. The results shown in this work prove that better results are found in terms of time of flight for the lightness numbers smaller than this nominal value. This is shown in Table 10, where the results of this work are compared to the proposed relation of $\sqrt{\frac{\beta_{nom}}{\beta}}$ by Heller et al. (2017) [7]. Indeed, an average improvement in time of flight of 30% is found.

C. Sensitivity Analyses

Next to the results shown above, the following sensitivity analyses were considered: (1) the effect of capturing about the alternative star to the one presented in Section VI.B, (2) the effect of arriving in a retrograde orbit, (3) the effect of increasing the minimum distance to the stars, and (4) the effect of an eccentric arrival orbit.

1. Capture about the other star

To assess the sensitivity of the capture trajectories based on the star at which capture takes place, the results for the capture trajectories into an orbit about either star is shown in Table 11. The results in bold represent the trajectories as shown in Section VI.B. For the same sail, it is clear that the time of flight differs significantly by performing a capture orbit about the other star. When considering the four sails, the improvement is smaller for larger lightness numbers, going from sail A to sail D.

2. Retrograde orbits

Another analysis is based on the change from prograde orbits to retrograde orbits for the phases of capture and star transfer. Note that both types of orbits are still in the orbital plane of Alpha Centauri. As stated before, all previous results are based on arriving in prograde orbits. However, when changing this condition to a retrograde orbit, better results were found in terms of time of flight for capture and the transfer trajectories to the other star. As an example, Figure 30 shows the capture trajectory for sail D into a retrograde orbit about Cen B. Overall, the trajectory is similar to

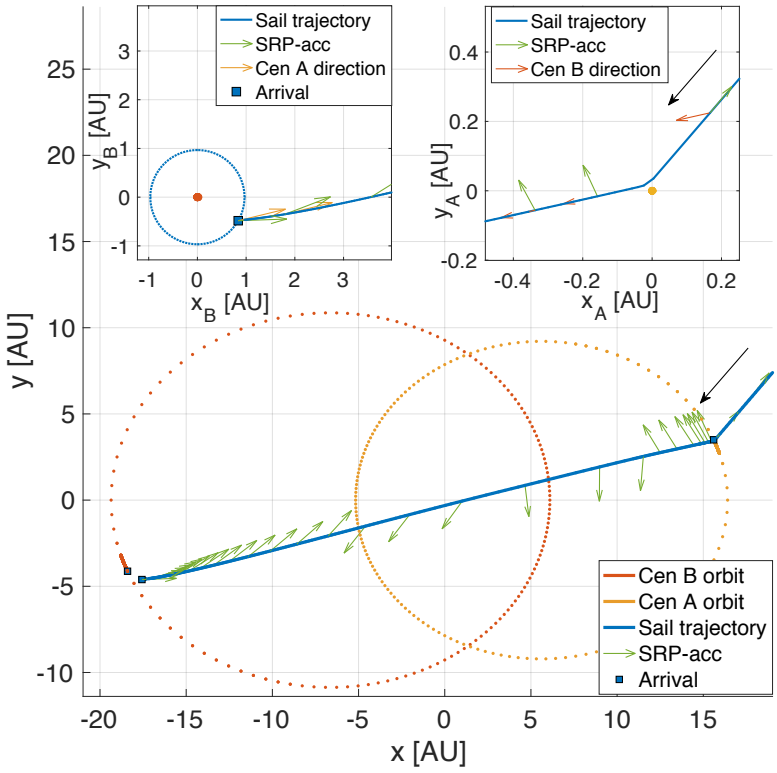

Fig. 30 Sail D: capture trajectory into a retrograde orbit about Cen B in the BSRS.

the case for the capture into a prograde orbit. However, the time of flight from the Sun to a circular orbit about Cen B is reduced by approximately 10 years to 101 years, which is an improvement of approximately 10%, with an injection velocity of 4.25% of c, corresponding to 7.3 AU a day.

The same conclusion holds for a transfer trajectory to the other star. As an example, Figure 31 shows a transfer trajectory from a prograde orbit about Cen A to a retrograde orbit about Cen B for sail B. For this case, the improvement in time of flight for the retrograde arrival orbit is approximately 35%.

3. Minimum distance to the stars

Next, the effect of changing the minimum distance to the stars from five to ten stellar radii was investigated. The minimum distance of ten stellar radii would be applicable to a sail with a reflectivity of 99.8% based on Eq. 30 and is analogous to the constraint of minimum distance to the Sun for the Parker Solar Probe, which will get as close as 8.86 solar radii in 2024, while still allowing thermal management of the spacecraft [40]. Although the optimized trajectories do not change in terms of shape, there is a significant increase in the time of flight of the capture trajectories, which can be explained by the inverse square law for the SRP-acceleration with the distance to the star. Two examples are shown in Table 12, for sail C and sail D. Increasing the minimum distance to the stars from five to ten stellar radii results in an increase of time of flight of on average 35%.

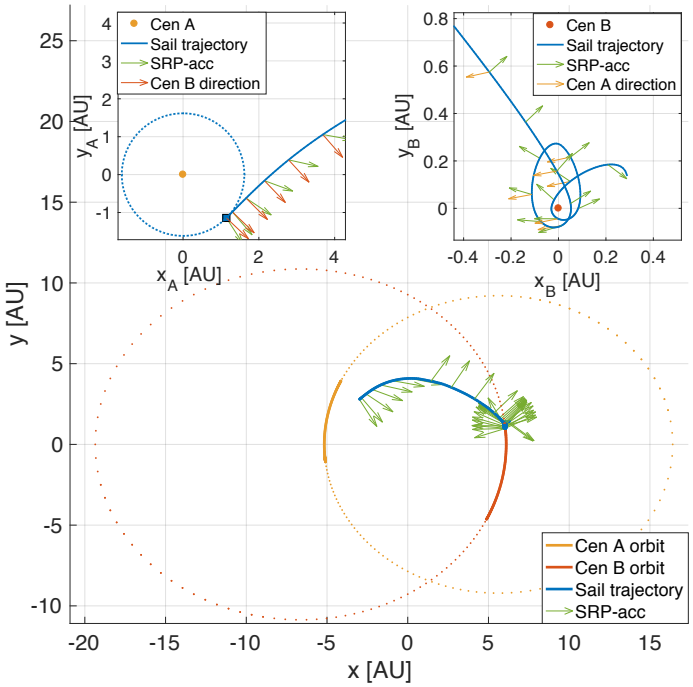

Fig. 31 Sail B: transfer trajectory from Cen A into a retrograde orbit about Cen B in the BSRS for sail B.

Table 12 Sensitivity to an increase in minimum distance to the stars. The increase in time of flight due to the increase in minimum distance to the stars is shown in percentages.

	Time of flight [yrs]		
Sail	$\tilde{n} = 5$	$\tilde{n} = 10$	Increase in time of flight in %
Sail C	1950	2669	36.9
Sail D	111.5	148.5	33.2

4. Eccentric arrival orbit

Finally, eccentric arrival orbits were investigated instead of the sail being captured into a circular orbit. For this investigation, the previous sensitivity analysis based on retrograde orbits was used as the reference transfer time for sail D being captured into a retrograde and circular orbit about Cen B. The time of flight of this reference trajectory was found to be 101 years.

Two values for the eccentricity were investigated: $e = 0.5$ and $e = 0.9$, while the other orbital elements did not change, i.e., $a = 0.967$ AU. The results of this sensitivity analysis are shown in Table 13. The improvements of the eccentric orbits with respect to the circular orbit are commensurate going from a circular orbit to an orbit with $e = 0.5$ and from that latter orbit to one with $e = 0.9$. The orbit with a high eccentricity of 0.9 results in a travel time from the Solar System to a closed orbit about Cen B of 77.6 years, with an injection speed of approximately 5.5% of c, corresponding to approximately 9.5 AU/day. This result is very similar to the result found by Heller et al. (2017) [7].

Table 13 Sensitivity to an eccentric orbit at arrival after being captured into a retrograde orbit about Cen B for sail D.

Sail D	Time of Flight [yrs]	Relative improvement w.r.t. $e = 0$ in %
$e = 0.0$	101	-
$e = 0.5$	88.4	12.5
$e = 0.9$	77.6	23.2

VII. Conclusion

This work investigated the orbital dynamics of a photon sail in the Alpha Centauri system as well as time-optimal trajectories from our Solar System to Alpha Centauri, which is seen as the prime target of interstellar travel. Contrary to the Breakthrough Starshot project, this research focused on capture into Alpha Centauri to increase the scientific yield of the mission. After showing the feasibility of the sail being captured into a bound orbit about a star, more mission applications were examined, in particular: transfer orbits to the other star and orbit raising about a star. These trajectories were optimized using an adapted version of InTrance, a trajectory optimization toolbox combining artificial neural networks and evolutionary algorithms.

Although it is technically possible to perform capture with a one-sided reflective sail, the time of flight would be eight times longer than for a sail that is reflective on both sides.

It was furthermore found that a high-technological graphene-based sail could travel from our Solar System into an orbit about Alpha Centauri B within less than 80 years, which is complementary with previous work. However, it is found to be extremely challenging for such a futuristic sail to perform transfer and orbit-raising trajectories after capture. Therefore, it is suggested to jettison the sail at arrival.

The Breakthrough Starshot project aims to travel to Alpha Centauri within 20 years as a flyby-mission. This work has shown that a capture would increase the time of flight to 2,000 years. However, through capture, an increase in exploration of the binary star system is achieved.

In addition, to indicate the need for technological improvement, a Sunjammer-like sail would need approximately 20,000 years to arrive at an orbit about Cen A.

Finally, for sails with lightness numbers lower than the high-technological graphene-based sail, the results in this work show an improvement in transfer time of approximately 30% over previous work.

Appendix: Apparent Orbit and True Orbit

Observing a star from Earth, the visible orbit is the apparent orbit, an orbit that is projected on the plane of the sky, the plane perpendicular to the line of sight. The reference frame of the observer is $\mathcal{B}(\hat{\mathbf{X}}, \hat{\mathbf{Y}}, \hat{\mathbf{Z}})$, with the Z-direction pointing towards the observer. However, the true orbit of the star is inclined to the plane of the sky. To obtain the real orbital plane from the observed orbit, two rotations are necessary, while one other rotation re-orients the orbit in the true

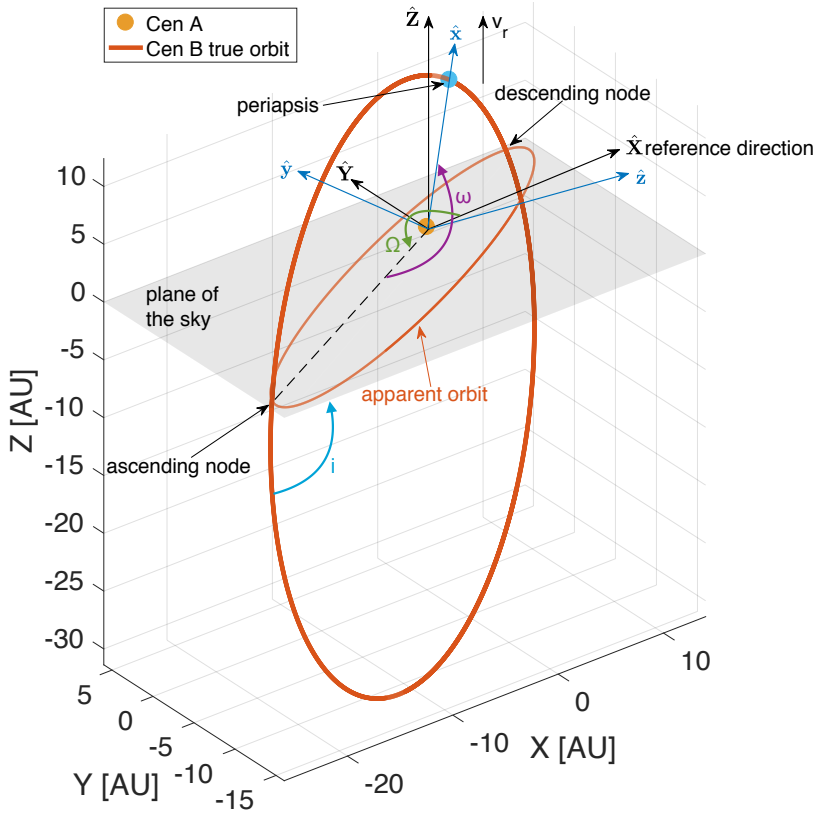

Fig. 32 Relative Cen B orbit about Cen A in the XYZ- and xyz-reference frames with the inclination i, longitude of ascending node Ω and argument of periapsis ω.

orbital plane. The reference frame for the true orbit is the BSRS, $\mathcal{J}_1(\hat{\mathbf{x}}, \hat{\mathbf{y}}, \hat{\mathbf{z}})$. The relationship between both reference frames is depicted in Figure 32, where the three rotations to transform from one frame to another are indicated: Ω as the green angle, i as the blue angle, and ω as the purple angle.

To transform a state vector from $\mathcal{B}(\hat{\mathbf{X}}, \hat{\mathbf{Y}}, \hat{\mathbf{Z}})$ to $\mathcal{J}_1(\hat{\mathbf{x}}, \hat{\mathbf{y}}, \hat{\mathbf{z}})$, the following transformation needs to be applied:

$$\begin{pmatrix} x \\ y \\ z \end{pmatrix} = \mathbf{T}_Z(-\omega)\mathbf{T}_X(i)\mathbf{T}_Z(-\Omega) \begin{pmatrix} X \\ Y \\ Z \end{pmatrix} \tag{31}$$

In the $\mathcal{B}(\hat{\mathbf{X}}, \hat{\mathbf{Y}}, \hat{\mathbf{Z}})$ reference system, the direction of the line connecting the barycenter of Alpha Centauri and the Sun, $\mathbf{s}_{XYZ}$, only has a component in the Z-direction. Given that the distance between Alpha Centauri and the Sun is 4.36 light years or 275,731 AU, the $\hat{\mathbf{X}}, \hat{\mathbf{Y}}, \hat{\mathbf{Z}}$-components are $\mathbf{s}_{XYZ}$ = [0; 0; 275,731] AU. Using Eq. 31 and the orbital elements Ω, ω and i as listed in Table 3, the $\hat{\mathbf{x}}, \hat{\mathbf{y}}, \hat{\mathbf{z}}$-components of the direction of the line connecting the barycenter of Alpha Centauri and the Sun are $\mathbf{s}_{xyz}$ = [213,533; 166,794; 51,101] AU, which results in $\hat{\mathbf{s}}_{xyz}$ = [0.774; 0.605; 0.185].

References

[1] Tsuda, Y., Mori, O., Funase, R., Sawada, H., Yamamoto, T., Saiki, T., Endo, T., and Kawaguchi, J., "Flight status of IKAROS deep space solar sail demonstrator," *Acta Astronautica*, Vol. 69, No. 9–10, 2011, pp. 833 – 840. doi:10.1016/j.actaastro.2011.06.005.

[2] Johnson, L., Whorton, M., Heaton, A., Pinson, R., Laue, G., and Adams, C., "NanoSail-D: A solar sail demonstration mission," *Acta Astronautica*, Vol. 68, No. 5–6, 2011, pp. 571 – 575. doi:10.1016/j.actaastro.2010.02.008.

[3] Ridenoure, R. W., Munakata, R., Wong, S. D., Diaz, A., Spencer, D. A., Stetson, D. A., Betts, B., Plante, B. A., Foley, J. D., and Bellardo, J. M., "Testing The LightSail Program: Advancing Solar Sailing Technology Using a CubeSat Platform," *Journal of Small Satellites*, Vol. 5, No. 2, 2016, pp. 531 – 550.

[4] Betts, B., Spencer, D., Nye, B., Munakata, R., Bellardo, J., Wong, S., Diaz, A., Ridenoure, R., Plante, B., Foley, J., and Vaughn, J., "LightSail 2: Controlled Solar Sailing Using a CubeSat," *Fourth International Symposium on Solar Sailing 2017*, Kyoto, Japan, 2017, p. 7.

[5] McInnes, C. R., *Solar Sailing: Technology, Dynamics and Mission Applications*, Springer - Praxis Books in Astronautical Engineering, Springer-Verlag, Berlin, Germany, 1999.

[6] Heller, R., and Hippke, M., "Deceleration of High-velocity Interstellar Photon Sails into Bound Orbits at α Centauri," *The Astrophysical Journal Letters*, Vol. 835, No. L32, 2017. doi:10.3847/2041-8213/835/2/L32.

[7] Heller, R., Hippke, M., and Kervella, P., "Optimized Trajectories to the Nearest Stars Using Lightweight High-velocity Photon Sails," *The Astronomical Journal*, Vol. 154, No. 115, 2017. doi:10.3847/1538-3881/aa813f.

[8] Aliasi, G., Mengali, G., and Quarta, A. A., "Artificial equilibrium points for a solar balloon in the α Centauri system," *Acta Astronautica*, Vol. 104, No. 2, 2014, pp. 464 – 471. doi:10.1016/j.actaastro.2014.03.006.

[9] Pino, T., and Circi, C., "A star-photon sailcraft mission in the Alpha Centauri system," *Advances in Space Research*, Vol. 59, 2017, pp. 2389 – 2397. doi:10.1016/j.asr.2017.02.014.

[10] Kervella, P., Thévenin, F., and Lovis, C., "Proxima's orbit around α Centauri," *Astronomy and Astrophysics*, Vol. 598, No. L7, 2017. doi:10.1051/0004-6361/201629930.

[11] Thévenin, F., Provost, J., Morel, P., Berthomieu, G., Bouchy, F., and Carrier, F., "Asteroseismology and calibration of α Cen binary system," *Astronomy and Astrophysics*, Vol. 392, No. 1, 2002, pp. L9–L12. doi:10.1051/0004-6361:20021074.

[12] Anglada-Escudé, G., Amado, P. J., Barnes, J., Berdiñas, Zaira M., Butler, R. Paul, Coleman, Gavin A. L., de la Cueva, Ignacio, Dreizler, Stefan, Endl, Michael, Giesers, Benjamin, Jeffers, Sandra V., Jenkins, James S., Jones, Hugh R. A., Kiraga, Marcin, Kürster, Martin, López-González, María J., Marvin, Christopher J., Morales, Nicolás, Morin, Julien, Nelson, Richard P., Ortiz, José L., Ofir, Aviv, Paardekooper, Sijme-Jan, Reiners, Ansgar, Rodríguez, Eloy, Rodríguez-López, Cristina, Sarmiento, Luis F., Strachan, John P., Tsapras, Yiannis, Tuomi, Mikko, and Zechmeister, Mathias, "A terrestrial planet candidate in a temperate orbit around Proxima Centauri," *Nature*, Vol. 536, 2016, pp. 437–440. doi:10.1038/nature19106.

[13] Kervella, P., and Thévenin, F., "A Family Portrait of the Alpha Centauri System," *European Southern Observatory*, 2003, p. eso0307. PR 05/03 - Science Release.

[14] Andrade-Ines, E., and Michtchenko, T. A., "Dynamical stability of terrestrial planets in the binary Alpha Centauri system," *Monthly Notices of the Royal Astronomical Society*, Vol. 444, No. 3, 2014, pp. 2167–2177. doi:10.1093/mnras/stu1591.

[15] Kopparapu, R. K., Ramirez, R. M., SchottelKotte, J., Kasting, J. F., Domagal-Goldman, S., and Eymet, V., "Habitable Zones around Main-sequence Stars: Dependence on Planetary Mass," *The Astrophysical Journal*, Vol. 787, No. 2, 2014, p. L29. doi:10.1088/2041-8205/787/2/L29.

[16] Henry, T. J., Backman, D. E., Blackwell, J., and Okimura, T., "Nearby Stars (NStars) Research," *American Astronomical Society Meeting Abstracts*, Bulletin of the American Astronomical Society, Vol. 32, 2000, p. 1596.

[17] Verbunt, F., and van Gent, R. H., "The star catalogues of Ptolemaios and Ulugh Beg Machine-readable versions and comparison with the modern HIPPARCOS Catalogue," *Astronomy and Astrophysics*, Vol. 544, 2012, p. A31. doi:10.1051/0004-6361/201219596.

[18] Kervella, P., Mignard, F., Mérand, A., and Thévenin, F., "Close stellar conjunctions of α Centauri A and B until 2050 - An m_K = 7.8 star may enter the Einstein ring of α Cen A in 2028," *Astronomy and Astrophysics*, Vol. 594, 2016, p. A107. doi:10.1051/0004-6361/201629201.

[19] Wakker, K., "Fundamentals of Astrodynamics," , 2015. Delft University of Technology Aerospace Engineering lecture notes.

[20] Ridpath, I., *A dictionary of astronomy*, Oxford University Press, Oxford, UK, 2012.

[21] Murray, C. D., and Correia, A. C. M., *Exoplanets*, University of Arizona Press, Tucson, Arizona, USA, 2010, Chap. Keplerian Orbits and Dynamics of Exoplanets, pp. 15–23.

[22] Argyle, R. W., *Observing and Measuring Visual Double Stars*, Springer Science & Business Media, 2012, Chap. The Orbital Elements of a Visual Binary Star, pp. 53–61.

[23] Matthews, R. A. J., "The Close Approach of Stars in the Solar Neighborhood," *Quarterly Journal of the Royal Astronomical Society*, Vol. 35, No. 1, 1994, p. 9.

[24] Pourbaix, D., Nidever, D., McCarthy, C., Butler, R. P., Tinney, C. G., Marcy, G. W., Jones, H. R. A., Penny, A. J., Carter, B. D., Bouchy, F., Pepe, F., Hearnshaw, J. B., Skuljan, J., Ramm, D., and Kent, D., "Constraining the difference in convective blueshift between the components of α Centauri with precise radial velocities," *Astronomy and Astrophysics*, Vol. 386, No. 1, 2002, pp. 280 – 285. doi:10.1051/0004-6361:20020287.

[25] Pourbaix, D., and Boffin, H. M. J., "Parallax and masses of α Centauri revisited," *Astronomy and Astrophysics*, Vol. 586, No. A90, 2016, p. 4. doi:10.1051/0004-6361/201527859.

[26] Pourbaix, D., Tokovinin, A. A., Batten, A. H., Fekel, F. C., Hartkopf, W. I., Levato, H., Morrell, N. I., Torres, G., and Udry, S., "S_{B_9}: The ninth catalogue of spectroscopic binary orbits," *Astronomy and Astrophysics*, Vol. 424, No. 2, 2004, pp. 727–732. doi:10.1051/0004-6361:20041213.

[27] Farres, A., Heiligers, J., and Miguel Baños, N., "Road Map to L4/L5 with a solar sail," *28th AIAA/AAS Space Flight Mechanics Meeting*, Kissimmee, Florida, USA, 2018, p. 21. doi:10.2514/6.2018-0211.

[28] Farrés, A., and Jorba, À., "Periodic and quasi-periodic motions of a solar sail close to SL1 in the Earth–Sun system," *Celestial Mechanics and Dynamical Astronomy*, Vol. 107, No. 1, 2010, pp. 233–253. doi:10.1007/s10569-010-9268-4.

[29] Baoyin, H., and Mcinnes, C. R., "Solar Sail Halo Orbits at the Sun–Earth Artificial L1 Point," *Celestial Mechanics and Dynamical Astronomy*, Vol. 94, No. 2, 2006, pp. 155–171. doi:10.1007/s10569-005-4626-3.

[30] Narayan, A., and Singh, N., "Motion and stability of triangular equilibrium points in elliptical restricted three body problem under the radiating primaries," *Astrophysics and Space Science*, Vol. 352, No. 1, 2014, pp. 57–70. doi:10.1007/s10509-014-1903-1.

[31] Biggs, J. D., McInnes, C. R., and Waters, T., "Control of Solar Sail Periodic Orbits in the Elliptic Three-Body Problem," *Journal of Guidance, Control, and Dynamics*, Vol. 32, No. 1, 2009, pp. 318–320. doi:10.2514/1.38362.

[32] Dachwald, B., "Low-Thrust Trajectory Optimization and Interplanetary Mission Analysis Using Evolutionary Neurocontrol," Ph.D. thesis, Universität der Bundeswehr München, 2004.

[33] Baoyin, H., and McInnes, C. R., "Solar Sail Equilibria in the Elliptical Restricted Three-Body Problem," *Journal of Guidance, Control and Dynamics*, Vol. 29, No. 3, 2006, pp. 538–543. doi:10.2514/1.15596.

[34] Farres, A., "Catalogue on the Dynamics of a Solar Sail around L1 and L2," *The Fourth International Symposium on Solar Sailing*, Kyoto, Japan, 2017, p. 9.

[35] Borggräfe, A., Ohndorf, A., Dachwald, B., and Seboldt, W., "Analysis of Interplanetary Solar Sail Trajectories with Attitude Dynamics," *1st IAA Conference on Dynamics and Control of Space Systems*, Porto, Portugal, 2012, pp. 1553–1569.

[36] Ohndorf, A., "Multiphase Low-Thrust Trajectory Optimization Using Evolutionary Neurocontrol," Ph.D. thesis, Delft University of Technology, 2016.

[37] Dachwald, B., Ohndorf, A., and Wie, B., "Solar Sail Trajectory Optimization for the Solar Polar Imager (SPI) Mission," *AIAA/AAS Astrodynamics Specialist Conference and Exhibit*, Keystone, Colorado, 2006, p. 18. doi:10.2514/6.2006-6177.

[38] Dachwald, B., "Optimal Solar Sail Trajectories for Missions to the Outer Solar System," *Journal of Guidance, Control, and Dynamics*, Vol. 28, No. 6, 2005, pp. 1187–1193. doi:10.2514/1.13301.

[39] Heiligers, J., Diedrich, B., Derbes, W., and McInnes, C., "Sunjammer: Preliminary End-to-End Mission Design," *AIAA/AAS Astrodynamics Specialist Conference*, San Diego, California, USA, 2014, p. 27. doi:10.2514/6.2014-4127.

[40] Guo, Y., "Parker Solar Probe Mission Design," *AAS/AIAA Astrodynamics Specialist Conference*, Portland, Maine, USA, 2019, p. 18.

3

Conclusion and Recommendations

In this thesis work, capture trajectories were optimized for a photon sail coming from our Solar System into Alpha Centauri, which is seen as the prime target for interstellar travel. By introducing a capture phase to the mission, the idea of a flyby-mission is surpassed, meaning that there is more scientific yield on such an innovative mission. In this chapter, the results of the work are evaluated in section 3.1 based on the research questions introduced in chapter 1, after which recommendations for future work are provided in section 3.2.

3.1. Conclusion

To represent the conclusions from the paper in another way, this section provides the answers to the research questions. Note that additional research was performed after the below research question were answered. Next to a capture phase, two phases were added: a transfer phase from the star about which the sail is captured to the other star of the binary system of Alpha Centauri and a subsequent orbit-raising phase about the latter star. Time-optimal solutions were found for these two phases and were based on the outcome of the capture phase. By adding two mission applications, more knowledge was gained into the orbital dynamics of a photon sail in Alpha Centauri.

1) Is it possible to get captured into an orbit about Centauri A or B?

With this thesis, it is shown that it is possible to get captured into an orbit in the habitable zone of one of the stars, using the stellar photons of Alpha Centauri A and Alpha Centauri B, two Sun-like stars, and their gravitational attraction. Although it is technically possible to perform capture trajectories with a one-sided reflective sail, the time of flight from our Solar System to Alpha Centauri would be eight times longer than for a two-sided reflective sail. As a result, it was concluded that a two-sided reflective sail would be a requirement to perform the proposed mission scenario. The latter sail configuration allows to perform photogravitational assists at the stars, maneuvers that are crucial to dispose of kinetic energy at arrival.

Table 3.1: Time of flight comparison of capture trajectories about Cen A and Cen B coming from our Solar System for a two-sided reflective sail.

		Capture into orbit about ...		
Sail	Lightness number wrt Sun	Cen A (yrs)	Cen B (yrs)	Improvement in %
Sail A	0.04	**18,790**	>70,000	73.2
Sail B	0.765	**2293**	3618	36.6
Sail C	4.37	2409	**1950**	19.1
Sail D	1779	132.3	**111.5**	15.7

Table 3.1 shows the time-optimal results for capture trajectories into a circular and prograde orbit about Alpha Centauri A and Alpha Centauri B for four different sails - sail A to sail D - with their corresponding lightness number with respect to the Sun as shown in Table 3.1. The time of flight in bold is the best solution for a given sail. When considering the four sails, the improvement for capture about the optimal star compared to the other star is smaller for larger lightness numbers, going from sail A to sail D. In addition, the star

about which the sail gets captured changes from Cen A to Cen B for lightness numbers larger than one, as the radiation pressure of the star is the dominant factor for sail C and sail D, whereas for sail A and sail B the gravitational acceleration is the dominant factor. As a result, for sail C and sail D, the more luminous star is used to maximize deceleration.

2) What is the maximum injection speed at which the spacecraft can still be captured into an orbit about Centauri A or B?

While Voyager 1 is traveling in outer space with a velocity of 0.01 AU a day, the sail proposed by the Breakthrough Starshot project would arrive at Alpha Centauri with an injection speed of 35 AU a day. In this work, however, the maximum injection speeds are found well within those extremes. The injection velocity was part of the objective function for the optimization of the capture phase, such that the maximum injection velocity was found for which capture is still possible. Figure 3.1 shows an overview of the results for the four different lightness numbers investigated with respect to the time of flight and the percentage of speed of light. The sails and lightness numbers are the same as those presented in Table 3.1. Note that the results shown in Figure 3.1 are for capture maneuvers resulting in a prograde and circular orbit about the star. Figure 3.1 shows that maximum injection velocities of 0.023%, 0.19 % , 0.23% and 3.9% of the speed of light are found for sails A to D, respectively. However, when arriving in a retrograde and highly elliptical orbit at Alpha Centauri B, a maximum injection velocity of up to 5.52% of the speed of light was found for sail D, corresponding to a travel time of 77.6 years from our Solar System to the eccentric orbit about Alpha Centauri B, which is similar to the result found by the referenced work by Heller and Hippke (2017) [17]. Note, however, that this reference work did not consider that the sail is being captured into an orbit about that star. Instead, it focused on using the characteristics of the binary star to travel to Proxima Centauri. Finally, for sails with lightness numbers smaller than the lightness number of sail D, the results in this work show an improvement in transfer time of approximately 30% over previous work.

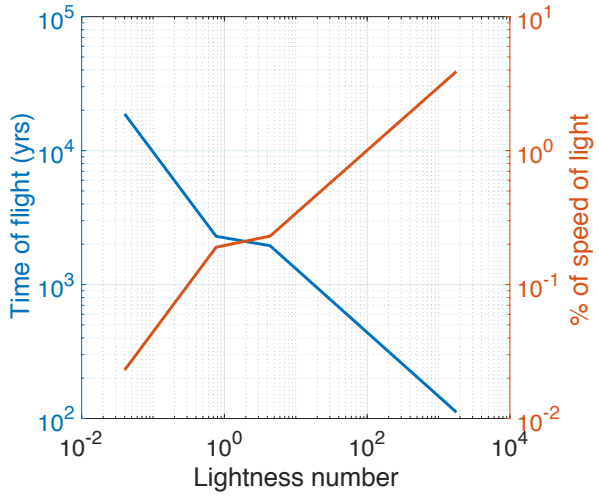

Figure 3.1: Overview of the results. The left vertical axis shows the time of flight in years, while the right vertical axis shows the percentage of speed of light for the investigated lightness numbers.

3) What is the required performance of the sail for interstellar travel to Alpha Centauri?

The four sails considered during this thesis are ranging from nowadays technology to a very optimistic graphene-based sail. The latter sail could travel from our Solar System to Alpha Centauri within 100 years. However, it is found to be extremely challenging for such a futuristic high-technology sail to perform orbit raising at arrival, as the force of the stellar radiation pressure acting on the sail is too large while being close to the star. Therefore, it is suggested to jettison the sail at arrival when those maneuvers are considered a part of the mission.

A sail configuration as proposed by the Breakthrough Starshot project would be capable to explore the binary star system by transferring between the stars and by increasing its orbit from the center of the habitable zone to its outer edge, for example. Although the Breakthrough Starshot project aims to travel to Alpha

Centauri within 20 years, a travel time of a hundred times more was found in case that sail would be captured into the binary star system, instead of performing a flyby.

Therefore, to be captured in Alpha Centauri and to keep the travel time within a few generations, a sail with the performance such as sail D would be required. However, the graphene-based sail technology is not expected to be ready for launch in the coming years. With this in mind, it is suggested to consider a flyby-mission, as proposed by the Breakthrough Starshot project, as the inaugural mission. By then, the technology might have been developed such that the capture phase can be added to the mission.

3.2. Recommendations

This research project conducted a first examination of an ideal photonic sail performing multiple orbital maneuvers in a binary star system. The results obtained show an abundance of potential for interstellar exploration in Alpha Centauri. After performing such an innovative research project, the list of recommendations for future work is endless, such is the potential of mission applications of a photon sail in Alpha Centauri. Taking into account that this work is the first in what could be a series of various theses topics, three different paths as a follow-up research topic are suggested below:

1. Implement the real sail model into the software, such that the trajectories can be considered with a more realistic non-perfectly reflective sail. As a result, more physical and technological aspects of a real mission can be considered, such as the temperature of the sail or relativistic effects during close encounters with the stars.

2. Build on this work and extend the mission applications to periodic orbits about an artificial equilibrium point. The area about the L_1-point in between the binary stars is considered as a perfect target for such a periodic orbit, as this is one of the locations where both stars could be observed simultaneously. In this work, the elliptical restricted three-body problem is examined, as well as the artificial equilibrium points and its periodic orbits. However, the results shown were in Alpha Centauri's orbital plane. It would be interesting to show out-of-plane periodic orbits in this system. The two methods proposed by Biggs et al. (2009) (numerical continuation and a time-delayed feedback mechanism) can be of use to kick-off this research [20].

3. Close the gap to the Breakthrough Starshot project and target Proxima Centauri or even Proxima b, the Earth-like planet. Optimizing transfer trajectories to the closest star to the Earth (after the Sun) or to planets around it is believed to be very attractive and valued research to contribute to interstellar travel.

Finally, some other recommendations are made based on the applied software InTrance. The benefits of the toolbox were obvious during the course of this work. After tailoring the software for this specific interstellar problem - by implementing a new stellar system and updating the sail's force model - the tool was ready to be used without having to make major changes elsewhere in the structure of the software. InTrance was proven to be applicable to a wide variety of mission scenarios without the need for heavy modifications. By making small adjustments to the input files (see an example in Appendix B), the software is immediately ready to switch from a capture trajectory optimization problem to a transfer rendezvous with another body. Also, the fact that no astrodynamical knowledge is required to perform optimization runs was clear from the results. Without the need to steer the optimization tool into the right direction, the evolutionary neurocontroller found that photogravitational assists about the companion star resulted in the best time-optimal trajectories. However, since InTrance only requires a broad description of the mission scenario, the results of each simulation run were found to differ slightly for the same simulation configuration. Therefore, it can be concluded that InTrance may not be the most robust optimization tool. Although this optimization problem can be solved with another, potentially more robust optimization algorithm such as PSOPT[1], there would be a need for an initial guess, resulting in removing that degree of freedom which is seen as a major benefit of InTrance. Although a comparison between optimization algorithms is out of the scope of this thesis work, a list of recommendations related to the optimization tool is provided below:

- In a search for better results, an additional constraint could be added to set the number of close encounters at the binary stars. By increasing that number for a relatively small lightness number, more photogravitational assists would be performed, which could result in a decrease in travel time.

[1] See the open-source optimal control software package at `http://www.psopt.org`, Retrieved August 19 2019

- In InTrance, the capture problem was considered as an escape problem, such that the target orbit after capturing becomes the initial condition of the escape problem. However, the orbital parameters of this initial condition had to be provided, without any freedom. Therefore, it is recommended to implement an additional routine that optimizes the initial orbital parameters as well. As an example, a window of options for the mean anomaly or eccentricity could be provided.
- In the current version of InTrance, the equations of motion are based on Cartesian and polar coordinates to represent the state of the spacecraft, with the orbital elements described by the classical Keplerian elements. During the course of this research, however, a singularity was found when the eccentricity of the sail's orbit approaches one, such that the trajectory is parabolic. This is a known problem and the proposed solution is to implement the modified equinoctial orbital elements, which would result in singularity-free orbital elements for a parabolic trajectory.
- Look into the library of the evolutionary neurocontrol. In this work, the optimization technique itself was considered as a black box. However, over the years since the first development of InTrance, the evolutionary algorithms, aritificial intelligence and machine learning methods improved. Therefore, it is recommended to update the optimization technique in InTrance with those improved algorithms.
- Make InTrance compatible with Linux systems, such that simulations can run on more powerful servers at the faculty of Aerospace Engineering at the Delft University of Technology.

A

Verification and Validation

This first appendix discusses the verification and validation of the major methods applied during this thesis work.

A.1. Alpha Centauri configuration

An extensive portion of the workload focused on determining the configuration of Alpha Centauri's binary star, to understand the entry conditions of a photon sail coming from our solar system. Here, it is shown that the implemented configuration of Alpha Centauri matches with references and with the observations made [17, 21].

Figure A.1 shows the relative orbit of Alpha Centauri B about Alpha Centauri A as seen from Earth for both the result of this work and the result of the reference that is based on observations [21]. Comparing both figures, it can be seen that both configurations match one-to-one.

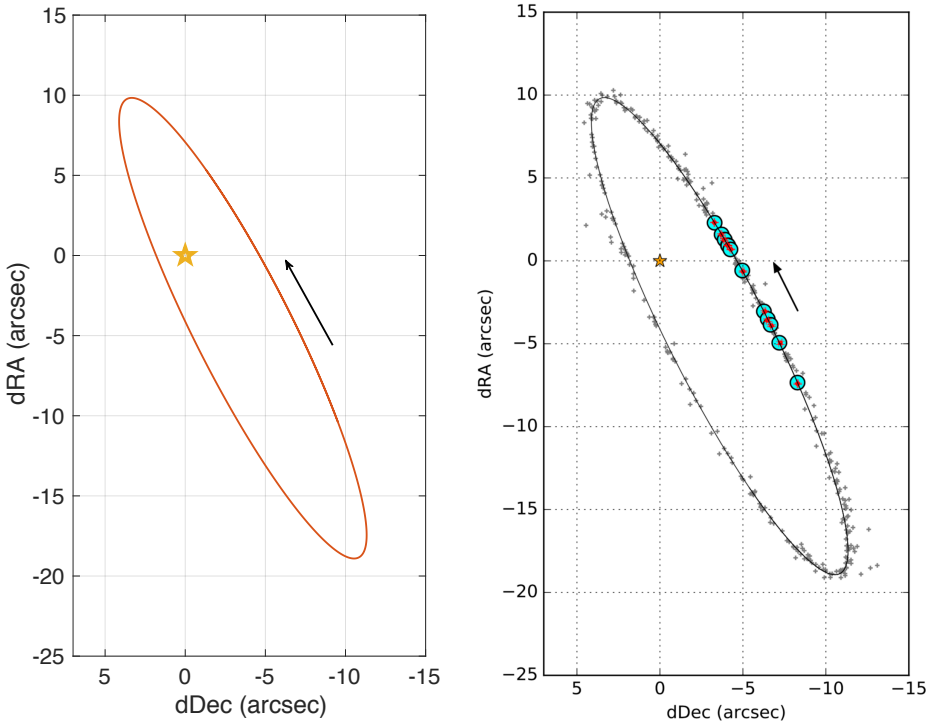

(a) Result of this research project.

(b) Reference result showing observations [21].

Figure A.1: Relative orbit of Alpha Centauri B about Alpha Centauri A as seen from Earth.

Alpha Centauri's configuration can also be verified with its absolute orbits about the barycenter of the

binary stars. Figure A.2 can be used to realize that, again, the implemented configuration for Alpha Centauri is in agreement with the reference [17].

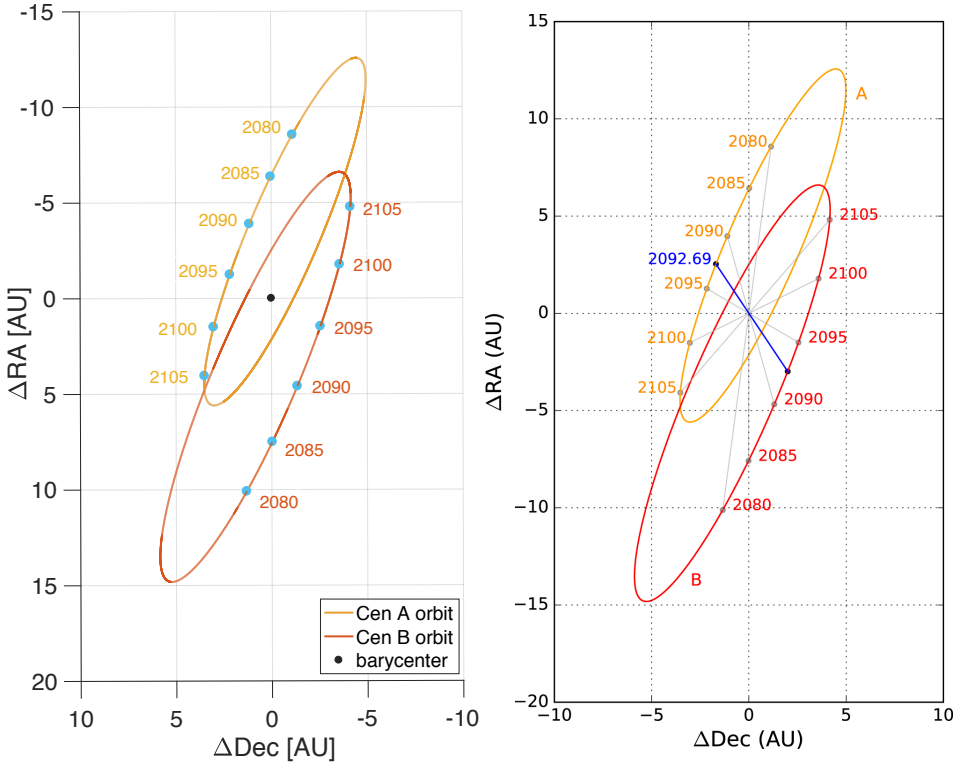

(a) Result of this research project, showing the position of the stars for various dates.

(b) Reference result, indicating the position of the stars for certain years [17].

Figure A.2: Absolute orbit of Alpha Centauri's binary star system as seen from Earth.

A.2. Lightness number contour plots

The implementation of the elliptical restricted three body problem for this work resulted in new insights in artifical equilibrium points for a photon sail subjected to stellar photonic pressure of two radiative bodies. To verify the correct implementation of this model, the characteristics of Alpha Centauri A and B were changed to those of the Sun and the Earth. This way, the outcome of the newly implemented model can be compared to the well-known equilibrium curves for the Sun-Earth circular restricted three body problem. Therefore, the model was changed to a circular case by setting the eccentricity to zero. Moreover, the luminosities of the two bodies of the model were modified. While one body was given the characteristics of the Sun, the other body representing Earth was given a very small luminosity, to assure that the equations of the new model for two radiative bodies were still considered. The outcome of this circular restricted three body problem considering two radiative bodies - although one very small - is compared with solar sail lightness number contours from the literature [22] (Figure 5.26, page 220).

Figures A.3 - A.5 show the results obtained with the modified elliptical restricted three body model for two radiative bodies on one side, while the other side shows the result obtained with the circular restricted three body model for one radiative body. The reference frame (x, y, z) used in these figures is a rotating frame that is common for the classical restricted three-body problem, with the barycenter of the system as the origin, the x-axis connecting the Sun and Earth, pointing in Earth's direction. The z-axis is defined perpendicular to the orbital plane of both bodies, while the y-axis completes the right-handed reference frame [22]. For the xy-view, the xz-view and the detail of the xz-view, the same results are obtained as the reference [22].

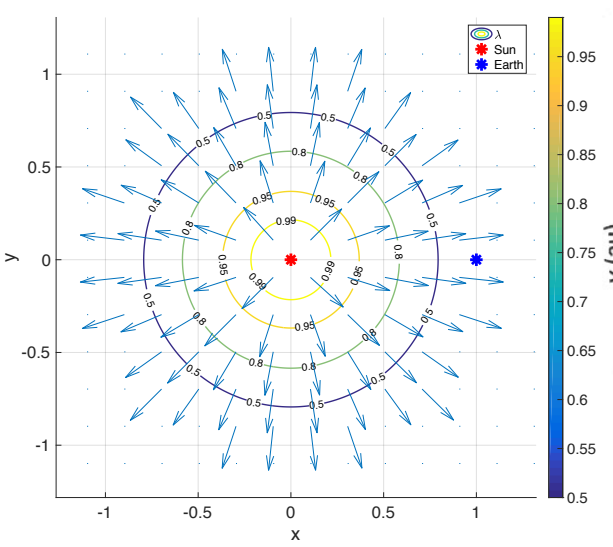

(a) Result of the modified elliptical restricted three body model for two radiative bodies.

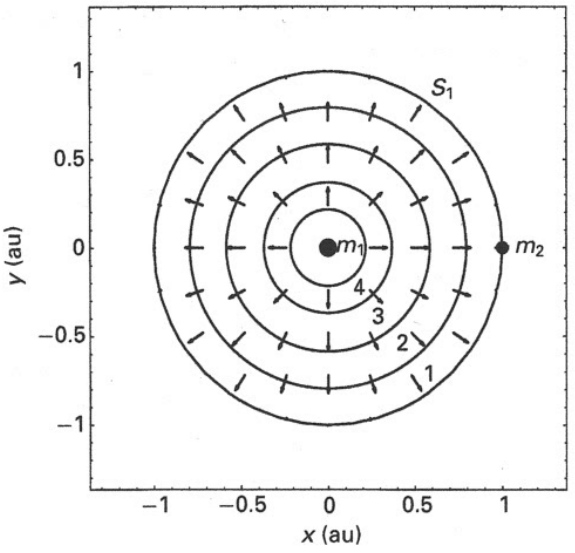

(b) Result of the circular restricted three body model for one radiative body. Lightness numbers: n° 1 = 0.5, n° 2 = 0.8, n° 3 = 0.95 and n° 4 = 0.99 [22].

Figure A.3: Lightness number contour plots in xy-plane.

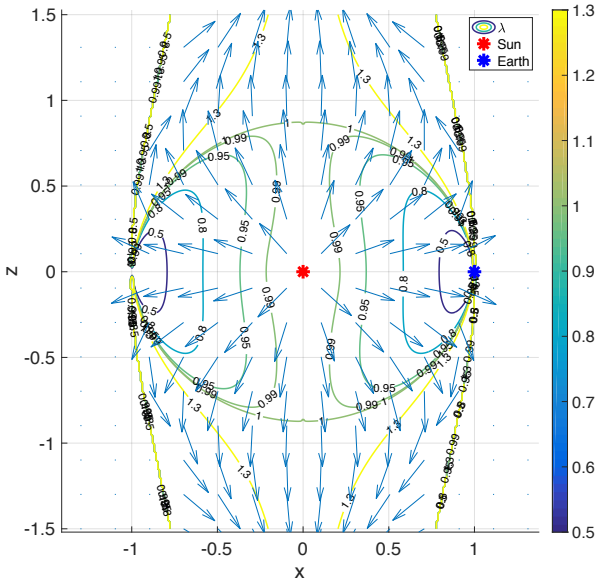

(a) Result of the modified elliptical restricted three body model for two radiative bodies.

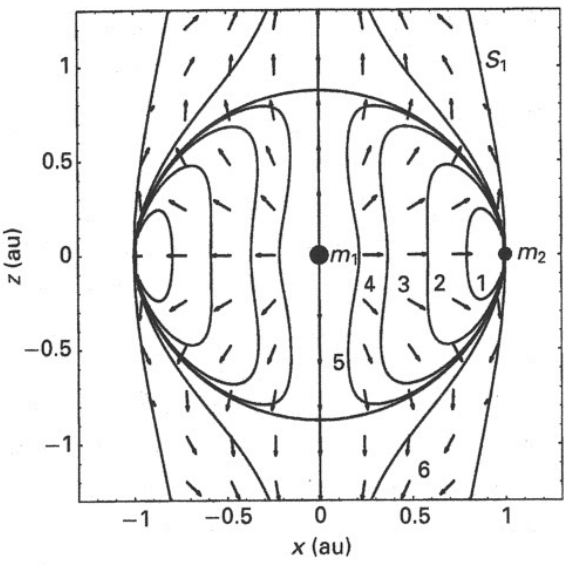

(b) Result of the circular restricted three body model for one radiative body. Lightness numbers: n° 1 = 0.5, n° 2 = 0.8, n° 3 = 0.95, n° 4 = 0.99 and n° 5 = 1.0 [22].

Figure A.4: Lightness number contour plots in xz-plane.

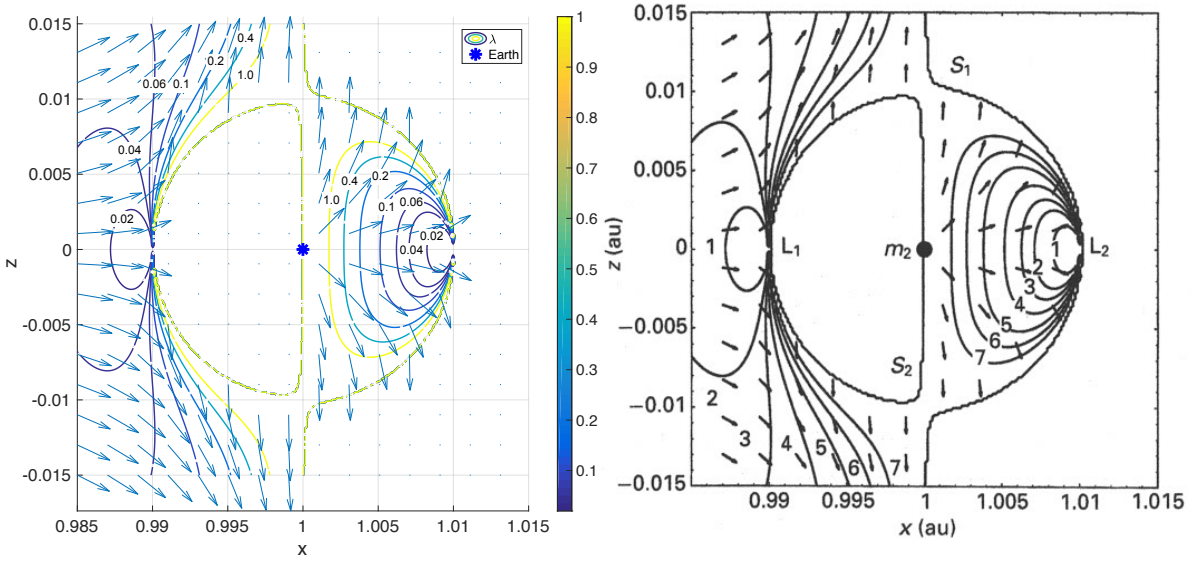

(a) Result of the modified elliptical restricted three body model for two radiative bodies.

(b) Result of the circular restricted three body model for one radiative body. Lightness numbers: n° 1 = 0.02, n° 2 = 0.04, n° 3 = 0.06, n° 4 = 0.1, n° 5 = 0.2, n° 6 = 0.4 and n° 7 = 1.0 [22].

Figure A.5: Detail of lightness number contour plots in xz-plane.

A.3. Force model

Besides adapting the stellar system within InTrance, the force model also required an update. With a sail orbiting in a binary star system, an additional stellar photonic pressure force was added to the model.

To verify the model, a straightforward orbit raising maneuver was performed for an initial orbit of two AU to a target orbit of three AU around Cen A, as is illustrated in Figure A.6.

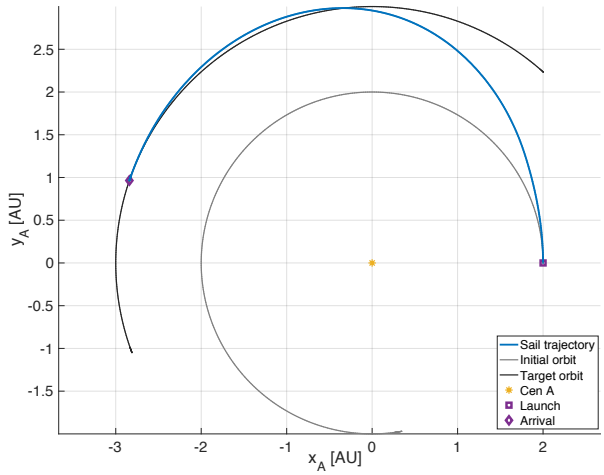

Figure A.6: Orbit raising maneuver used for the verification of the force model.

The result of the simulation was then used in a Matlab-script that integrates the trajectory again based on the steering strategy of InTrance's simulation. Thus, with the initial condition of the Matlab-based verification script being the same as the InTrance simulation, the cone and clock angles are used to reintegrate the trajectory.

The Matlab simulation and more specifically the integration of the equations of motion was verified throughout the thesis work using the results of multiple references [22–24]. Two examples of this verification is shown in Figure A.7. Note that the left side shows the result from this thesis work, while the right side shows the result of the reference [23, 24].

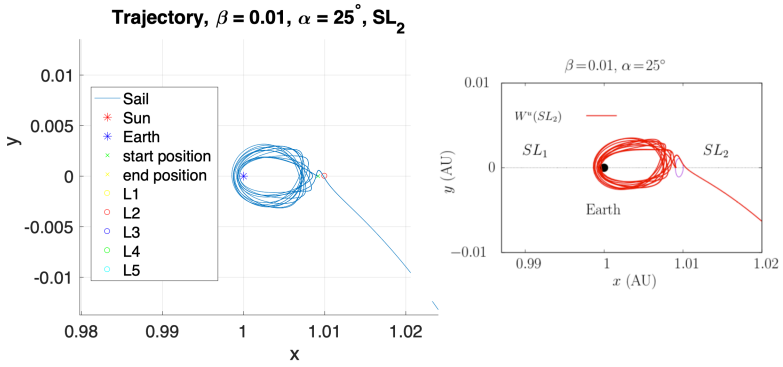

(a) Comparing the propagation of an initial condition on the SL_2 unstable manifold with [23].

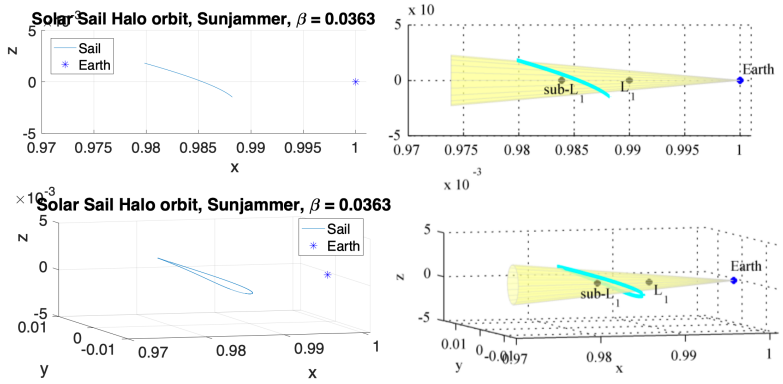

(b) Comparing the Halo orbit for Sunjammer's ideal solar sail with [24].

Figure A.7: Verification of Matlab integration script.

The difference between the reintegrated trajectory in Matlab (left column) and the outcome of InTrance (centered column) in terms of position and velocity in x-, y- and z-direction are presented in Figure A.8 and Figure A.9, respectively. In the latter figure, the build-up of numerical integration errors are observable. With such an accuracy, it can be concluded that the force model was correctly implemented into InTrance.

A.4. Backwards integration

Since the problem of finding the time-optimal capture trajectory was solved in InTrance as an escape problem, the trajectory was propagated backwards in time. Such a major change compared to forwards propagation requires verification.

A similar orbit maneuver as for the verification of the force model was used as a test case for verification of the backwards integration, as shown in Figure A.10. The difference, however, is that this orbit is decreased in its distance to the star from three to two AU about Cen A.

The process of backwards integration is then verified by integrating the trajectory forwards in time in the Matlab verification script. Therefore, the final state conditions of the InTrance simulation was used as the initial conditions for the Matlab simulation.

The difference between the forwards-reintegrated trajectory in Matlab (left column) and the outcome of the backwards-integrated InTrance simulation (centered column) in terms of position and velocity in x-, y- and z-direction are presented in Figure A.11 and Figure A.12, respectively, with the arrows indicating the forwards or backwards integration. Again, the difference in velocity shows a build-up in numerical error. With an accuracy of up to tenths of kilometers over a transfer time of about two years, the accuracy is found to be sufficient to verify the process of backwards integration.

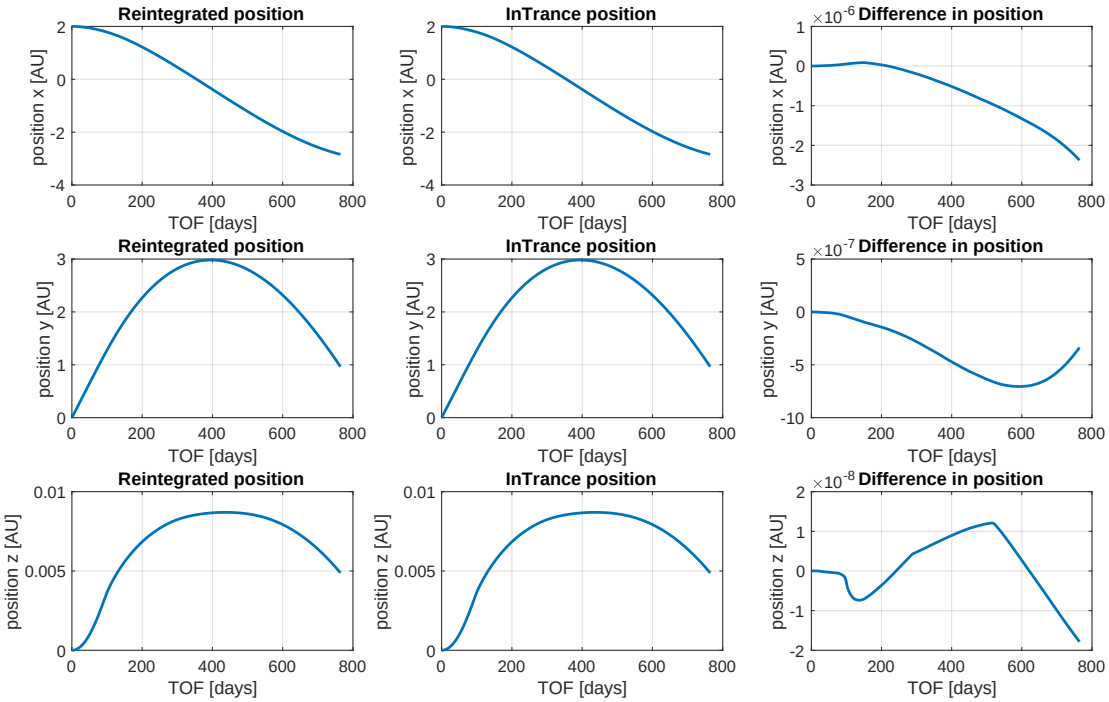

Figure A.8: Verification of the new force model, Cartesian position.

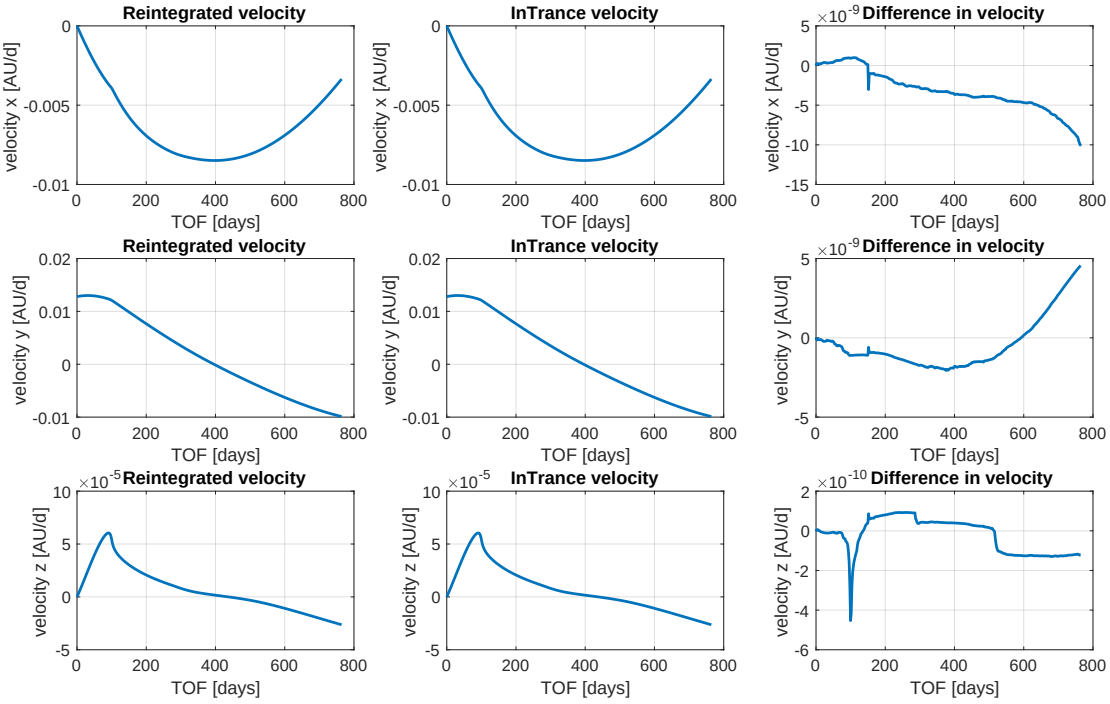

Figure A.9: Verification of the new force model, Cartesian velocity.

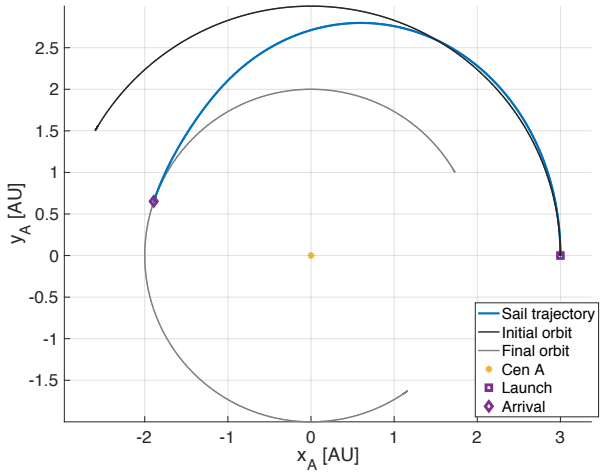

Figure A.10: Example of an orbital reduction in distance from three to two AU to verify the backwards integration.

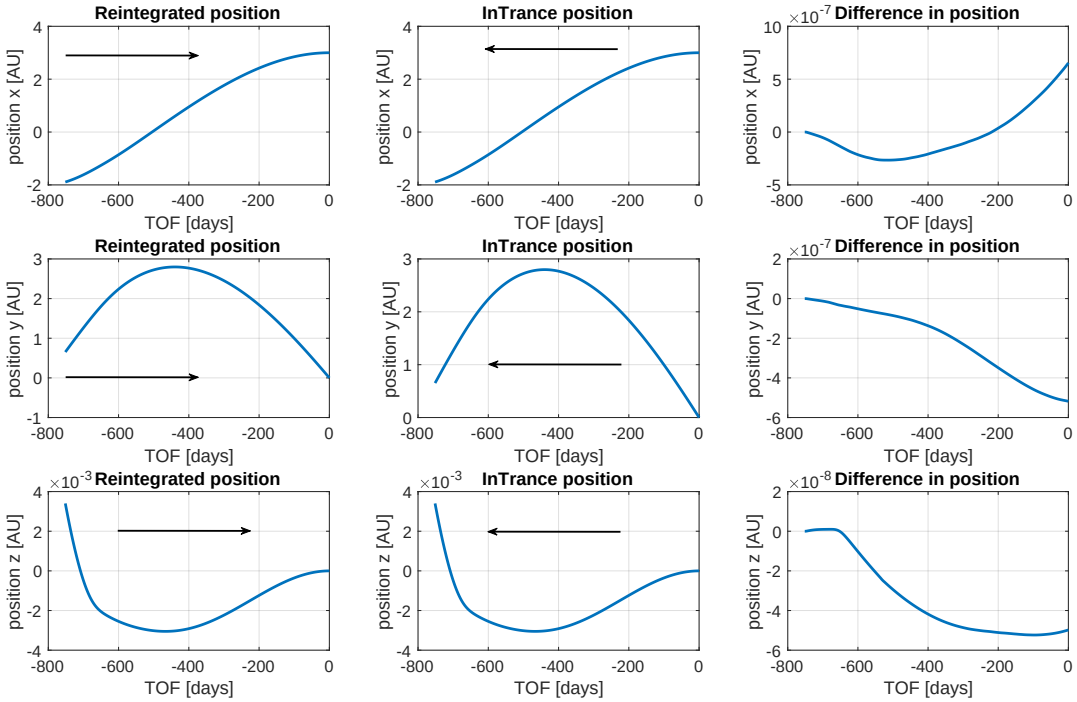

Figure A.11: Verification of the process of backwards integration, Cartesian position.

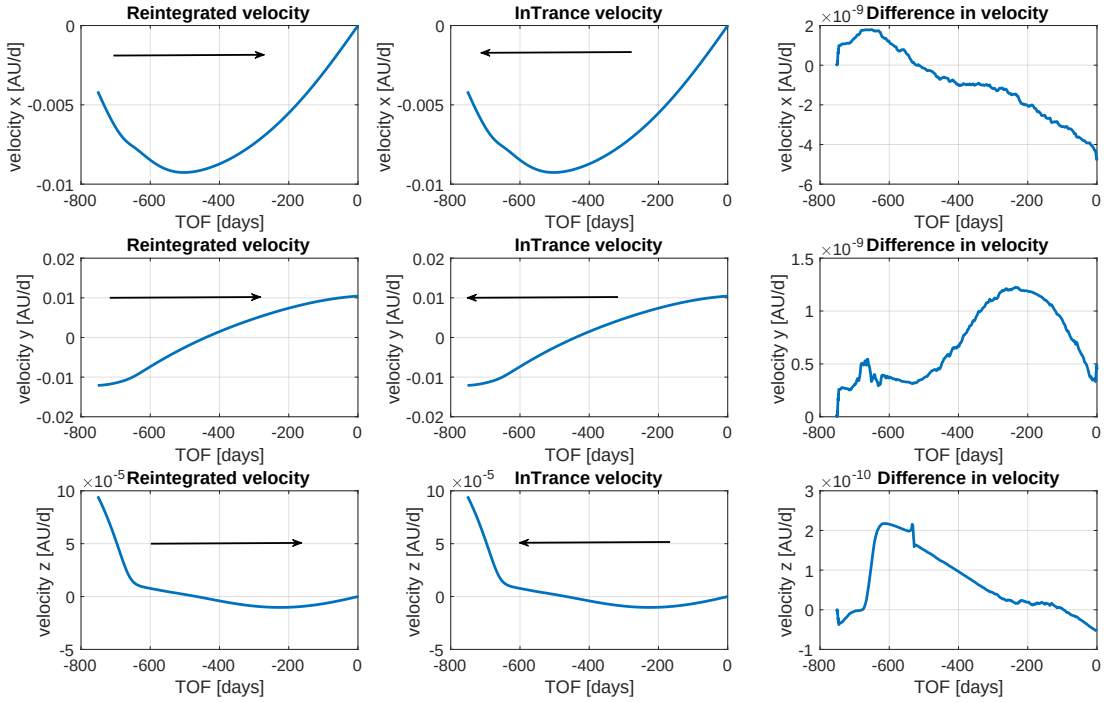

Figure A.12: Verification of the process of backwards integration, Cartesian velocity.

B

InTrance

This appendix shows the input configuration files used in InTrance. With these five files, all information is provided to perform a capture trajectory optimization.

B.1. InTrance Configuration

```
RANDOM_SEED = 92500

COMMAND             = optimize

SIM_PARAM_FILE_1    = coldstart_solarsail.sim

EA_PARAM_FILE       = coldstart_solarsail.eap

COLDSTART           = YES

SIM_DATA_FILE       = ..\Output files\coldstart_solarsail.csv
TRAJ_DATA_FILE      = ..\Output files\coldstart_solarsail.dat
GESOP_FILE          = ..\Output files\coldstart_solarsail.gesop.txt
VRML_FILE           = ..\Output files\coldstart_solarsail.wrl
CTRL_FILE           = ..\Output files\coldstart_solarsail.ctr
BEST_CHROM_FILE     = ..\Output files\coldstart_solarsail.eac
REPORT_FILE         = ..\Output files\coldstart_solarsail.rep
```

B.2. Evolutionary Algorithm Configuration

```
SEARCH_SPACE_HYPERCUBE_SIZE       = 1.0
HYPERCUBE_START_SIZE              = 1.0
HYPERCUBE_SHRINKING_FACTOR        = 0.75
HYPERCUBE_FACTOR_ON_GOOD_REPRODUCTION = 1.0
HYPERCUBE_FACTOR_ON_BAD_REPRODUCTION = 1.1
POPULATION_SIZE                   = 50
POPULATION_SIZE_SSS               = 200
SEARCH_SCAN_EPOCHS                = 12
FITNESS_FUNCTION_TYPE             = J_AND
CHROMOSOME_MUTATION_PROBABILITY = 0.8
CHROMOSOME_INIT_MODEL             = RANDOM_LINEAR
GENOM_MUTATION_PROBABILITY        = 1E-3
SELECTION_PRESSURE_ON_TIME        = 0.03
HYPERCUBE_UPPER_LIMIT             = 1.0E-2
```

```
FBC_MET_FITNESS                 = 0.00
IL_POP_CONV_FBC_MET             = 1.0E-6
IL_POP_CONV_FBC_NOT_MET         = 1.0E-5
IL_EA_CONV_FBC_MET              = 1.0E-6
IL_EA_CONV_FBC_NOT_MET          = 1.0E-4
DYN_OP_PROB                     = TRUE
```

B.3. Neurocontroller Configuration

```
HIDDEN_LAYERS               = 1
NEURONS_IN_HIDDEN_LAYER1 = 12
//NEURONS_IN_HIDDEN_LAYER2 = 5
NC_OUTPUT                   = direct
TRANSFER_FUNCTION           = sigmoid
```

B.4. Spacecraft Configuration

```
SC_TYPE                     = solar sail
LIGHTNESS_NUMBER = 981
OPTICAL_SAIL_MODEL = ideal
CONE_ANGLE_MAX = 90DEG
```

B.5. Simulation Configuration

```
SIM_START_TIME_MIN                  = 38760
SIM_START_TIME_MAX                  = 67980
FLIGHT_TIME_MIN             = 1JYR
ARRIVAL_DATE_MIN                    = 0
INTEGRATION_INTERVAL                = 15JYR
INTEGRATION_STEPS                   = 1000
MIN_OUTPUT_POINTS                   = 100
MODIFY_INIT_PARAMETERS      = yes
MODIFY_LAUNCH_DATE = yes
MODIFY_INIT_DISTANCE = yes
MODIFY_INIT_AZI = yes
MODIFY_INIT_ELE = yes
MODIFY_INIT_VEL = yes
MODIFY_INIT_OFA = yes
MODIFY_INIT_FPA = yes
DYN_INTEGRATION_INTERVAL            = YES
MIN_CEN_B_DISTANCE                  = 0.0200512212au
MIN_CEN_A_DISTANCE                  = 0.0284182855au

DISTURBING_BODIES                   = "disturbingbodies.sim"

USE_DSSC                            = YES
DSSC_STEP_DISTANCE_CONTROL          = NO
DSSC_STEP_ANGLE_CONTROL             = YES
DSSC_MAX_STEP_ANGLE                 = 2.0deg
DSSC_MAX_STEP_SIZE                  = 0.1JYR
DSSC_MIN_STEP_SIZE                  = 2.0day
DSSC_APPROACH_CONTROL               = NO
DSSC_DISTURBING_CONTROL               = YES
```

```
INITIAL_STATE                          = orbit
INITIAL_CENTRAL_BODY                   = SUN
INITIAL_BODY_NAME                      = SUN
INITIAL_FRAME_EQUATORIAL               = false
INITIAL_SEMIMAJOR_AXIS                 = 0.967au
INITIAL_ECCENTRICITY                = 0.0
INITIAL_INCLINATION                 = 0.0deg
INITIAL_MEAN_ANOMALY                = 0deg
INITIAL_VINF_MIN = 0.0KM/S
INITIAL_VINF_MAX = 0.0KM/S
INITIAL_VINF_AZIMUTH_MIN = 0.0RAD
INITIAL_VINF_AZIMUTH_MAX = 360deg
INITIAL_VINF_ELEV_MIN = -180deg
INITIAL_VINF_ELEV_MAX = 180deg
INITIAL_DISTANCE_MIN = 0.693au
INITIAL_DISTANCE_MAX = 1.241au
INITIAL_AZIMUTH_MIN = -360deg
INITIAL_AZIMUTH_MAX = 360deg
INITIAL_ELEVATION_MIN = -360deg
INITIAL_ELEVATION_MAX = 360deg
INITIAL_ORBIT_ANGLE_MIN = -180deg
INITIAL_ORBIT_ANGLE_MAX = 180deg
INITIAL_FPA_MIN = -180deg
INITIAL_FPA_MAX = 180deg

TARGET_STATE                           = body flyby
TARGET_BODY_NAME                       = pluto

TARGET_DIST_MAX_INIT                   = 4.0au
TARGET_DIST_MAX_FINAL                  = 4.0au
TARGET_DIST_MAX_SHRINK                 = 0.5
TARGET_DIST_MAX_DECREASE               = 50.0au
TARGET_DIST_MAX_REDUCTION_USE_MAX = FALSE

OPTIMIZATION_GOAL                      = minimum transfer time
ACCURACY_FITNESS_FRACTION              = 0.1
INTEGRATOR                             = RKF54
DES_CALLS_MAX                          = 5000000
MAX_RELATIVE_ERROR                     = 1.0E-9
MAX_ABSOLUTE_ERROR                     = 1.0E-9
USE_ITGR_STOPPER                       = yes
ALWAYS_USE_OBJ_FCN                     = yes

SC_CONF                                = spacecraft.scp

NAV_TYPE                               = ANN
NAV_ANN_CONF                           = control.ncp

//USE_ROTATION_DYNAMICS                    = TRUE

STEERING_DYN_UNIT_CALC              = TRUE
STEERING_USE_RANGE                     = yes
STEERING_USE_RANGE_RATE                = yes
STEERING_USE_ACC_THRUST_MAX         = FALSE
STEERING_USE_ACC_THRUST_MAX_DRY     = FALSE
STEERING_USE_STEP_SIZE              = TRUE
```

```
STEERING_USE_TIME_UNTIL_PERI_SC  = no
STEERING_USE_TIME_UNTIL_PERI_TGT = no

STEERING_USE_ABS_CART_POS_X      = TRUE
STEERING_USE_ABS_CART_POS_Y      = TRUE
STEERING_USE_ABS_CART_POS_Z      = TRUE

STEERING_USE_ABS_CART_VEL_X      = TRUE
STEERING_USE_ABS_CART_VEL_Y      = TRUE
STEERING_USE_ABS_CART_VEL_Z      = TRUE

STEERING_USE_ABS_POLAR_POS_R     = TRUE
STEERING_USE_ABS_POLAR_POS_AZI   = TRUE
STEERING_USE_ABS_POLAR_POS_ELE   = TRUE

STEERING_USE_ABS_POLAR_VEL_R     = TRUE
STEERING_USE_ABS_POLAR_VEL_AZI   = TRUE
STEERING_USE_ABS_POLAR_VEL_ELE   = TRUE

//STEERING_USE_TGT_CART_POS_X      = yes
//STEERING_USE_TGT_CART_POS_Y      = yes
//STEERING_USE_TGT_CART_POS_Z      = yes

//STEERING_USE_TGT_CART_VEL_X      = yes
//STEERING_USE_TGT_CART_VEL_Y      = yes
//STEERING_USE_TGT_CART_VEL_Z      = yes

STEERING_USE_TGT_CART_POS_REL_X    = yes
STEERING_USE_TGT_CART_POS_REL_Y    = yes
STEERING_USE_TGT_CART_POS_REL_Z    = yes

//STEERING_USE_TGT_CART_VEL_REL_X    = yes
//STEERING_USE_TGT_CART_VEL_REL_Y    = yes
//STEERING_USE_TGT_CART_VEL_REL_Z    = yes
```

Bibliography

[1] P. Lubin. A roadmap to interstellar flight. *Journal of the British Interplanetary Society*, 69(2):40 – 77, 2016.

[2] Y. Tsuda, O. Mori, R. Funase, H. Sawada, T. Yamamoto, T. Saiki, T. Endo, and J. Kawaguchi. Flight status of ikaros deep space solar sail demonstrator. *Acta Astronautica*, 69(9–10):833 – 840, 2011.

[3] L. Johnson, M. Whorton, A. Heaton, R. Pinson, G. Laue, and C. Adams. Nanosail-d: A solar sail demonstration mission. *Acta Astronautica*, 68(5–6):571 – 575, 2011.

[4] R. W. Ridenoure, R. Munakata, S. D. Wong, A. Diaz, D. A. Spencer, D. A. Stetson, B. Betts, B. A. Plante, J. D. Foley, and J. M. Bellardo. Testing the lightsail program: Advancing solar sailing technology using a cubesat platform. *Journal of Small Satellites*, 5(2):531 – 550, 2016.

[5] B. Betts, D. Spencer, B. Nye, R. Munakata, J. Bellardo, S. Wong, A. Diaz, R. Ridenoure, B. Plante, J. Foley, and J. Vaughn. Lightsail 2: Controlled solar sailing using a cubesat. In *Fourth International Symposium on Solar Sailing 2017*, page 7, Kyoto, Japan, 2017.

[6] R. McKay, M. Macdonald, J. Biggs, and C. McInnes. Survey of highly non-keplerian orbits with low-thrust propulsion. *Journal of Guidance, Control, and Dynamics*, 34(3):645–666, 2011.

[7] J. Heiligers, M. Macdonald, and J. S. Parker. Extension of earth-moon libration point orbits with solar sail propulsion. *Astrophysics and Space Science*, 361(7):20, 2016.

[8] J. Heiligers, B. Diedrich, W. Derbes, and C. McInnes. Sunjammer: Preliminary end-to-end mission design. In *AIAA/AAS Astrodynamics Specialist Conference*, page 27, San Diego, California, USA, 2014.

[9] J. Heiligers and C. McInnes. Novel solar sail mission concepts for space weather forecasting. In *Advances in the Astronautical Sciences*, volume 152, page 20, Santa Fe, New Mexico, USA, 2014. 24th AAS/AIAA Space Flight Mechanics Meeting.

[10] J. Heiligers, T. D. van den Oever, M. Ceriotti, P. Mulligan, and C. McInnes. Continuous planetary polar observation from hybrid pole-sitters at venus, earth, and mars. In *Fourth International Symposium on Solar Sailing (ISSS 2017)*, page 10, Kyoto, Japan, 2017.

[11] B. Dachwald. Optimal solar sail trajectories for missions to the outer solar system. *Journal of Guidance, Control, and Dynamics*, 28(6):1187–1193, 2005.

[12] R. L. Forward. Roundtrip interstellar travel using laser-pushed lightsails. *Journal of Spacecraft and Rockets - J SPACECRAFT ROCKET*, 21(2):187–195, 1984.

[13] R. L. Forward. Pluto - the gateway to the stars. *Missiles and Rockets*, 10:26 – 28, 1962.

[14] G. Marx. Interstellar vehicle propelled by terrestrial laser beam. *Nature*, 211:22–23, 1966.

[15] J. L. Redding. Interstellar vehicle propelled by terrestrial laser beam. *Nature*, 213:588–589, 1967.

[16] R. Heller and M. Hippke. Deceleration of high-velocity interstellar photon sails into bound orbits at α centauri. *The Astrophysical Journal Letters*, 835(L32), 2017.

[17] R. Heller, M. Hippke, and P. Kervella. Optimized trajectories to the nearest stars using lightweight high-velocity photon sails. *The Astronomical Journal*, 154(115), 2017.

[18] G. Aliasi, G. Mengali, and A. A. Quarta. Artificial equilibrium points for a solar balloon in the α centauri system. *Acta Astronautica*, 104(2):464 – 471, 2014.

[19] T. Pino and C. Circi. A star-photon sailcraft mission in the alpha centauri system. *Advances in Space Research*, 59:2389 – 2397, 2017.

[20] J. D. Biggs, C. R. McInnes, and T. Waters. Control of solar sail periodic orbits in the elliptic three-body problem. *Journal of Guidance, Control, and Dynamics*, 32(1):318–320, 2009.

[21] P. Kervella, F. Mignard, A. Mérand, and F. Thévenin. Close stellar conjunctions of α centauri a and b until 2050 - an m_k = 7.8 star may enter the einstein ring of α cen a in 2028. *Astronomy and Astrophysics*, 594:A107, 2016.

[22] C. R. McInnes. *Solar Sailing: Technology, Dynamics and Mission Applications*. Springer - Praxis Books in Astronautical Engineering, Springer-Verlag, Berlin, Germany, 1999.

[23] A. Farres, J. Heiligers, and N. M. Baños. Road map to l4/l5 with a solar sail. In *28th AIAA/AAS Space Flight Mechanics Meeting*, page 21, Kissimmee, Florida, USA, 2018.

[24] J. Heiligers et al. Sunjammer: Preliminary end-to-end mission design. *American Institute of Aeronautics and Astronautics*, 2014. doi:10.2514/6.2014-4127.